

EFFECTS OF SPECIFIC PfEMP1 LIGATION INTERACTIONS WITH ICAM-1,  
INTEGRIN  $\alpha$ V $\beta$ 3, AND CD36 ON MONOCYTES IN AN *IN VITRO* MALARIA-  
NAÏVE HOST MODEL

by

Jordan Merritt

A Dissertation Submitted to the Faculty of

Charles E. Schmidt College of Science

In Partial Fulfillment of the Requirements for the Degree of

Doctor of Philosophy

Florida Atlantic University

Boca Raton, FL

December 2019

Copyright 2019 by Jordan Merritt

EFFECTS OF SPECIFIC PfEMP1 LIGATION INTERACTIONS WITH ICAM-1,  
INTEGRIN  $\alpha$ V $\beta$ 3, AND CD36 ON MONOCYTES IN AN *IN VITRO* MALARIA-  
NAÏVE HOST MODEL

by

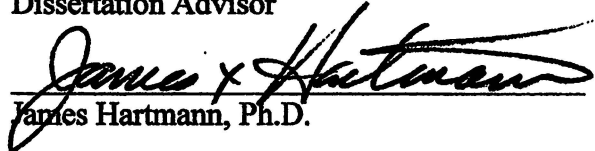
Jordan Merritt

This dissertation was prepared under the direction of the candidate's dissertation advisor, Dr. Andrew Oleinikov, Department of Biomedical Science, and has been approved by all members of the supervisory committee. It was submitted to the faculty of the Charles E. Schmidt College of Science and was accepted in partial fulfillment of the requirements for the degree of Doctor of Philosophy.

SUPERVISORY COMMITTEE:



Andrew Oleinikov, Ph.D.  
Dissertation Advisor



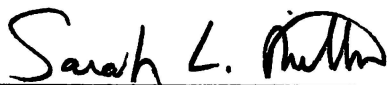
James Hartmann, Ph.D.



Vijaya Ragavarapu, Ph.D.



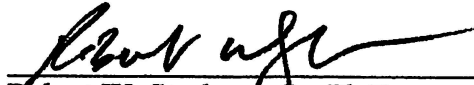
Yoshimi Shibata, Ph.D.



Sarah Milton, Ph.D.  
Interim Chair, Department of  
Biological Sciences



Ata Sarajedini, Ph.D.  
Dean, Charles E. Schmidt College of  
Science



Robert W. Stackman Jr., Ph.D.  
Dean, Graduate College

December 5, 2019  
Date

## ACKNOWLEDGEMENTS

I would like to thank the members of my dissertation committee, Dr. James Hartmann, Dr. Vijaya Iragavarapu, and Dr. Yoshimi Shibata for their support and guidance through coursework and research. I would like to thank my PI, Dr. Andrew Oleinikov, for accepting me into his lab and guiding me every step of the way. I also would like to thank the members of the lab, Dr. Olga Chesnokov, Irina Oleinikov, and Tonya Aaron for teaching me how to use the machinery in the lab. Without their support, this journey would have been a lot more difficult.

## ABSTRACT

Author: Jordan Merritt

Title: Effects of Specific PfEMP1 Ligation Interactions with ICAM-1, Integrin  $\alpha V\beta 3$ , and CD36 on Monocytes in an in vitro Malaria-Naïve Host Model

Institution: Florida Atlantic University

Dissertation Advisor: Dr. Andrew Oleinikov, Ph.D.

Degree: Doctor of Philosophy

Year: 2019

Malaria is a severe global health problem that causes approximately 435,000 deaths per year. Any non-immune individual traveling to malaria endemic regions can be affected too, including humanitarian volunteers, travelers, and US troops.

Under physiological conditions, damaged or malaria-infected RBCs would be removed within the spleen, but *Plasmodium falciparum* infected RBCs (iRBCs) sequester to microvascular endothelial cells to avoid entering the spleen. Adhesion interactions and parasite sequestration to endothelial cells are mediated by *Plasmodium falciparum* erythrocyte membrane protein 1 family (PfEMP1) proteins expressed on the iRBC's surface. The PfEMP1 proteins bind to existing endothelial cell surface receptors that already serve primary functions, including ICAM-1, integrin  $\alpha V\beta 3$ , and CD36.

Traditionally, these receptors are explored in the context of endothelial cell sequestration, but this project examines the consequence of receptor: PfEMP1 interaction on immune cells, namely monocyte-like THP-1 cells.

Since most deaths occur when non-immune individuals are exposed to the parasite, it is important to investigate the interaction the naïve immune system will have, when first encountering a PfEMP1-expressing iRBC. The circulating innate immune monocyte's ability to travel through the bloodstream, increases the probability of encountering an iRBC and serves as an interesting target to further understand the naïve host's initial reaction to malaria infection. We incubated THP-1 cells or soluble ICAM-1, integrin  $\alpha V\beta 3$ , and CD36 receptors with PfEMP1-coated 5 $\mu$ m beads, surface-immobilized PfEMP1 proteins, and iRBCs to simulate the host's naïve interaction toward iRBCs *in vitro*. Using strong ICAM-1, integrin  $\alpha V\beta 3$ , and CD36 binding PfEMP1 proteins, we determined if PfEMP1 overall protein sequence similarity has an effect on binding strength, if binding strength leads to a stronger ability to ligate to our target receptors and THP-1 cells, and if this ligation will result in an inflammatory immune response by monocyte-like THP-1 cells to eliminate the parasite.

Our study determined that overall protein sequence similarity toward the strong CD36 binding PfEMP1 protein was correlated with CD36-binding strength and ability to ligate to CD36 on a monocyte-like THP-1 cell. Overall sequence similarity did not predict ability of PfEMP1 proteins to bind to ICAM-1 and integrin  $\alpha V\beta 3$ . Ligation of THP-1 to surface-immobilized ICAM-1, integrin  $\alpha V\beta 3$ , and CD36 strong binding PfEMP1 proteins produced mainly anti-inflammatory effects. Incubation of THP-1 cells with live iRBCs, which bind to ICAM-1 (3G8 line), integrin  $\alpha V\beta 3$  (E9 line), and CD36

(E9 line) produced mainly pro-inflammatory effects. We speculate that the resulting pro-inflammatory effects might have been partially limited by the anti-inflammatory effects of PfEMP1::THP-1 ligation through our target receptors.

To my wife, Crystal Merritt, who has supported me throughout this journey.



EFFECTS OF SPECIFIC PfEMP1 LIGATION INTERACTIONS WITH ICAM-1,  
 INTEGRIN  $\alpha$ V $\beta$ 3, AND CD36 ON MONOCYTES IN AN *IN VITRO* MALARIA-  
 NAÏVE HOST MODEL

LIST OF TABLES .....	xiii
LIST OF FIGURES .....	xiv
CHAPTER I: GENERAL INTRODUCTION .....	1
CHAPTER II: ICAM-1 STUDIES .....	12
Abstract .....	12
Introduction.....	13
Materials and Methods.....	16
THP-1 Culture.....	16
Plasmids coding for PfEMP1 domains .....	16
PfEMP1 Protein sequence similarity analysis .....	17
Bead-based ICAM-1 binding assay and statistical analysis .....	18
Bead-based equilibrium constant ( $K_D$ ) analysis.....	19
THP-1:Bead-based ligation analysis and statistical comparison .....	20
PfEMP1 domain::THP-1 cytokine and chemokine analysis and statistical comparison .....	21
Results.....	22
BLASTp protein sequence similarity analysis.....	22
Sequence similarities to DBL2 $\beta$ <sub>Pf11 0521</sub> do not determine ICAM-1 binding.....	24

Equilibrium constant ( $K_D$ ): ICAM-1 has strong avidity toward DBL2 $\beta$ <sub>PF11 0521</sub> ....	26
Control beads ligated ICAM-1 on THP-1 cells more than DBL2 $\beta$ <sub>PF11 0521</sub> coated beads .....	27
THP-1 cell ligation to DBL2 $\beta$ <sub>PF11 0521</sub> produces anti-inflammatory effects .....	28
Discussion .....	30
CHAPTER III: INTEGRIN $\alpha$ V $\beta$ 3 STUDIES .....	37
Abstract .....	37
Introduction.....	38
Materials and Methods.....	42
THP-1 Culture.....	42
Plasmids coding for PfEMP1 domains .....	43
PfEMP1 Protein sequence similarity analysis .....	43
Bead-based integrin $\alpha$ V $\beta$ 3 binding assay and statistical analysis.....	44
Bead-based equilibrium constant ( $K_D$ ) analysis.....	45
THP-1:Bead-based ligation analysis and statistical comparison .....	46
PfEMP1::THP-1 cytokine and chemokine analysis and statistical comparison .....	47
THP-1::DBL2 $\delta$ <sub>PFL 2665c</sub> global gene expression analysis .....	48
Results.....	49
BLASTp protein sequence similarity analysis.....	49
Overall sequence similarity to DBL2 $\beta$ <sub>PF11 0521</sub> does not determine integrin $\alpha$ V $\beta$ 3 binding .....	51
Equilibrium constant ( $K_D$ ): Strong avidity of integrin $\alpha$ V $\beta$ 3 toward DBL2 $\delta$ <sub>PFL 2665c</sub>	53
DBL2 $\delta$ <sub>PFL 2665c</sub> coated beads ligated integrin $\alpha$ V $\beta$ 3 on THP-1 cells.....	54

THP-1 cell ligation to surface-immobilized DBL2 $\delta_{\text{PFL 2665c}}$ produces anti-inflammatory effects .....	55
THP-1 cell ligation to surface-immobilized DBL2 $\delta_{\text{PFL 2665c}}$ downregulates inflammatory gene expression .....	56
Discussion .....	59
CHAPTER IV: CD36 STUDIES .....	67
Abstract .....	67
Introduction.....	68
Materials and Methods.....	73
THP-1 Culture.....	73
Plasmids coding for PfEMP1 domains .....	73
PfEMP1 Protein sequence similarity analysis .....	74
Bead-based CD36 binding assay and statistical analysis.....	74
Bead-based equilibrium constant ( $K_D$ ) analysis.....	76
THP-1:Bead-based ligation analysis and statistical comparison .....	77
PfEMP1::THP-1 cytokine and chemokine analysis and statistical comparison .....	78
THP-1::CIDR1 $\alpha_{\text{PF08 0106}}$ global gene expression analysis.....	79
Results.....	80
Survey of CIDR1 $\alpha$ containing PfEMP1 domains for CD36 binding ability .....	80
BLASTp protein sequence similarity analysis.....	81
PfEMP1 Degree and specificity of binding to CD36 is correlated with E-value .....	83
Equilibrium constant ( $K_D$ ): CD36 avidity is correlated with E-value .....	85

THP-1 surface bound CD36 ligates PfEMP1 coated beads; correlated with E-value and $K_D$ .....	88
THP-1 ligation to CIDR1 $\alpha$ -containing PfEMP1 subset produces anti-inflammatory effects .....	92
THP-1 cell ligation to CIDR1 $\alpha_{PF08\ 0106}$ has a mixed effect on gene expression.....	95
Discussion .....	96
CHAPTER V: iRBC STUDIES AND CONCLUSION .....	101
Abstract .....	101
Introduction.....	102
Materials and Methods.....	103
THP-1 Culture.....	103
Parasite Culture .....	103
iRBC::THP-1 cytokine and chemokine analysis and statistical comparison.....	104
Results.....	105
THP-1::3G8 iRBC interaction produces mainly pro-inflammatory effects.....	105
THP-1::E9 iRBC interaction produces mainly pro-inflammatory effects .....	107
Discussion and Overall Conclusion .....	110
REFERENCES .....	117

## LIST OF TABLES

Table 1: Summary of DBL2 $\beta$ BLASTp Sequence Analysis .....	24
Table 2: Summary of DBL2 $\delta$ BLASTp Sequence Analysis.....	51
Table 3: Summary of CIDR1 $\alpha$ BLASTp Sequence Analysis.....	83

## LIST OF FIGURES

Figure 1: BLASTp Sequence Alignment for PfEMP1s targeting ICAM-1 .....	23
Figure 2: ICAM-1 Bound to PfEMP1 Domains .....	26
Figure 3: Avidity of ICAM-1 for DBL2 $\beta$ <sub>Pf11 0521</sub> .....	27
Figure 4: Percentage of DBL2 $\beta$ <sub>Pf11 0521</sub> coated beads ligated by THP-1 .....	28
Figure 5: Cytokine/Chemokine production from ICAM-1::DBL2 $\beta$ <sub>Pf11 0521</sub> ligation .....	29
Figure 6: BLASTp Sequence Alignment for PfEMP1s targeting Integrin $\alpha$ V $\beta$ 3 .....	50
Figure 7: Integrin $\alpha$ V $\beta$ 3 Bound to PfEMP1 Domains .....	52
Figure 8: Avidity of integrin $\alpha$ V $\beta$ 3 for DBL2 $\delta$ <sub>PfL 2665c</sub> .....	54
Figure 9: Percentage of DBL2 $\delta$ <sub>PfL 2665c</sub> coated beads ligated by THP-1 .....	55
Figure 10: Cytokine/Chemokine production from integrin $\alpha$ V $\beta$ 3::DBL2 $\delta$ <sub>PfL 2665c</sub> ligation .....	56
Figure 11: RNA <sub>Seq</sub> Analysis from THP-1 ligation to HAE and DBL2 $\delta$ <sub>PfL 2665c</sub> .....	58
Figure 12: Integrin $\alpha$ V $\beta$ 3 binding to various PfEMP1 proteins.....	60
Figure 13: Integrin $\alpha$ V $\beta$ 3 binding to various RGD-containing PfEMP1 proteins .....	61
Figure 14: Survey of CIDR1 $\alpha$ containing PfEMP1 proteins for CD36 binding.....	81
Figure 15: BLASTp Sequence Alignment for PfEMP1s targeting CD36 .....	82
Figure 16: CD36 Bound to PfEMP1 Domains .....	84
Figure 17: Correlation between bound CD36 (MFI) and protein sequence similarity .....	85
Figure 18: Avidity of CD36 for PfEMP1 Domains .....	87
Figure 19: Correlation between E-value and Equilibrium Constant of CD36.....	88

Figure 20: Percentage of CIDR1 $\alpha$ <sub>PF07 0049</sub> coated beads ligated by THP-1 .....	89
Figure 21: Percentage of CIDR1 $\alpha$ <sub>MAL7P1.56</sub> coated beads ligated by THP-1 .....	90
Figure 22: Percentage of CIDR1 $\alpha$ <sub>PF08 0106</sub> coated beads ligated by THP-1 .....	91
Figure 23: Correlation between % beads ligated to THP-1, E-value and $K_D$ of CD36 ....	92
Figure 24: Cytokine/Chemokine production from CD36::CIDR1 $\alpha$ <sub>PF07 0049</sub> ligation.....	93
Figure 25: Cytokine/Chemokine production from CD36::CIDR1 $\alpha$ <sub>MAL7P1.56</sub> ligation.....	94
Figure 26: Cytokine/Chemokine production from CD36::CIDR1 $\alpha$ <sub>PF08 0106</sub> ligation.....	95
Figure 27: RNA <sub>Seq</sub> Analysis from THP-1 ligation to HAE and CIDR1 $\alpha$ <sub>PF08 0106</sub> .....	96
Figure 28: Cytokine/Chemokine production from 3G8 iRBC::THP-1 interaction .....	107
Figure 29: Cytokine/Chemokine production from E9 iRBC::THP-1 interaction.....	110
Figure 30: 3G8 iRBC sequestered to ICAM-1 .....	111
Figure 31: E9 iRBC binding to surface-immobilized recombinant human receptors ....	113

## CHAPTER I: GENERAL INTRODUCTION

Malaria is a severe global health problem with approximately 435,000 documented deaths in 2017 (1). This is a striking number because the deaths are concentrated in impoverished, tropical and subtropical regions. In addition to the risk to the residents, any non-immune individuals traveling to malaria endemic regions can be affected too, including humanitarian volunteers, travelers, and US troops.

Malaria is an obligate endoparasite belonging to the phylum Apicomplexa and the genus *Plasmodium*. Humans can be infected with 5 different species of malaria: *P. falciparum*, *P. malariae*, *P. ovale*, *P. vivax*, and *P. knowlesi*. However, *P. falciparum* is the only species of malaria that substantially sequesters within the host's vasculature, leading to severe malaria complications and in many cases, death.

*P. falciparum* is transmitted by the female *Anopheles* mosquito. Parasites in a sporozoite form are transferred to the host through the saliva of mosquito, when it takes a blood meal. Following vascular migration to the liver, sporozoites gain entry to Kupffer cells and hepatocytes. Within hepatocytes, sporozoites develop into merozoites and are released into the bloodstream. Erythrocyte binding-like (EBL) and reticulocyte binding-like (RBL) protein family ligands on the merozoite surface bind to specific red blood cell (RBC) membrane receptors to gain entry. One example is EBL-1 on the



merozoite surface, which binds specifically to glycophorin B on the RBC to facilitate parasite invasion (2). The asexual reproduction cycle, consisting of a haploid genome, begins when the RBC's membrane is breached by the parasite. Once the RBC is infiltrated, the parasites will progress through three distinct life stages (ring, trophozoite, and schizont) before releasing daughter merozoites to infect other RBCs (3).

Under physiological conditions, damaged, aged, or infected RBCs would be removed within the spleen, but *P. falciparum* infected RBCs (iRBCs) sequester to microvascular endothelial cells to avoid entering the spleen (4). Endothelial sequestration provides iRBCs the appropriate time needed to complete their 48-hour life cycle, to potentially infect additional RBCs. Sequestered schizonts are able to release merozoites leading to an increase in the parasitemia within the host (5). Furthermore, prolonged circulating malarial parasites are required for the production of male and female gametocytes, which are removed during mosquito blood meals to undergo the sexual reproductive cycle of the parasite within the mosquito's gut. The sexual and asexual reproductive cycles are essential for further transmission of the parasite. The hallmark of severe malaria (SM) complications is the ability of *P. falciparum* iRBCs to sequester to the endothelium of blood vessels, uninfected red blood cells, other iRBCs, and tissues of the body (6). SM complications include, but are not limited to, cerebral malaria, severe anemia, organ failure, respiratory distress, and placental malaria resulting in infant and maternal mortality (7, 8). Sequestration also causes blood flow problems, immune cell recruitment, inflammation, tissue damage, and disruption of normal cell function (9).

In order to sequester, iRBCs will present malaria specific proteins on their surface that interact with the host's cell membrane surface receptors. The malaria specific

proteins belong to the *Plasmodium falciparum* erythrocyte membrane protein 1 family (PfEMP1) (10). There are approximately 60 *var* genes, with only one expressed at a time, within the haploid malaria genome that codes for all PfEMP1 proteins (11). *var* genes are divided into 6 groups (UpsA, UpsB, UpsC, UpsD, UpsE, and UpsBC), which are classified by their associated upstream (Ups) promoter sequences (12, 13). Each PfEMP1 protein is constructed of various Duffy binding-like domains (DBL) and cysteine rich interdomain regions (CIDR). There are 5 major types of DBL domains ( $\alpha$ ,  $\beta$ ,  $\gamma$ ,  $\delta$ , and  $\epsilon$ ) and three major types of CIDR domains ( $\alpha$ ,  $\beta$ , and  $\gamma$ ) that are organized according to their primary protein structure (14). For sequestration, the malaria parasite uses extracellular DBL and CIDR domains to adhere to existing cell surface receptors. These extracellular domains are highly variable in sequence but preserve a substantial level of homology and similar 3D architecture.

Adhesion interactions and parasite sequestration to endothelial cells are mediated by expressed PfEMP1 domains on the iRBCs surface. Endothelial cells are simple squamous cells that line the inner surface of blood vessels. This type of cell is important for immune cell trafficking, blood clotting, and the control of blood pressure through dilation and constriction. iRBCs have been shown to bind to various endothelial cell receptors, including ICAM-1 (15), integrin  $\alpha V\beta 3$  (16), and CD36 (17).

ICAM-1, intercellular adhesion molecule 1, is a transmembrane protein that facilitates immune cell migration by acting as a docking point within blood vessels for circulating immune cells to adhere (43, 56). Integrin  $\alpha V\beta 3$  is a transmembrane receptor found on endothelial cells, which functions in adhesion, and signal transduction (66). CD36 is an integral cell membrane scavenger receptor that is expressed in various tissues

throughout the body. The main function of CD36 is to recognize and facilitate the removal of macromolecules possessing a negative charge, including uptake of long-chain fatty acids and oxidized low density lipoproteins (LDL) (96). iRBCs utilize specific DBL and CIDR regions within PfEMP1 proteins to bind to these receptors (18). More specifically, in the 3D7 strain of *P. falciparum*, the CIDR1 $\alpha$  domain has been shown to bind to CD36, while the CIDR $\beta$  and CIDR $\gamma$  domains do not bind to CD36 (19). It is interesting to note, that out of all the CIDR domains, along with CIDR $\delta$ , CIDR1 $\alpha$  had the highest amino acid sequence similarities (93). Further, in the same strain of *P. falciparum*, the DBL2 $\beta$  domain of the PF11 0521 allele binds to ICAM-1 with high affinity (20, 21). Recently, we have demonstrated that the DBL2 $\delta$  domain of the PFL2665c allele binds to integrin  $\alpha$ V $\beta$ 3 (16).

PfEMP1s are from malarial origin; therefore, they are recognized by the immune system as foreign. In the case of pregnancy malaria (PM), the ability of the mother's immune system to recognize iRBCs sequestered in the placenta can result in developed, adaptive immunity (22). Therefore, the antigen-presenting innate immune cells are important to phagocytose the iRBC and present it to T- and B-cells to promote an adaptive immune response. Serum samples, containing antibodies, from multigravid women are able to inhibit PfEMP1 binding to chondroitin sulfate A (CSA) on syncytiotrophoblast of the placenta compared to serum samples from men and primigravid women (23). PM is a severe malaria syndrome where adaptive immunity develops only after multiple pregnancies (24). Over multiple pregnancies, the specific nature of the placental sequestration interaction provides a conserved immune target for antibodies to be produced toward the malaria parasite. Before immunity to PM develops,

PM may lead to low birth weight, stillborn death, and/or death of the mother, predominantly in the primigravid population.

Unfortunately, individuals without substantial exposure to malaria, like newborns and travelers, are at the highest risk of severe malaria leading to death. High diversity of *var* gene variants in the field and ability of iRBCs to switch expressed *var* genes, producing different PfEMP1 proteins, makes it difficult for individuals living in malaria-endemic areas to efficiently develop broad immunity. Therefore, formation of a natural adaptive immune response to clinical malaria requires decades of constant exposure and infection, resulting in ~500,000 deaths from malaria complications yearly (1).

Further, the efficacy of current drug treatments, especially the most commonly prescribed anti-malarial drugs, are rapidly declining. Additionally, many of the commonly administered antimalarial drugs have severe side effects. For example, chloroquine is an antimalarial drug that creates toxic heme-complexes, causing the RBC to lyse and destroy the parasite (25). The release of toxic compounds from the lysed RBC can lead to severe side effects like blindness, uncontrolled movements, and hearing loss (26). Additionally, malaria has developed resistance to drug treatment at an alarming rate, which has made many treatments obsolete, even though they are still being utilized (27). Overuse leading to parasite selection and parasite drug target variability is thought to contribute to drug resistance (28). Currently, prophylactic drugs are the most effective drug treatment for travelers (29). To be effective, prophylactic drug regimens need to be started 1-2 weeks before traveling to a malaria endemic region and usually continued for 1 week after leaving the region. The problem with prophylactic treatment is that the

majority of people dying from malaria live in endemic regions and are not able to leave to begin and end their treatment in a malaria eradicated area.

People living in malaria endemic regions have found some reprieve from the parasite by attacking the vector (mosquito), instead of the parasite within the human host. Common vector control methods include mosquito nets, larvicides, insecticides, and residual spraying within homes. Residual spraying when combined with insecticide treated mosquito nets is 61% more effective at reducing parasitemia than insecticide treated mosquito nets alone (30). Residual spraying consists of spraying insecticides on the inner walls of a dwelling to kill mosquitoes. After taking a blood meal, mosquitoes will land on a solid surface to digest. When the mosquitoes land on the wall, they will be killed by the insecticides that were sprayed there. Unfortunately, malaria can still be transmitted to the host of the dwelling during the initial blood meal; however, the mosquito would be prevented from further spreading the parasite after interacting with the insecticides on the walls of the dwelling.

The World Health Organization (WHO) recommends four different classes of insecticides for indoor residual spraying: carbamates, organochlorines, organophosphates, and pyrethroids (31). However, the limited options for safe, effective, indoor insecticides has led to their overuse in both quantity and duration. Similar to the malaria parasite developing drug resistance to anti-parasitic medications, the mosquito is developing resistance to insecticides. Currently, mosquitoes that have developed resistance to organophosphates and pyrethroids around Shanghai may derail China's national program goal of eliminating malaria in China by 2020 (32). Anti-parasitic medication and insecticide resistance combined with the difficulties in acquiring an adaptive immune

response places importance on figuring out ways to make the immune system more efficient at combating malaria infection.

Recently, the treatment strategies have shifted to immune system manipulation to assist the host in developing long-term immunity to malaria. In 2015, the European Medicines Agency (EMA) approved a malaria vaccine that was trialed in seven African countries. Mosquirix, or RTS,S/AS01 vaccine, was developed by the GlaxoSmithKline vaccine research laboratory to help the host produce antibodies toward a pre-erythrocytic stage of the parasite. The recombinant vaccine targets the circumsporozoite protein (CSP); therefore, when immune cells encounter the vaccine, they will produce antibodies against the CSP malarial protein. If the host possess anti-CSP antibodies, then they should be able to mount an immune response to the sporozoite, before it enters and matures within hepatocytes of the liver.

The vaccine completed phase 3 trials at 11 health facilities throughout Kenya, Tanzania, Mozambique, Gabon, Malawi, Ghana, and Burkina Faso between March 2009 and January 2014. For the safety of the participants, indoor residual spraying and mosquito bed nets were also used. The vaccine was administered once a month for 3 months to children 6 to 12 weeks of age and children 5 to 17 months of age. The study was extended to include a subpopulation of the treatment group who also received an 18 month booster treatment. In the infant (6 to 12 weeks) population, the clinical episodes of malaria were reduced by approximately 24%, but no long-term protection against severe malaria infection developed (33). As a result, the infant population does not serve as an effective target population for RTS,S vaccine treatment. Excitingly, the 5 to 17 month treatment group who received the 18 month booster were able to see reductions in clinical

episodes and a 32% reduction in severe malaria after 4 years. The participants who did not receive the RTS,S vaccine booster treatment did not see any long-term protection against severe malaria (34).

The mixed results of the RTS,S vaccine provides hope that the scientific community is on the right track by attempting to promote an immune response to eradicate malaria; however, it also signifies that more research needs to be conducted on immune interactions with the malaria parasite to create more efficient and effective treatment methods. In addition to the adaptive, antibody-producing arm of the immune system that the RTS,S vaccine targets, the rapid, nonspecific innate arm of the immune system could offer key information on the naïve host's initial interaction with the malaria parasite. This information could lead to innate immune manipulation therapy or the discovery of novel vaccine targets. During the innate immune response, immune cell surface-bound pattern recognition receptors (PRRs) recognize and bind to a wide array of pathogen-associated molecular patterns (PAMPs) on infectious materials to eliminate them from the host. Interestingly, many of the cell surface-bound receptors implicated in sequestration of iRBCs to endothelial cells can also be found on innate immune cells, including monocytes.

Monocytes use surface bound receptors for recognition of pathogens and to facilitated phagocytosis and elimination of the pathogens, including iRBCs expressing PfEMP1s on their surface. PfEMP1 recognition by immune cells can lead to an immune response characterized by an increase in cytokine and chemokine production, inflammation, and immune cell recruitment (35). However, an over-reactive immune response may lead to severe complications instead of protection. Inflammatory

microenvironments, created by the innate immune response toward malaria, may be responsible for tissue damage and organ dysfunction (36). In mouse models, depletion of neutrophils early during malaria infection decreased the production of IL-12, IL-18, IFN- $\gamma$ , TNF- $\alpha$ , and MIP-1 $\alpha$ . The reduction in inflammatory cytokines resulted in a decrease in monocyte recruitment to brain microvasculature, which ultimately inhibited the development of CM (132). Therefore, inflammation can be a major contributor to severe malaria complications. Conversely, an under-reactive immune response may lead to parasite survival, increasing the risk of dangerous hyperparasitemia. The type of immune response is dependent on the signaling pathways from specific immune cell receptors involved in recognition of PfEMP1 proteins.

As common and expensive treatment methods become less effective, any further attempts at treatment strategies would benefit from a better understanding of how the immune system interacts with malaria. An understanding of PfEMP1 interactions with specific immune cell surface receptors is needed to fully combat SM cases. Cell surface receptors ICAM-1 (15), integrin  $\alpha$ V $\beta$ 3 (16), and CD36 (17) are the most common sequestration receptors utilized by circulating *P. falciparum* parasites and have been shown to interact with specific PfEMP1 constructs (121). Traditionally, these receptors are explored in the context of endothelial cell sequestration, but this project examines the immune consequence of receptor::PfEMP1 interaction on monocyte-like THP-1 cells. Since most deaths occur when non-immune individuals are exposed to the parasite, it is important to investigate the interaction the naïve immune system will have, when first encountering a PfEMP1. As a result of the less specific and more broad approach to pathogen elimination, the innate immune system is the first line of defense against



pathogens. The innate immune system utilizes leukocytes that travel through the bloodstream to search for pathogens. Circulating innate immune monocytes create reactive oxygen species and inflammatory mediators, referred to as an oxidative burst, to directly eliminate a pathogen. Additionally, monocytes and dendritic cells can phagocytose pathogens, process, and present portions of the pathogen to T- and B-cells to mount an adaptive immune response. A monocyte's location, circulating through the bloodstream, increases the probability of encountering an iRBC and serves as an interesting target to further understand the naïve host's initial immune reaction to malaria infection.

For this project, unstimulated monocyte-like THP-1 cells were used to simulate a circulating immune mononuclear cell. PfEMP1 protein constructs were attached individually to 5µm Bio-Plex beads, simulating a 5µm iRBC, to determine binding abilities and consequences of interaction with ICAM-1, integrin  $\alpha V\beta 3$ , and CD36. The three main aims of this project are: 1) Determine if PfEMP1 constructs, with similar protein sequences to known sequestration implicated PfEMP1 proteins, will bind to ICAM-1, integrin  $\alpha V\beta 3$ , and CD36 with the same avidity, lending importance to protein sequence and binding characteristics, 2) Determine the ability of our surface-immobilized target PfEMP1 protein domains to induce cytokine/chemokine production by monocyte-like THP-1 cells and also comparing differential expression of genes (upon CD36 and integrin  $\alpha V\beta 3$  ligation) in monocyte-like THP-1 cells. 3) Compare the effects of 3G8 (IT4 genetic background) and E9 (NF54 genetic background) infected red blood cell, which bind to ICAM-1 and CD36/integrin  $\alpha V\beta 3$ , respectively, interactions with THP-1

cells to the effects of surface-immobilized PfEMP1 domain interactions with THP-1 cells on cytokine/chemokine secretion.

## CHAPTER II: ICAM-1 STUDIES

### Abstract

The role of ICAM-1 has expanded as the list of ligands for ICAM-1 has expanded. The three main ligands of ICAM-1 are fibrinogen, Mac-1, and LFA-1. During the cellular phase of coagulation, fibrinogen crosslinks platelets together through ICAM-1. The ICAM-1::fibrinogen interaction also plays a major role in leukocyte adhesion to endothelial cells. During tight adhesion prior to leukocyte transmigration to damaged tissues, ICAM-1 on endothelial cells binds to Mac-1 via fibrinogen crosslink, Mac-1 directly, or LFA-1 directly on leukocytes. Similarly, tight adhesion between ICAM-1 on endothelial cells with PfEMP1 proteins containing appropriate DBL $\beta$  domains on iRBCs facilitates sequestration of iRBCs to the microvasculature, prolonging the parasite infection. Interestingly, the innate immune consequences of PfEMP1::ICAM-1 interactions have not been extensively researched. In this study, we examine the effects of PfEMP1 protein sequence similarity, toward the known ICAM-1 binding DBL2 $\beta$ <sub>PF11 0521</sub> protein construct, on ICAM-1 binding strength and avidity. Additionally, we examine if DBL2 $\beta$ <sub>PF11 0521</sub>::ICAM-1 ligation will induce cytokine/chemokine release by monocyte-like THP-1 cells. Overall sequence similarity toward the DBL2 $\beta$ <sub>PF11 0521</sub> PfEMP1 protein construct did not predict ability to bind to ICAM-1 and THP-1 cell ligation to surface-immobilized DBL2 $\beta$ <sub>PF11 0521</sub> produced mainly anti-inflammatory effects.

## Introduction

Intercellular Adhesion Molecule 1 (ICAM-1), also known as Cluster of Differentiation 54 (CD54), is a transmembrane protein found on the surface of endothelial cells, innate immune cells, and lymphocytes. Historically, ICAM-1 has been described as a simple adhesion molecule, but its role has expanded as the list of ligands for ICAM-1 has expanded. Three main ligands of ICAM-1 are fibrinogen, macrophage adhesion ligand-1 (Mac-1, integrin  $\alpha M\beta 2$ , CD11b/CD18), and leukocyte function associated antigen-1 (LFA-1, integrin  $\alpha L\beta 2$ , CD11a/CD18).

Fibrinogen is a protein that is secreted by hepatocytes into the blood stream. Once circulating in the blood, fibrinogen is converted to fibrin by thrombin in order to form a fibrin clot during the fluid phase of coagulation (37). Fibrinogen is constructed from 2 sets of  $\alpha$ ,  $\beta$ ,  $\gamma$  polypeptide chains, linked by disulfide bonds. Amino acid substitutions in the  $\beta$  polypeptide chain reduces the interaction of thrombin to its substrate, fibrinogen, thus reducing the production of fibrin and clotting ability (38). Fibrinogen also cross links integrin  $\alpha IIa\beta 3$  surface receptors on adjacent platelets to aid in aggregation during the cellular phase of coagulation (39, 40). Amino acid substitutions in the  $\gamma$  polypeptide chain of fibrinogen reduced its ability to aggregate platelets compared to substitutions within  $\alpha$  and  $\beta$  polypeptide chains, which showed no change in ability to aggregate platelets (41). Similarly, platelet aggregation was also decreased by blocking the ICAM-1 and fibrinogen interaction via targeted anti-ICAM-1 antibodies (42).

The ICAM-1::fibrinogen interaction also plays a major role in leukocyte adhesion to endothelial cells. ICAM-1 on endothelial cells binds to fibrinogen, which in turn, binds to Mac-1 on the surface of leukocytes (43, 44). Tight leukocyte adhesion to the vascular

endothelium is one of the four steps in leukocyte extravasation out of the bloodstream and into specific tissues and organs. The steps include: chemoattraction, rolling adhesion, tight adhesion (where ICAM-1 becomes important), and transmigration.

Following tissue damage, chemical signals in the form of chemokines, are secreted by immune cells near the damaged tissue to chemoattract additional immune cells to the area. The concentration of chemokines, and therefore, the chemoattractant signal decreases as distance from the damaged tissue increases. Circulating leukocytes, following the chemical signal, will use cell surface carbohydrate ligands to loosely bind to selectins on the surface of endothelial cells. As a result of the quick association and dissociation with selectins, leukocytes can break and make bonds simultaneously to slowly roll in the direction of blood flow along the endothelium (45). Immune cells near the site of damage will also produce cytokines that stimulate endothelial cells to upregulate stronger adhesion molecules, including ICAM-1, to stop the leukocytes from rolling (46). At this point, ICAM-1 on the endothelial cells can interact with Mac-1 via fibrinogen crosslink (44), Mac-1 directly (47), or LFA-1 (48) on the leukocytes. Once the leukocytes stop rolling, ligated ICAM-1 translocates to caveolae, which are small invaginations of plasma membrane. Leukocytes located at the caveolae, via ICAM-1, are transcytosed for migration through a transcellular pathway (49) instead of a paracellular pathway (50), which was previously suggested as the exclusive route for leukocyte cell migration. In the paracellular pathway, ICAM-1 on the endothelial cell surface co-localizes with LFA-1 on leukocytes into a ring like structure that promotes cell migration through cell junctions (51).

Similar to ICAM-1-mediated leukocyte adhesion, ICAM-1 has been implicated in malaria-infected red blood cell (iRBC) sequestration to the endothelium (52). Upon testing each of the 5 distinct PfEMP1 DBL domain types ( $\alpha$ ,  $\beta$ ,  $\gamma$ ,  $\delta$ ,  $\epsilon$ ) for binding to ICAM-1, only the DBL $\beta$  domain bound to ICAM-1 (15). Further analysis of 16 PfEMP1 proteins containing DBL $\beta$  domains from the 3D7 parasite line determined that only the DBL2 $\beta$ 3<sub>PF11 0521</sub> protein construct binds ICAM-1 strongly compared to the other PfEMP1 proteins tested (20). ICAM-1 interactions are known to facilitate cerebral malaria (53); therefore, a DBL2 $\beta$ 3<sub>PF11 0521</sub>-like PfEMP1 domains may be the ICAM-1 ligands that facilitate iRBC sequestration in brain capillaries leading to cerebral malaria syndrome.

ICAM-1 can also be found on immune cells. ICAM-1 ligation on astrocytes, a subset of glial cells in the brain, leads to internal cell signaling that produces pro-inflammatory TNF- $\alpha$  (54). Similarly, ICAM-1 signaling in cerebral and dermal microvascular endothelial cells (MVEC) produced the pro-inflammatory cytokines and immune recruiting chemokines TNF- $\alpha$ , IL-8 (CXCL8), CCL3, CCL4, VCAM-1 and COX-2 through mitogen-activated protein kinase (MAPK) activation (55). Further, it has been proposed that ICAM-1 signaling plays a direct role in promoting inflammation of endothelial cells at the blood vessel wall (56). Unfortunately, the immune interaction between PfEMP1 proteins and ICAM-1 on immune cells has not been studied extensively. Since DBL $\beta$ 3<sub>PF11 0521</sub> was previously determined, by our lab, to significantly bind ICAM-1 compared to other DBL $\beta$  containing PfEMP1 domains, DBL $\beta$ 3<sub>PF11 0521</sub> serves as our reference PfEMP1 protein for our ICAM-1 studies.

In this study, we determine if protein sequence similarity toward the DBL2 $\beta$ 3<sub>PF11 0521</sub> protein construct plays a role in ICAM-1 binding strength and avidity using PfEMP1-

coated Bio-Plex beads. Additionally, we determine if DBL $\beta$ 3<sub>PF11 0521</sub>::ICAM-1 ligation will induce cytokine/chemokine release by monocyte-like THP-1 cells, which possess ICAM-1 receptors (57). We hypothesize that protein sequence similarity toward the strong ICAM-1-binding DBL2 $\beta$ 3<sub>PF11 0521</sub> PfEMP1 protein construct would predict similar ICAM-1 binding strength and avidity. Based on ICAM-1s function in leukocyte extravasation and immune signaling (51, 55, 56), we predicted that PfEMP1::ICAM-1 ligation would induce pro-inflammatory cytokine/chemokine release by monocyte-like THP-1 cells.

## **Materials and Methods**

### **THP-1 Culture**

THP-1 cells, kindly provided by Dr. Yoshimi Shibata from Florida Atlantic University, were cultured in RPMI 1640 growth medium, supplemented with 25 $\mu$ g/ml gentamicin sulfate, 0.125 $\mu$ g/ml Amphotericin B, and 10% heat-inactivated FBS. The cells were cultured below 5X10<sup>5</sup>cells/ml in order to maintain an unstimulated, nonadherent monocyte population to simulate naïve host immune cells cytokine analysis.

For ligation of PfEMP1-coated beads and interaction with surface-immobilized PfEMP1 proteins, THP-1 cells were incubated with Goat IgG (Jackson Laboratories, Cat# 005-000-002) to block the cells from interacting with our PfEMP1 capture antibody, Goat anti-GFP (Rockland, Cat# 600-101-215). Antibiotic and anti-fungal additives were withheld from the media for all experiments requiring binding.

### **Plasmids coding for PfEMP1 domains**

PfEMP1 plasmids were created previously using the methods described in (120). Briefly, all PfEMP1 domains were cloned into the pHisAdEx vector, expressed by COS-7 cells, harvested, and immobilized on either COOH Bio-Plex beads (BioRad, Cat# 1715060##) or individual wells of a 96 well plate. Immobilization steps are mentioned in corresponding sections below. The pHisAdEx vector containing a 54kDA malaria-irrelevant protein fragment that is a part of all PfEMP1 domain-containing constructs, thus being present in all recombinant PfEMP1 domains tested, was used as the control in all PfEMP1 experiments.

#### *PfEMP1 Protein sequence similarity analysis*

The National Institute of Health's (NIH) Basic Local Alignment Search Tool (BLAST) was used to compare known PfEMP1 protein sequences to determine related PfEMP1 proteins. Query searches were conducted using the non-redundant protein sequence database, BLASTp (protein-protein BLAST) algorithm, and *Plasmodium falciparum* isolate 3D7 (taxid: 36329) as the organism. Search results are organized by query cover, percent identical, and expected value (E-value). Query cover refers to the percentage of the original query sequence that can be compared to the sequences from the results. Percent identical refers to the percentage of identical amino acids in the same location between the original query sequence and the sequences from the results. The E-value was the measurement of how many times, by chance, in a given search the exact same sequence will exist. Therefore, as E-values approach zero, the results are more likely to be specific to the sequence searched. Related proteins were determined by how close their E-value was to zero. The protein sequence from the PfEMP1 construct



DBL2 $\beta$ 3<sub>PF11 0521</sub>, shown to strongly bind to ICAM-1, was used as our initial BLASTp search query.

*Bead-based ICAM-1 binding assay and statistical analysis*

HisAdEx (HAE, control), DBL2 $\beta$ 6<sub>PF07 0050</sub>, DBL2 $\beta$ 3<sub>PF1235w</sub>, and DBL2 $\beta$ 3<sub>PF11 0521</sub> PfEMP1 proteins were expressed as GFP-fusion proteins by COS-7 cells. COOH Bio-Plex beads of various fluorescence color (bead region) were coated with Goat anti-GFP antibody and incubated with COS-7 cell lysates expressing each individual PfEMP1 domain (one bead region per one domain), overnight at 4°C with rotation. The PfEMP1 coupled beads were washed and stored at -80°C in 1xPBS with 0.1% BSA, 0.02% Tween-20, 0.05% sodium azide, and 15% glycerol until experimentation, but no longer than 1 month. The solution was switched to 1x TBS, 0.05% tween-20, and 0.1% BSA Fraction V for binding experiments. To determine binding ability and specificity to ICAM-1, 2 $\mu$ g/ml of recombinant human ICAM-1-FC (R&D Systems, Cat# 720-IC) was incubated with PBS, 5 $\mu$ g/ml anti-CD36 monoclonal antibody (Abcam, Cat# ab17044), or 5 $\mu$ g/ml anti-ICAM-1 monoclonal antibody (Invitrogen, Cat# MA5407) for 1 hour with shaking at room temperature. Following pre-incubation with blocking agents, the ICAM-1 recombinant proteins were incubated with HAE, DBL2 $\beta$ 6<sub>PF07 0050</sub>, DBL2 $\beta$ 3<sub>PF1235w</sub>, and DBL2 $\beta$ 3<sub>PF11 0521</sub> coated beads for 1 hour with shaking at room temperature. Any unbound ICAM-1 was washed out of the system through vacuum filtration and then the beads were incubated with a 1:250 dilution of Goat anti-human IgG-Phycoerythrin (R&D Systems, Cat# 109-116-170) with shaking at room temperature, to target bound ICAM-1 through the FC portion of the recombinant protein.

Mean fluorescent intensity (MFI) of bound fluorescently-labeled ICAM-1 was determined by the Bio-Plex 200 suspension array system (BioRad) using Bio-Plex Manager Software 5.0. All binding experiments were conducted in triplicate and repeated at least once. MFI values were compared for statistical significance to the control by a two-tailed T. Test with two sample equal variance and a 95% confidence interval using both Microsoft Excel and Bio-Plex Manager 5.0 (\* =  $P \leq 0.05$ , \*\* =  $P \leq 0.01$ , \*\*\* =  $P \leq 0.001$ , \*\*\*\* =  $P \leq 0.0001$ ). All graphical error bars are Standard Error of Means (SEM).

#### *Bead-based equilibrium constant ( $K_D$ ) analysis*

Various concentrations of recombinant ICAM-1-FC (3.0 $\mu$ g/ml, 1.0 $\mu$ g/ml, and 0.3 $\mu$ g/ml) were incubated with a 1:250 dilution of Goat anti-human IgG-PE, to fluorescently label the ICAM-1 receptor. Following fluorescent labeling, the various concentrations of ICAM-1 were incubated with HAE and DBL2 $\beta$ 3<sub>PF11 0521</sub> coated Bio-Plex beads for 0, 5, 10, and 15 minutes. The change in MFI ( $\Delta$ MFI) of bound fluorescently labeled ICAM-1 was compared to change in time ( $\Delta$ Time) to determine the velocity of binding for 3.0 $\mu$ g/ml, 1.0 $\mu$ g/ml, and 0.3 $\mu$ g/ml of recombinant ICAM-1. The inverse velocities ( $1/V = \Delta$ Time/ $\Delta$ MFI) were plotted against their corresponding inverse concentrations ( $1/C$ ) on a Lineweaver-Burk double reciprocal scatter plot. On a Lineweaver-Burk plot, the x-intercept of the linear line of best fit equals  $1/-K_D$ , where  $K_D$  represents the equilibrium dissociation constant. In this case, the equilibrium constant signifies the concentration of ICAM-1 where 50% of ICAM-1 is bound to DBL2 $\beta$ 3<sub>PF11 0521</sub> and 50% of ICAM-1 is not bound to DBL2 $\beta$ 3<sub>PF11 0521</sub>. Mean fluorescent intensity (MFI) of bound fluorescently-labeled ICAM-1 was determined by the Bio-Plex 200

suspension array system using Bio-Plex Manager Software 5.0. All  $K_D$  experiments were conducted in duplicate and repeated at least once. Data was plotted using Microsoft Excel to determine  $K_D$  values. All graphical error bars are Standard Error of Means (SEM).

*THP-1: Bead-based ligation analysis and statistical comparison*

THP-1 cells were incubated with PBS, 10  $\mu\text{g/ml}$  of anti-CD36 monoclonal antibody, or 10  $\mu\text{g/ml}$  of anti-ICAM-1 monoclonal antibody for 30 minutes at 37°C with shaking. The cells were washed and then incubate with either HAE or DBL2 $\beta$ 3<sub>PF11 0521</sub> coated beads, at a 1:20 ratio of Beads:THP-1 cells, for 2 hours with shaking at 0°C and 37°C. The 0°C samples were used as a ligation control (no phagocytosis taking place) and the results at 0°C were subtracted as background from the 37°C samples. Others have confirmed phagocytosis takes place at 37°C, but not at 0°C by confocal microscopy also using THP-1 cells and PfEMP1-coated fluorescent beads (137). Therefore, reported values adjusted for the control signify ligation and possibly phagocytosis, further analysis is needed to confirm phagocytosis. Using the Attune NXT acoustic focusing flow cytometer (Life Technologies) and associated software, we were able to locate our beads and cells using side scatter (SSC) and front scatter (FSC) characteristics. The beads are smaller and have a more complex internal core than the THP-1 cells. The bead's complex internal core is made up of two fluorescent dyes that can be detected on the BL3 channel of the flow cytometer. To locate our ligated and possibly phagocytosed beads, we gated the THP-1 cells and analyzed the gated region for the BL3 channel. We compared the number of beads (positive signal in BL3) associated with THP-1 cells to the total amount of beads in the system to determine the percentage of beads ligated and possibly

phagocytosed. The percentage was compared for statistical significance to the control by a two-tailed T. Test with two sample equal variance and a 95% confidence interval using both Microsoft Excel and Bio-Plex Manager 5.0 (\* =  $P \leq 0.05$ , \*\* =  $P \leq 0.01$ , \*\*\* =  $P \leq 0.001$ , \*\*\*\* =  $P \leq 0.0001$ ). All ligation experiments were conducted in duplicate and repeated at least once. All graphical error bars are Standard Error of Means (SEM).

*PfEMP1 domain::THP-1 cytokine and chemokine analysis and statistical comparison*

Utilizing the same process as Bio-Plex bead coupling, HAE and DBL2 $\beta$ 3<sub>PF11 0521</sub> were immobilized on the surface of a 96-well flat bottom plate through Goat anti-GFP targeted attachment.  $4.0 \times 10^5$  THP-1 cells were added to each well and incubated at 37°C for 0, 12, and 24 hours. The supernatants were collected and analyzed using Bio-Plex Pro Human Cytokine kits (BioRad Cat# 171304090M and Cat# 171-AL003M) testing for the presence of IL-1 $\alpha$ , IL-1 $\beta$ , IL-2, IL-6, IL-8, IL-10, IL-12 (p40), IL-12 (p70), IL-13, IL-19, IL-20, IL-22, IL-26, IL-27, IL28a, IL29, IFN- $\gamma$ , MCP-1, MIP-1 $\alpha$ , and TNF- $\alpha$ . 4 parameter logistic (4PL) or 5 parameter logistic (5PL) standard curves for each cytokine/chemokine were created using the provided standards with the concentration on the x-axis and the MFI on the y-axis. Unknown sample concentrations were determined by fitting the MFI values to the standard curves using the Bio-Plex Manager 5.0 software and confirmed by MyCurveFit online-based application. All samples were analyzed with a one-way ANOVA followed by a two-tailed T. Test with two sample equal variance and a 95% confidence interval using both Microsoft Excel and Bio-Plex Manager 5.0 (\* =  $P \leq 0.05$ , \*\* =  $P \leq 0.01$ , \*\*\* =  $P \leq 0.001$ , \*\*\*\* =  $P \leq 0.0001$ ). Only statistically significant

experimental values compared to the HAE control are reported. All graphical error bars are Standard Error of Means (SEM).

## Results

### BLASTp protein sequence similarity analysis

PfEMP1 proteins consist of an intracellular, transmembrane, and an extracellular region. The extracellular portion of each PfEMP1 can be constructed using any combination of functional domains (CIDR and DBL regions). As malarial research progresses, there has been great progress in pinpointing specific functional groups that bind to human cell surface receptors.

The complete DBL2 $\beta$ 3 domain sequence coded by the PF11 0521 *var* gene served as the BLASTp search query to determine DBL2 $\beta$  segments from other *var* genes that are similar in protein structure (Figure 1A). DBL2 $\beta$ 3<sub>PF11 0521</sub> was selected for its strong ability to bind to ICAM-1. A small subset consisting of the two most similar PfEMP1 proteins to DBL2 $\beta$ 3<sub>PF11 0521</sub> was formed from BLASTp analysis. The first result from BLASTp analysis was a direct match to the DBL2 $\beta$ 3 protein sequence from the PF11 0521 *var* gene. Aligning the sequences produced a query cover of 100%, identical value of 100%, and an E-value of 0.0 (Figure 1B). The second result from BLASTp analysis corresponded to the DBL2 $\beta$ 3 protein sequence from the PFD1235w *var* gene. Aligning this sequence with the original query produced a query cover of 99%, an identical value of 49%, and an E-value of 5e-147 (Figure 1C). The third result from BLASTp analysis corresponded to the DBL2 $\beta$ 6 protein sequence from the PF07 0050 *var* gene. Aligning this sequence with the original query produced a query cover of 93%, an identical value

of 47%, and an E-value of 1e-128 (Figure 1D). The nomenclature used above for DBL2 domains is in accordance with (93).

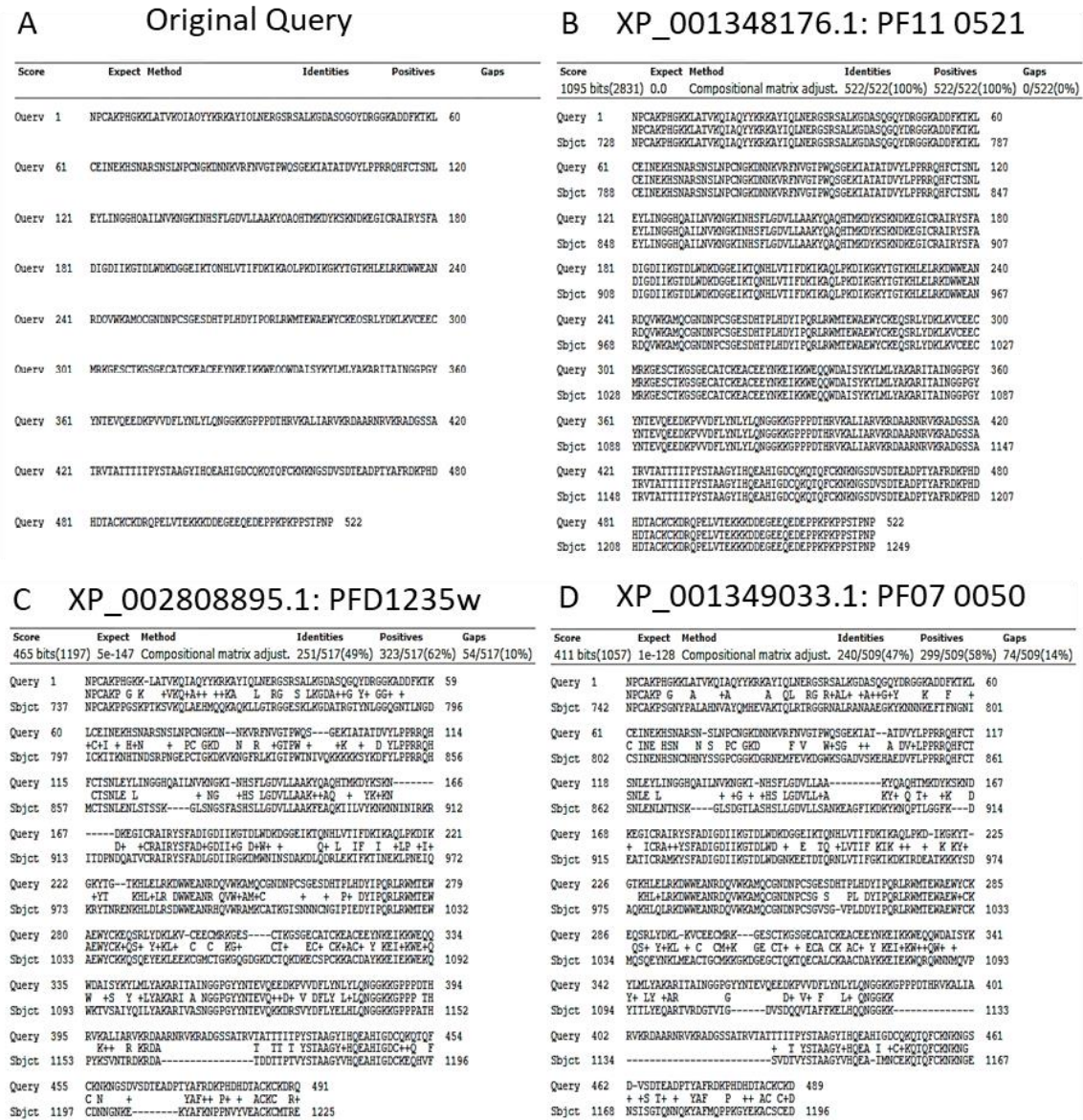


**Figure 1: BLASTp Sequence Alignment for PfEMP1s targeting ICAM-1: A.** The original query consisting of the DBL2β3 protein sequence (amino acids 1-522) from the PF11 0521 gene, which is compared to: **B.** DBL2β3<sub>PF11 0521</sub>, **C.** DBL2β3<sub>PFD1235w</sub>, & **D.** DBL2β6<sub>PF07 0050</sub>. The top line is the original query sequence, the second line lists which amino acids are shared between each sequence, and the third line is the sequence from BLASTp query results.

PF11 0521 and PFD1235w belong to the *var* gene subgroup A, while PF07 0050 belongs to intermediate subgroup B/C (Table 1). Group A genes are located near the telomere and transcription proceeds toward the telomere. Group B/C genes share qualities with both the subclass B and C genes (58).

Gene	NCBI Reference Sequence	Classification Group	Query Cover	E value	Identical	Experimental Construct
PF11 0521	XP_001348176.1	A	100%	0.0	100%	DBL2β3 PF11 0521
PFD1235w	XP_002808895.1	A	99%	5e-147	49%	DBL2β3 PFD1235w
PF07 0050	XP_001349033.1	B/C	93%	1e-128	47%	DBL2β6 PF07 0050

**Table 1: Summary of DBL2β BLASTp Sequence Analysis.** The DBL2β3 protein sequence from the PF11 0521 *var* gene was used as the original query. Genes showing the most sequence similarity, determined by E-values closest to zero, were chosen for further analysis.

Sequence similarities to DBL2β3<sub>PF11 0521</sub> do not determine ICAM-1 binding

HisAdEx (HAE, control), DBL2β6<sub>PF07 0050</sub>, DBL2β3<sub>PFD1235w</sub>, and DBL2β3<sub>PF11 0521</sub> coated Bio-Plex beads, pre-incubated with PBS, showed mean fluorescent intensity (MFI) values of bound ICAM-1 to be  $308 \pm 11.56$ ,  $39.25 \pm 0.43$ ,  $37.38 \pm 2.70$ , and  $4931.63 \pm 105.37$  respectively. Control, DBL2β6<sub>PF07 0050</sub>, DBL2β3<sub>PFD1235w</sub>, and DBL2β3<sub>PF11 0521</sub> coated Bio-Plex beads, pre-incubated with anti-ICAM-1 antibodies, showed MFI values of  $318.40 \pm 8.83$ ,  $39.00 \pm 1.22$ ,  $35.25 \pm 1.16$ , and  $68.75 \pm 4.81$  respectively. Control, DBL2β6<sub>PF07 0050</sub>, DBL2β3<sub>PFD1235w</sub>, and DBL2β3<sub>PF11 0521</sub> coated Bio-Plex beads, pre-incubated with anti-CD36 antibodies, showed MFI values of  $301.3 \pm 10.90$ ,  $37.25 \pm 1.03$ ,  $38.88 \pm 1.16$ , and  $4229 \pm 135.46$  respectively (Figure 2A).

DBL2 $\beta$ 3<sub>PF11 0521</sub> was the only domain with a statistically significant amount of bound ICAM-1 detected compared to the control ( $p \leq 0.0001$ , Figure 2B).

Since no bound ICAM-1 was found attached to DBL2 $\beta$ 6<sub>PF07 0050</sub> and DBL2 $\beta$ 3<sub>PF01235w</sub>, the beads that those domains were attached to were checked for functionality. When the beads in question were coated with DBL2 $\beta$ 3<sub>PF11 0521</sub> instead of the other domains, there was comparable bound ICAM-1 to the results reported in Figure 2A for DBL2 $\beta$ 3<sub>PF11 0521</sub> (Data not shown). Therefore, the bead regions were ruled out as a contributor to ICAM-1 not binding to DBL2 $\beta$ 6<sub>PF07 0050</sub> and DBL2 $\beta$ 3<sub>PF01235w</sub>. When adjusted for the control, pre-incubation with anti-CD36 reduced binding to DBL2 $\beta$ 3<sub>PF11 0521</sub> by 15.05%, while pre-incubation with anti-ICAM-1 antibody reduced binding by 100%, which was a statistically significant reduction ( $P \leq 0.0001$ , Figure 2C).



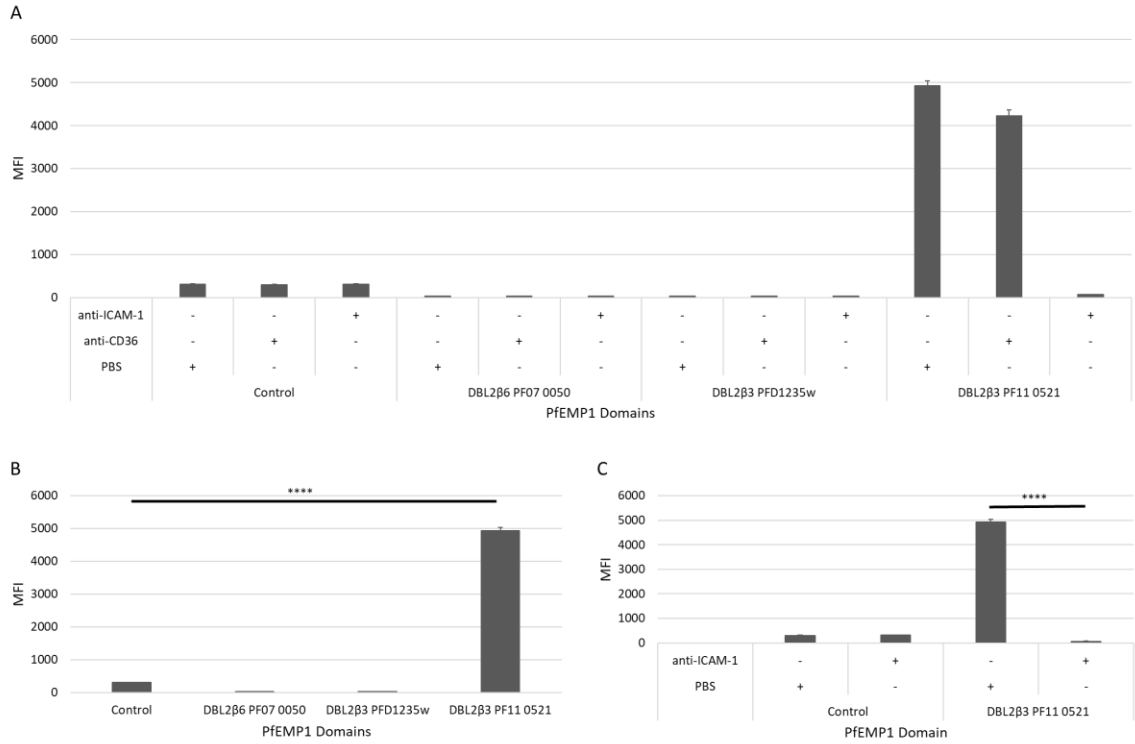


**Figure 2. ICAM-1 Bound to PfEMP1 Domains:** **A.** ICAM-1 bound to HisAdEx (control), DBL2β6<sub>PF07 0050</sub>, DBL2β3<sub>PFD1235w</sub>, and DBL2β3<sub>PF11 0521</sub> following pre-incubation with PBS, 2 μg/ml anti-CD36 monoclonal antibody, or 2 μg/ml anti-ICAM-1 monoclonal antibody. **B.** ICAM-1 bound to control, DBL2β6<sub>PF07 0050</sub>, DBL2β3<sub>PFD1235w</sub>, DBL2β3<sub>PF11 0521</sub> following pre-incubation with PBS. **C.** ICAM-1 bound to DBL2β3<sub>PF11 0521</sub> following pre-incubation with PBS, anti-CD36, or anti-ICAM-1 compared to control pre-incubated with PBS. Error bars are SEM. Asterisks indicate P-value from Student *t* test. \*\*\*\* =  $P \leq 0.0001$ .

*Equilibrium constant ( $K_D$ ): ICAM-1 has strong avidity toward DBL2β3<sub>PF11 0521</sub>*

Bio-Plex analysis demonstrated that there was a statistically significant amount of bound ICAM-1 to DBL2β3<sub>PF11 0521</sub> and no bound ICAM-1 to both DBL2β6<sub>PF07 0050</sub> and DBL2β3<sub>PFD1235w</sub>, when compared to the control (Figure 2A). Therefore, DBL2β6<sub>PF07 0050</sub> and DBL2β3<sub>PFD1235w</sub> were not included in future experiments. Interacting 3.0μg/ml of ICAM-1 with DBL2β3<sub>PF11 0521</sub> coated beads resulted in an average inverse velocity of  $0.017 \pm 0.002$ , 1.0μg/ml resulted in an average inverse velocity of  $0.062 \pm 0.023$ , and

0.3 $\mu$ g/ml resulted in an average inverse velocity of  $0.075 \pm 0.016$ . The inverse velocities ( $1/V = \Delta\text{Time}/\Delta\text{MFI}$ ) were plotted against their corresponding inverse concentrations ( $1/C$ ) on a Lineweaver-Burk double reciprocal plot. When you form a line of best fit to the points, the x-intercept equals  $1/K_D$  and resulted in an ICAM-1  $K_D$  of 7.62nM, specific to the DBL2 $\beta$ 3<sub>PF11 0521</sub> protein (Figure 3).

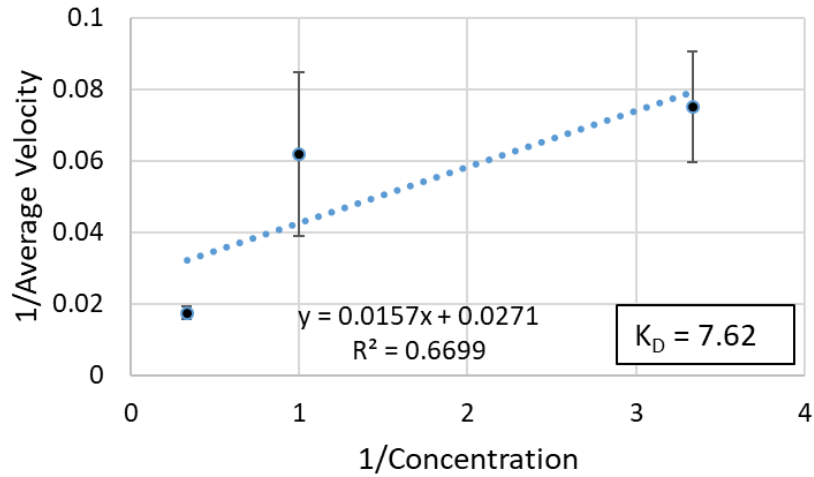


**Figure 3. Avidity of ICAM-1 for DBL2 $\beta$ 3<sub>PF11 0521</sub>:** The inverse of the ICAM-1 concentrations (3.0 $\mu$ g/ml, 1.0 $\mu$ g/ml, 0.3 $\mu$ g/ml) on the x-axis and the inverse of the average velocities on the y-axis.  $K_D$  value is derived where the x-intercept =  $1/K_D$ . Error bars are SEM.

Control beads ligated ICAM-1 on THP-1 cells more than DBL2 $\beta$ 3<sub>PF11 0521</sub> coated beads

The previous sections have shown that recombinant ICAM-1 binds strongly to DBL2 $\beta$ 3<sub>PF11 0521</sub>. To determine if this direct-binding ability translates to ability to ligate to ICAM-1 on monocyte-like THP-1 cells, HAE (control) and DBL2 $\beta$ 3<sub>PF11 0521</sub> coated beads were incubated with monocyte-like THP-1 cells. The percentage of control beads ligated by THP-1 cells when pre-incubated with PBS was  $18.51 \pm 0.02\%$ , with anti-CD36 was  $14.27 \pm 0.45\%$ , and with anti-ICAM-1 was  $14.14 \pm 0.02\%$  (Figure 4A). The percentage

of DBL2 $\beta$ 3<sub>PF11 0521</sub> coated beads ligated by THP-1 cells when pre-incubated with PBS was  $6.98 \pm 2.81\%$ , with anti-CD36 was  $7.51 \pm 0.23\%$ , and with anti-ICAM-1 was  $8.50 \pm 1.27\%$  (Figure 4B). Therefore, the control beads showed a better ability to ligate ICAM-1 on THP-1 cells than DBL2 $\beta$ 3<sub>PF11 0521</sub> coated beads.

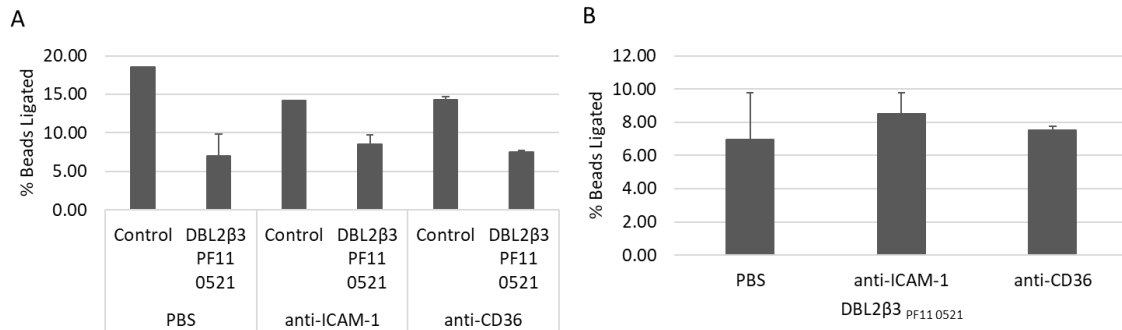


**Figure 4. Percentage of DBL2 $\beta$ 3<sub>PF11 0521</sub> coated beads ligated by THP-1:** **A.** The percentage of control and DBL2 $\beta$ 3<sub>PF11 0521</sub> coated beads ligated by ICAM-1 on THP-1 cells pre-incubated with PBS, anti-ICAM-1 antibody, and anti-CD36 antibody. **B.** The percentage of DBL2 $\beta$ 3<sub>PF11 0521</sub> coated beads ligated by ICAM-1 on THP-1 cells pre-incubated with PBS, anti-ICAM-1 antibody, and anti-CD36 antibody. Error bars are SEM.

#### THP-1 cell ligation to DBL2 $\beta$ 3<sub>PF11 0521</sub> produces anti-inflammatory effects

THP-1 cells were incubated for 0, 12, and 24 hours in a 48 well plate with empty wells, HAE (control) surface-immobilized wells, and DBL2 $\beta$ 3<sub>PF11 0521</sub> surface-immobilized wells. The supernatants were collected and tested for the production of IL-1 $\alpha$ , IL-1 $\beta$ , IL-2, IL-6, IL-8, IL-10, IL-12 (p40), IL-12 (p70), IL-13, IL-19, IL-20, IL-22, IL-26, IL-27, IL28 $\alpha$ , IL29, IFN- $\gamma$ , MCP-1, MIP-1 $\alpha$ , and TNF- $\alpha$ . Only detected cytokines and statistically significant reductions or increases in the production of cytokines were reported.

THP-1 cells incubated in DBL2 $\beta$ 3<sub>PF11 0521</sub> coated wells for 12 hours produced more IL-1ra (7494.56  $\pm$  60.92 pg/ml) than THP-1 cells alone (2903.33  $\pm$  133.28 pg/ml) and significantly more than the control incubated THP-1 cells (4850.39  $\pm$  256.30 pg/ml,  $P \leq 0.05$ , Figure 5A). THP-1 cells incubated for 24 hours in DBL2 $\beta$ 3<sub>PF11 0521</sub> coated wells produced 5.84  $\pm$  0.42 pg/ml of IL-1 $\beta$ , which was less than the THP-1 cells alone (9.74  $\pm$  0.36 pg/ml) and significantly less than the control incubated THP-1 cells (13.89  $\pm$  0.38 pg/ml,  $P \leq 0.05$ , Figure 5B). THP-1 cells incubated for 24 hours in DBL2 $\beta$ 3<sub>PF11 0521</sub> coated wells produced 182.58  $\pm$  1.05 pg/ml of IL-8, which was less than the THP-1 cells alone (636.73  $\pm$  36.09 pg/ml) and significantly less than the control incubated THP-1 cells (290.85  $\pm$  4.45 pg/ml,  $P \leq 0.05$ , Figure 5C).

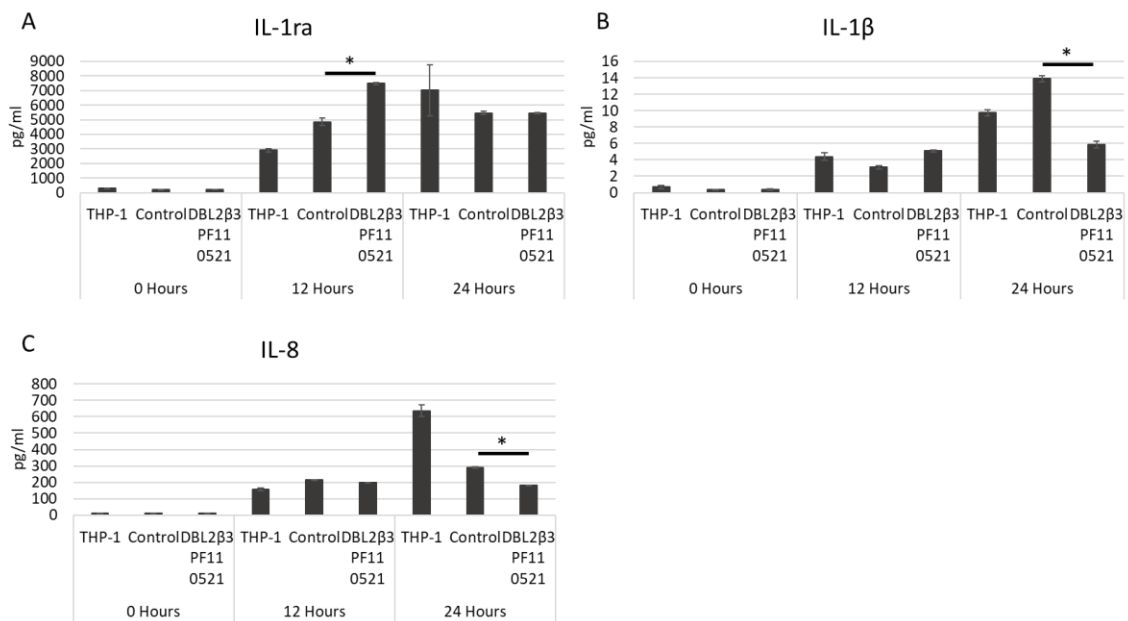


**Figure 5. Cytokine/Chemokine production from ICAM-1::DBL2 $\beta$ 3<sub>PF11 0521</sub> ligation:** The amount of A. IL-1ra, B. IL-1 $\beta$ , C. IL-8 produced after 0, 12, 24 hours of incubation in empty, HAE coated, or DBL2 $\beta$ 3<sub>PF11 0521</sub> coated wells. All samples were analyzed with a one-way ANOVA followed by a two-tailed T. Test with two sample equal variance and a 95% confidence (\* =  $P \leq 0.05$ ). Error bars are SEM.

## Discussion

Historically, ICAM-1 has been described as a simple adhesion molecule; however, “simple” does not adequately describe its role, which includes complex crosslinking for platelet aggregation (42), tight adhesion for leukocyte extravasation (43, 44), and recognition of PfEMP1 proteins for *Plasmodium falciparum* infected red blood cell (iRBC) sequestration (52).

In the case of malaria sequestration, ICAM-1 facilitates iRBC adherence within brain capillaries leading to cerebral malaria syndrome (54). Specifically, of the 5 distinct PfEMP1 DBL region types ( $\alpha$ ,  $\beta$ ,  $\gamma$ ,  $\delta$ ,  $\epsilon$ ), only the DBL $\beta$  region bound to ICAM-1 (15). Interestingly, all of the ICAM-1 binding domains belong to the  $\beta$ 3 or  $\beta$ 5 subclasses of the DBL domain (122). Analysis of 16 PfEMP1 proteins from the NF54 parasite line containing the DBL $\beta$  domain determined that only the DBL2 $\beta$ 3<sub>PF11 0521</sub> protein construct binds ICAM-1 strongly (20). Although all domains were designed similarly, the authors noted that false negative results could not be excluded due to potential problems in domain folding.

ICAM-1s ability to facilitate iRBC sequestration to endothelial cells has been studied extensively (54, 60, 61); however, the immune interaction between individual PfEMP1 proteins and ICAM-1 on immune cells has not been studied. Since DBL2 $\beta$ 3<sub>PF11 0521</sub> was previously determined, by our lab, to significantly bind to ICAM-1 compared to other DBL $\beta$  PfEMP1 domains, DBL2 $\beta$ 3<sub>PF11 0521</sub> served as our reference point for our ICAM-1 studies.

In this study, we predicted that protein sequence similarity toward the DBL2 $\beta$ 3<sub>PF11 0521</sub> PfEMP1 protein construct would predict similar ICAM-1 binding strength and avidity. Based on ICAM-1s function in leukocyte extravasation and immune

signaling (51, 55, 56), we predicted that PfEMP1::ICAM-1 ligation would induce pro-inflammatory cytokine/chemokine release by monocyte-like THP-1 cells.

The complete DBL2 $\beta$ 3 domain sequence coded by the PF11 0521 *var* gene served as a NIH-BLASTp search query and determined the DBL2 $\beta$ 3<sub>PF11 0521</sub> (E-value = 5e-147) and DBL2 $\beta$ 6<sub>PF07 0050</sub> (E-value = 1e-128) PfEMP1 proteins to be the most closely related (Table 1). Previous studies noted that some PfEMP1 proteins derived from Group A *var* genes bind to ICAM-1 (59); however, of the two Group A PfEMP1 proteins tested only DBL2 $\beta$ 3<sub>PF11 0521</sub> bound to ICAM-1, while DBL2 $\beta$ 3<sub>PF11 0521</sub> did not bind to ICAM-1. Of the ICAM-1 binding DBL $\beta$  subclasses ( $\beta$ 1 (rare),  $\beta$ 3, and  $\beta$ 5), both DBL2 $\beta$ 3<sub>PF11 0521</sub> and DBL2 $\beta$ 3<sub>PF11 0521</sub> belong to the ICAM-1 binding  $\beta$ 3 subclass (93). Other groups have confirmed this distinction showing that the DBL $\beta$  domain coded by PFD1235w was able to bind to ICAM-1 (122). It is possible that the same domain in our hands was not active in ICAM-1 binding due to problems with folding (20).

The intermediate subgroup B/C PfEMP1 protein DBL2 $\beta$ 6<sub>PF07 0050</sub> also did not show an ability to bind to ICAM-1, compared to the control. DBL2 $\beta$ 6<sub>PF07 0050</sub> belongs to the  $\beta$ 6 subclass, which is classified as a non-ICAM-1 binding subclass (93). Thus, our results with DBL2 $\beta$ 6<sub>PF07 0050</sub> confirms this binding classification. DBL2 $\beta$ 6<sub>PF07 0050</sub> and DBL2 $\beta$ 3<sub>PF11 0521</sub> were not included in future experiments. Contrary to our predicted hypothesis, sequence similarity, in general, did not translate into ability to bind to ICAM-1. Since a single mutation in a conserved Glutamate-34 region within ICAM-1 can inhibit ICAM-1::LFA-1 ligation (62), it is believed that conserved and semi-conserved residues can determine the binding site for ICAM-1 on PfEMP1 proteins, thus rendering comparisons to the overall protein sequence unable to be a future predictor of ICAM-1

binding. Similarly, belonging to a known binding subclass does not necessarily mean that the domain will bind, which appears to depend more on the specifics of the structure (20, 122). Future data on more ICAM-1 binding domains will further justify this notion or provide a better prediction of binding.

The MFI of fluorescently labeled ICAM-1 bound to DBL2 $\beta$ 3<sub>PF11 0521</sub> was statistically significant compared to the control ( $P \leq 0.0001$ , Figure 2B). Further, we found a statistically significant 100% reduction in ICAM-1 binding to DBL2 $\beta$ 3<sub>PF11 0521</sub> after pre-incubation with anti-ICAM-1 antibody ( $P \leq 0.0001$ , Figure 2C), compared to only 15% reduction after pre-incubation with anti-CD36 antibody, demonstrating the specific nature of the ICAM-1::DBL2 $\beta$ 3<sub>PF11 0521</sub> interaction. In related studies, the specific PfEMP1::ICAM-1 interaction implicated in endothelial cell sequestration of iRBCs was also inhibited and, in this case, reversed using anti-ICAM-1 monoclonal antibodies, though reversal of binding was incomplete and varied in its efficiency between parasite isolates (63). The reversal behavior is similar to natural anti-DBL2 $\beta$ 3<sub>PF11 0521</sub> antibodies in adults that strongly inhibit, but poorly reverse binding to ICAM-1 (20).

The avidity of the specific ICAM-1::DBL2 $\beta$ 3<sub>PF11 0521</sub> interaction was determined by calculating the equilibrium constant ( $K_D$ ) of ICAM-1 toward DBL2 $\beta$ 3<sub>PF11 0521</sub>. The  $K_D$  of ICAM-1 toward the DBL2 $\beta$ 3<sub>PF11 0521</sub> protein was found to be 7.62nM. A 7.62nM concentration of ICAM-1 is very low and signifies a strong avidity of ICAM-1 toward the DBL2 $\beta$ 3<sub>PF11 0521</sub> domain. The calculated  $K_D$  value is very close to the range of 2.3-2.6nM, which was previously reported by our lab for the same interaction (21). More recently, another group determined a  $K_D$  of 3.2nM for the same DBL2 $\beta$ 3<sub>PF11 0521</sub> domain expressed

in similar boundaries (123). Additionally, the strong avidity of ICAM-1 to PfEMP1 proteins is supported by published results using surface plasmon resonance analysis that determined the  $K_D$  of ICAM-1 to the IT4VAR13 PfEMP1 protein was 2.8nM (124). For an avidity strength comparison, it is reported that the  $K_D$  of ICAM-1 towards its LFA-1 ligand is 133nM (64); therefore, DBL2 $\beta$ <sub>PF11 0521</sub> binding to ICAM-1 requires 16 times less ICAM-1 to reach equilibrium, compared to LFA-1 binding.

Since we wanted to determine the immune response in naïve hosts, those who suffer the highest mortalities, we chose non-stimulated THP-1 cells to simulate a circulating monocyte, which would encounter a PfEMP1-expressing iRBC in the vasculature. Contrary to our stated hypothesis, the strength of binding and avidity of ICAM-1 directly to DBL2 $\beta$ <sub>PF11 0521</sub> did not translate to the ability to induce ligation through ICAM-1 on monocyte-like THP-1 cells. After adjustment for the 0°C ligation control, 18.51%  $\pm$  0.02 of control beads were ligated to THP-1 cells and only 6.98%  $\pm$  2.81 of DBL2 $\beta$ <sub>PF11 0521</sub> coated beads were ligated to THP-1 cells. Therefore, our DBL2 $\beta$ <sub>PF11 0521</sub> coated beads did not ligate to THP-1 cells more than the control beads.

To determine the immune response of ICAM-1::DBL2 $\beta$ <sub>PF11 0521</sub> interaction, THP-1 cells were incubated with and without DBL2 $\beta$ <sub>PF11 0521</sub> ligation through surface-immobilized domains, supernatants were collected, and analyzed for the presence of pro- and anti-inflammatory cytokine/chemokine production. It is worth noting that there was a detected increase in production of cytokines over time from our control THP-1 cells (incubated with PBS), which follows a similar pattern to THP-1 baseline cytokine profiles previously reported when incubated with LPS (133, 134). As we did not test our serum for the presence of LPS, it could not be excluded that our serum lot may introduce



some levels of LPS in the experiments, which could in turn stimulate the production of cytokines. It has been shown that LPS is often present in commercial FBS preparations (135). Additionally, all THP-1 cell cultures were incubated under the same conditions; therefore, an increase in cytokine production from a possible mycoplasma contamination would be visible in all samples. This, actually, provides an opportunity to test how THP-1 cells stimulated to produce cytokines non-specifically (not by malaria-relevant substances), respond to interactions with PfEMP1 domains. In the future, experiments with exclusion of serum, or with serum tested negative for LPS would be performed similarly.

Unlike the published studies in endothelial ICAM-1 interactions that led to a pro-inflammatory response (55, 56), ligation of ICAM-1 on THP-1 cells to the specific PfEMP1 protein DBL2 $\beta$ 3<sub>PF11 0521</sub> displayed an anti-inflammatory response. After 12 hours of incubation with DBL2 $\beta$ 3<sub>PF11 0521</sub>, THP-1 cells produced significantly more of the anti-inflammatory cytokine IL-1ra, compared to production by THP-1 cells alone and the control. Physiologically, IL-1ra binds to the IL-1 receptor (IL-1r) to inhibit IL-1 ligation, which inhibits the activation of transcription factors that tell the cell to produce pro-inflammatory cytokines (65). Blocking the IL-1r will inhibit a pro-inflammatory response from the affected cells. After 24 hours of incubation with DBL2 $\beta$ 3<sub>PF11 0521</sub>, THP-1 cells produced significantly less IL-1 $\beta$  and IL-8. The pro-inflammatory cytokine IL-1 $\beta$  is one of two ligands for the IL-1r, which upon ligation will signal the cell to activate transcription factors to promote the further production of pro-inflammatory cytokines. IL-8, also known as CXCL8, is a chemokine that aids in the recruitment of granulocytes. Upon the arrival of immune cells via chemotaxis from secreted IL-8, the IL-8 molecule

will also stimulate the cells to phagocytose pathogens. Therefore, through direct ICAM-1::DBL2 $\beta$ <sub>PF11 0521</sub> ligation without the participation of co-receptors found on RBCs, THP-1 cells insufficiently produce both IL-1 $\beta$  and IL-8 to mount a pro-inflammatory immune response and increased their production of anti-inflammatory IL-1ra, which could lead to the persistence of malaria infection.

In conclusion, our bead-based model to simulate an iRBC interacting with a circulating innate immune cell proved beneficial for characterizing binding characteristics and immune system consequences from the singular, specific interaction between ICAM-1 and the PfEMP1 protein domain DBL2 $\beta$ <sub>PF11 0521</sub>. Due to the strength in binding ability and avidity of ICAM-1 toward DBL2 $\beta$ <sub>PF11 0521</sub>, targeting the ICAM-1::DBL2 $\beta$ <sub>PF11 0521</sub> interaction may reduce one of the strongest sequestration interactions between a PfEMP1 protein and cell surface receptor. Targeting ICAM-1 directly has proven effective in the laboratory setting, with anti-ICAM-1 monoclonal antibodies successfully inhibiting and partially reversing ICAM-1 mediated iRBC sequestration (63). Unfortunately, antibodies toward ICAM-1 could not serve as a viable physiological treatment because of the systemic consequences that could arise. Since PfEMP1 proteins are of foreign origin, directly targeting the DBL2 $\beta$ <sub>PF11 0521</sub> PfEMP1 protein might be the best option to avoid systemic consequences. It is true that not all iRBCs display the specific DBL2 $\beta$ <sub>PF11 0521</sub> PfEMP1 protein; however, with the unique strength and specific nature of the interaction with ICAM-1, DBL2 $\beta$ <sub>PF11 0521</sub> may be the best available target for inhibiting ICAM-1 mediated sequestration. Additionally, since other PfEMP1 proteins with similar protein sequences did not bind to ICAM-1, the importance of the complete protein sequence of DBL2 $\beta$ <sub>PF11 0521</sub> in ICAM-1 binding is confirmed. Further,

the importance of the complete protein sequence of DBL2 $\beta$ 3<sub>PF11 0521</sub> for ICAM-1 binding is supported by the discovery that only antibodies to the full length DBL2 $\beta$ 3<sub>PF11 0521</sub> construct inhibit ICAM-1 interaction, compared to antibodies targeting truncated portions of DBL2 $\beta$ 3<sub>PF11 0521</sub> (21). Successfully blocking DBL2 $\beta$ 3<sub>PF11 0521</sub> from interacting with ICAM-1 might inhibit the ability of relevant iRBC to sequester, allowing the spleen to efficiently remove the circulating iRBCs, thus avoiding SM complications and death. In addition, instead of specific antibodies, small molecules targeting the PfEMP1::ICAM-1 interaction of geographically unrelated heterologous strains might prove to be more useful in reducing sequestration of iRBC to endothelial cells (125); however, the small molecules effect on iRBC::monocyte interaction and consequences should be studied further. Not to be ignored, iRBCs can change their expressed PfEMP1 protein at any point; therefore, targeting a single PfEMP1 protein may not be effective; however, with the discovery of other strong PfEMP1::receptor interactions, similar to those addressed in the following chapters, a combination strategy targeting the strongest interacting PfEMP1 proteins could prove to be a very effective and comprehensive immune-modulatory treatment strategy.

### CHAPTER III: INTEGRIN $\alpha$ V $\beta$ 3 STUDIES

#### **Abstract**

Integrins are transmembrane receptors consisting of an  $\alpha$ -subunit and  $\beta$ -subunit that play an important role in cell::cell adhesion and signaling. Integrins recognize distinct protein sequence patterns within their associated ligands to facilitate binding. The collagen-binding integrins have a conserved  $\beta$ 1-subunit that attaches at GFOGER regions, laminin-binding integrins have individual  $\alpha$ -subunits with varying affinities for laminin isoforms, fibrinogen-binding integrins recognized fibrinogen through KRLDGS sequences, and integrins recognize ICAM-1 by a conserved Glutamate-34 region. Collagen and laminin can also be recognized by a conserved RGD sequence. Remarkably, malaria has incorporated RGD sequences in some PfEMP1 proteins to potentially prolong parasite exposure via integrin-mediated iRBC sequestration to endothelial cells. Interestingly, the immune consequences of PfEMP1::integrin interaction have not been extensively researched. In this study, we examine if the presence of a RGD sequence has an effect on integrin binding. Additionally, we examine if PfEMP1::integrin ligation will induce cytokine/chemokine release by monocyte-like THP-1 cells. Of the PfEMP1 proteins tested, only the PfEMP1 proteins containing a RGD motif were able to bind to integrin  $\alpha$ V $\beta$ 3. Incubation of beads coated with strong integrin  $\alpha$ V $\beta$ 3-binding DBL2 $\delta$ <sub>PFL 2665c</sub> PfEMP1 protein did not lead to a significant increase in ligation by THP-1 cells

compared to control beads, while cell ligation to surface-immobilized DBL2 $\delta$ <sub>PFL 2665c</sub> produced mainly anti-inflammatory effects.

## Introduction

Integrins are transmembrane receptors that play an important role in adhering the extracellular matrix (ECM) to the cytoskeleton of a cell and in cell::cell adhesion and signaling in blood cells. Integrins are heterodimers made of two glycoprotein subunits: one  $\alpha$ -subunit and one  $\beta$ -subunit. As cell signaling facilitators, integrins participate as bidirectional signalers. Integrins can participate in outside-in signaling by ligation to one of many corresponding external ligands and integrins can also participate in inside-out signaling by inducing cytoskeleton proteins talin and kindlin to associate with the cytoplasmic tail of the  $\beta$ -subunit, thus activating the typical external ligand-binding function (66, 67, 68). There is great variation in integrin construction and function, since there are 18  $\alpha$ -subunits and 8  $\beta$ -subunits contributing to 24 heterodimers found in humans (69). As a result of the variation in subunit construction, integrins can bind to numerous ligands.

The common direct ligands in integrin-mediated ECM adhesion are collagen, laminin, and fibrinogen, while the common indirect ligands in integrin-mediated ECM adhesion are fibronectin and vitronectin (70). Attachment of the ECM found outside of the cell, to the cytoskeleton within the cell, is important for ontogenesis. The ECM acts as the cell's framework and stores growth factors and cytokines, while collagen forms the connective tissue between the ECM and cytoskeleton (71, 72). Collagen::integrin interactions also commonly occur during wound healing. Interestingly, all of the collagen-binding integrins contain various  $\alpha$ -subunits dimerized with a conserved  $\beta$ 1-

subunit. More specifically, integrins  $\alpha 1\beta 1$ ,  $\alpha 2\beta 1$ ,  $\alpha 10\beta 1$ , and  $\alpha 11\beta 1$  bind to glycine-phenylalanine-hydroxyproline-glycine-glutamate-arginine (GFOGER) regions found within the triple helical collagen peptide (73, 74).

Similar to the conserved  $\beta 1$ -subunit having an affinity towards collagen, the  $\alpha$ -subunit determines the integrins specificity towards different laminin isoforms (75). Laminins are made up of five  $\alpha$ , three  $\beta$ , and three  $\gamma$ -subunits. Integrin  $\alpha 3\beta 1$  and  $\alpha 6\beta 4$  bind to laminin isoforms with  $\alpha 3$  and  $\alpha 5$  subunits,  $\alpha 6\beta 1$  binds to all laminin isoforms, and  $\alpha 7\beta 1$  binds to isoforms with  $\alpha 2$  and  $\alpha 5$  subunits (76). Laminins are primarily found in the basal lamina, which combines with connective tissue containing collagen, to create the basement membrane. The basement membrane is the ECM of tissues that forms a barrier between internal and external body surfaces, including the epithelial lining of the skin and respiratory/gastrointestinal tracts.

The before mentioned ligands for ICAM-1, LFA-1 and Mac-1 are also named integrin  $\alpha L\beta 2$  and integrin  $\alpha M\beta 2$ , respectively. Mac-1 binds to fibrinogen via a lysine-arginine-leucine-aspartate-glycine-serine (KRLDGS) sequence and the  $\beta 2$ -subunit of LFA-1 requires a conserved Glutamate-34 region within ICAM-1 for adhesion (44, 62). Integrin  $\alpha IIa\beta 3$  also binds fibrinogen during the cellular phase of coagulation. Integrin interactions contributing to leukocyte migration was reviewed in the previous chapter, Chapter II: ICAM-1 Studies.

An extensively studied arginine-glycine-aspartic acid (RGD) sequence that is recognized by many integrins was first discovered in fibronectin in 1984 (77, 78). Crystal structures of integrin  $\alpha IIb\beta 3$  and  $\alpha V\beta 3$  bound to RGD-containing ligands determined that the RGD motif binds at the interface between the integrin  $\alpha$  and  $\beta$ -subunits (79, 80). It is

possible that variations in the  $\alpha/\beta$ -subunit interface can contribute to varying affinities for RGD-containing ligands (81). Since 1984, the RGD sequence has been discovered in integrin ligands vitronectin, collagen, and laminin, which can be recognized by integrin  $\alpha V\beta 3$ ,  $\alpha 5\beta 1$ , and  $\alpha IIb\beta 3$  (82). In-direct integrin binding ligands, fibronectin and vitronectin, form the link between collagens and integrins on the cell surface. Through RGD recognition, plasma fibronectin finds its way into damaged tissue to form a provisional matrix that is later replaced by cellular fibronectin during wound healing (83). Vitronectin anchors to collagen within the ECM to act as an adhesion facilitator for integrin expressing cells. Overall, cell::extracellular matrix adhesion, directly or indirectly via integrin, activates signal transduction pathways that lead to cell growth, cell division, cell survival/apoptosis, and differentiation (70).

Remarkably, viruses have also incorporated an RGD sequence in their viral envelope to interact with RGD recognizing integrins. Therefore, integrins can serve as entry receptors for viruses (84). The human papillomavirus-16 (HPV-16) is inhibited from entering human adult keratinocytes by inhibiting the function of RGD recognizing integrins (85). Similarly, the glycoprotein H portion of the herpes simplex virus type 2 (HSV-2), containing an RGD motif, is recognized by integrin  $\alpha V\beta 3$ , which facilitates HSV-2 entry into human genital tract epithelial cells (86). Non-enveloped adenoviruses are also able to gain cellular entry through integrins recognizing a RGD sequence found in the adenovirus's penton subunits (87). Whether naturally occurring or developed to survive, a virus's ability to exploit integrin's specific affinity for RGD motifs has proven effective for the persistence of disease.

Integrins are found on the surface of almost every type of cell, including on cells found in the brain. Recognition of the RGD motif can be exploited in microvascular cells found in the brain, if the pathogen can cross the blood brain barrier (BBB). Viruses do not cross the BBB, but instead infect the surrounding brain parenchyma. However, malaria can infiltrate brain microvasculature through the bloodstream. Once the iRBCs enter the brain they will sequester in the microvasculature, causing blockage that can lead to coma, stroke, and death. Under continuous flow, *in vitro*, iRBC adhere to HDMEC at least 7-fold greater than uninfected red blood cells (RBC). Additionally, inhibition of integrin  $\alpha V\beta 3$  on HDMEC by anti-integrin  $\alpha V$  antibodies was able to decrease the ability of iRBC to sequester by 45% (89).

Integrin  $\alpha V\beta 3$  is also found on immune cells, including monocyte-like THP-1 cells (57). Integrin  $\alpha V\beta 3$ , along with ICAM-1, facilitates monocyte transmigration through the endothelium (90). Additionally, integrin  $\alpha V\beta 3$  on macrophage can recognize RGD sequences on apoptotic cells to facilitate phagocytosis and cell-mediated cytotoxicity (91, 92). However, the immune interaction between PfEMP1 proteins and integrin  $\alpha V\beta 3$  on immune cells has not been studied extensively.

Out of all possible PfEMP1 proteins in the 3D7 clone of malaria, 23 contain RGD motifs (93). Therefore, malaria could be designating almost 30% of its PfEMP1 protein repertoire to integrin binding, possibly through integrin  $\alpha V\beta 3$ . Interestingly, only 1 of the 23 PfEMP1 domains reported contains two RGD sequences, DBL2 $\delta_{PFL\ 2665c}$ . Since DBL2 $\delta_{PFL\ 2665c}$  possesses two RGD motifs and, thus, two possible integrin binding sites, DBL2 $\delta_{PFL\ 2665c}$  serves as our reference point for our integrin  $\alpha V\beta 3$  studies.



In this study, we determine if protein sequence similarity toward the DBL2 $\delta_{\text{PFL 2665c}}$  protein construct and/or presence of a RGD sequence motif plays a role in integrin  $\alpha\text{V}\beta 3$  binding strength and avidity using PfEMP1-coated Bio-Plex beads. Additionally, we determine if DBL2 $\delta_{\text{PFL 2665c}}$ ::integrin  $\alpha\text{V}\beta 3$  ligation will induce cytokine/chemokine release by monocyte-like THP-1 cells. We hypothesize that sequence similarity will be less important compared to possessing a RGD motif on ability to bind to Integrin  $\alpha\text{V}\beta 3$ . Based on integrin  $\alpha\text{V}\beta 3$ 's role in adhesion and facilitation of phagocytosis, it is predicted that ligation through Integrin  $\alpha\text{V}\beta 3$  will induce the production of inflammatory cytokines/chemokines by THP-1 cells.

## **Materials and Methods**

### **THP-1 Culture**

THP-1 cells, kindly provided by Dr. Yoshimi Shibata from Florida Atlantic University, were cultured in RPMI 1640 growth medium, supplemented with 25 $\mu\text{g/ml}$  gentamicin sulfate, 0.125 $\mu\text{g/ml}$  Amphotericin B, and 10% heat-inactivated FBS. The cells were cultured below 5X10<sup>5</sup> cells/ml in order to maintain an unstimulated, nonadherent monocyte population to simulate naïve host immune cells for cytokine analysis.

For interaction with surface-immobilized PfEMP1 proteins, THP-1 cells were incubated with Goat IgG (Jackson Laboratories, Cat# 005-000-002) to block the cells from interacting with our PfEMP1 capture antibody, Goat anti-GFP (Rockland, Cat# 600-101-215). Antibiotic and anti-fungal additives were withheld from the media for all experiments requiring binding.

### Plasmids coding for PfEMP1 domains

PfEMP1 plasmids were created previously using the methods described in (120). Briefly, all PfEMP1 domains were cloned into the pHisAdEx vector, expressed by COS-7 cells, harvested, and immobilized on either COOH Bio-Plex beads (BioRad, Cat# 1715060##) or wells of a 48 well plate. Immobilization steps are mentioned in subsequent corresponding sections below. The pHisAdEx vector without inserted malarial DNA was used as the control in all PfEMP1 experiments. This plasmid contains a 54kDA malaria-irrelevant protein fragment that is a part of all PfEMP1 domain-containing constructs and thus is a perfect control for all recombinant PfEMP1 domains tested.

### PfEMP1 Protein sequence similarity analysis

The National Institute of Health's (NIH) Basic local Alignment Search Tool (BLAST) was used to compare known PfEMP1 protein sequences to determine related PfEMP1 proteins. Query searches were conducted using the non-redundant protein sequence database, BLASTp (protein-protein BLAST) algorithm, and *Plasmodium falciparum* isolate 3D7 (taxid: 36329) as the organism. Search results are organized by query cover, percent identical, and expected value (E-value). Query cover refers to the percentage of the original query sequence that can be compared to the sequences from the results. Percent identical refers to the percentage of identical amino acids in the same location between the original query sequence and the sequences from the results. The E-value was the measurement of how many times, by chance, in a given search the exact same sequence will exist. Therefore, as E-values approach zero, the results are more

likely to be specific to the sequence searched. Related proteins were determined by how close their E-value was to zero. The protein sequence from the PfEMP1 construct DBL2 $\delta$ <sub>PFL 2665c</sub>, shown to react to integrin  $\alpha$ V $\beta$ 3, was used as our initial BLASTp search query.

*Bead-based integrin  $\alpha$ V $\beta$ 3 binding assay and statistical analysis*

HisAdEx (HAE, control), DBL2 $\delta$ <sub>PF10 0406</sub>, DBL2 $\delta$ <sub>PF10 0406</sub>, and DBL2 $\delta$ <sub>PFL 2665c</sub> PfEMP1 proteins were expressed as GFP-fusion proteins by COS-7 cells. COOH Bio-Plex beads of various fluorescence color (bead region) were coated with Goat anti-GFP antibody and incubated with COS-7 cell lysates expressing each individual PfEMP1 domain (one bead region per one domain), overnight at 4°C with rotation. The PfEMP1 coupled beads were washed and stored at -80°C in 1xPBS with 0.1% BSA, 0.02% Tween-20, 0.05% sodium azide, and 15% glycerol until experimentation, but no longer than 1 month. The solution was switched to 1x TBS, 0.05% tween-20, 0.1% BSA Fraction V, 1mM calcium chloride, and 1mM magnesium chloride for binding experiments. Recombinant human integrin  $\alpha$ V $\beta$ 3 (R&D Systems, Cat #3050-AV) was labeled with biotin by incubation with 10mM EZ-Link Sulfo-NHS-LC-Biotin (ThermoFisher Scientific), according to the manufacturer's directions. The biotin-labeled integrin  $\alpha$ V $\beta$ 3 was dialyzed in a Slide-A-Lyzer 10K Dialysis Cassette (ThermoFisher Scientific) in 1x PBS buffer.

To determine binding ability and specificity to integrin  $\alpha$ V $\beta$ 3, 5 $\mu$ g/ml of recombinant integrin  $\alpha$ V $\beta$ 3-Bio was incubated with PBS, 25 $\mu$ g/ml anti- $\beta$ 1 monoclonal antibody (R&D Systems, Cat# MAB17781), 25 $\mu$ g/ml anti-integrin  $\alpha$ V $\beta$ 3 monoclonal

antibody (R&D Systems, Cat# MAB3050), or PfEMP1 coated beads were incubated in 1 $\mu$ g/ml cycloRGDFV inhibitory peptide (RGD-IP, Sigma Aldrich, Cat# SCP0111) for 1 hour with shaking at room temperature. Following pre-incubation with blocking agents, the integrin  $\alpha$ V $\beta$ 3-Bio recombinant proteins were incubated with HAE, DBL2 $\delta$ <sub>PFD 1015c</sub>, DBL2 $\delta$ <sub>PF10 0406</sub>, and DBL2 $\delta$ <sub>PFL 2665c</sub> coated beads for 1 hour with shaking at room temperature. Any unbound integrin  $\alpha$ V $\beta$ 3-Bio was washed out of the system through vacuum filtration and then the beads were incubated with a 1:250 dilution of Streptavidin-Phycoerythrin (SA-PE, Jackson Laboratories Cat# 016-110-084, Inc. Minneapolis, MN.) with shaking at room temperature, to target bound integrin  $\alpha$ V $\beta$ 3 through the biotin label.

Mean fluorescent intensity (MFI) of bound fluorescently-labeled integrin  $\alpha$ V $\beta$ 3-Bio was determined by the Bio-Plex 200 suspension (BioRad) array system using Bio-Plex Manager Software 5.0. All binding experiments were conducted in triplicate and repeated at least once, MFI values were compared for statistical significance to the control by a two-tailed T. Test with two sample equal variance and a 95% confidence interval using both Microsoft Excel and Bio-Plex Manager 5.0 (\* =  $P \leq 0.05$ , \*\* =  $P \leq 0.01$ , \*\*\* =  $P \leq 0.001$ , \*\*\*\* =  $P \leq 0.0001$ ). All graphical error bars are Standard Error of Means (SEM).

#### Bead-based equilibrium constant ( $K_D$ ) analysis

Pre-incubation with SA-PE renders integrin  $\alpha$ V $\beta$ 3-Bio non-functional; therefore, labeling was accomplished after integrin  $\alpha$ V $\beta$ 3 and bead incubation. Various concentrations of recombinant integrin  $\alpha$ V $\beta$ 3-Bio (12.0 $\mu$ g/ml, 6.0 $\mu$ g/ml, and 3.0 $\mu$ g/ml)

were incubated with HAE and DBL2 $\delta$ <sub>PFL 2665c</sub> coated Bio-Plex beads for 0, 5, 10, and 15 minutes. The beads were then incubated with a 1:250 dilution of SA-PE for 15 minutes, to fluorescently label bound integrin  $\alpha$ V $\beta$ 3-Bio. The change in MFI of bound fluorescently labeled integrin  $\alpha$ V $\beta$ 3-Bio was compared to change in time to determine the velocity of binding for 12.0 $\mu$ g/ml, 6.0 $\mu$ g/ml, and 3.0 $\mu$ g/ml of recombinant integrin  $\alpha$ V $\beta$ 3-Bio. The inverse velocities ( $1/V = \Delta\text{Time}/\Delta\text{MFI}$ ) were plotted against their corresponding inverse concentrations ( $1/C$ ) on a Lineweaver-Burk double reciprocal scatter plot. On a Lineweaver-Burk plot, the x-intercept of the linear line of best fit equals  $1/-K_D$ , where  $K_D$  represents the equilibrium dissociation constant. In this case, the equilibrium constant signifies the concentration of integrin  $\alpha$ V $\beta$ 3 where 50% of integrin  $\alpha$ V $\beta$ 3 is bound to DBL2 $\delta$ <sub>PFL 2665c</sub> and 50% of integrin  $\alpha$ V $\beta$ 3 is not bound to DBL2 $\delta$ <sub>PFL 2665c</sub>. Mean fluorescent intensity (MFI) of bound fluorescently-labeled integrin  $\alpha$ V $\beta$ 3-Bio was determined by the Bio-Plex 200 suspension array system using Bio-Plex Manager Software 5.0. All  $K_D$  experiments were plotted using Microsoft Excel and conducted in duplicate with at least one repetition. All graphical error bars are Standard Error of Means (SEM).

#### THP-1: Bead-based ligation analysis and statistical comparison

THP-1 cells were incubated with PBS, 25 $\mu$ g/ml anti- $\beta$ 1 antibody, 25 $\mu$ g/ml anti-integrin  $\alpha$ V $\beta$ 3 antibody, or PfEMP1 coated beads were incubated in 1 $\mu$ g/ml cycloRGDFV inhibitory peptide for 30 minutes at 37°C with shaking. The cells were washed and then incubate with either HAE or DBL2 $\delta$ <sub>PFL 2665c</sub> coated beads, at a 1:20 ratio of Beads:THP-1 cells, for 2 hours with shaking at 0°C and 37°C. The 0°C samples were

used as a ligation control (no phagocytosis taking place) and the results at 0°C were subtracted as background from the 37°C samples. Others have confirmed phagocytosis takes place at 37°C, but not at 0°C by confocal microscopy also using THP-1 cells and PfEMP1-coated fluorescent beads (137). Therefore, reported values adjusted for the control signify ligation and possibly phagocytosis, further analysis is needed to confirm phagocytosis. Using the Attune NXT acoustic focusing flow cytometer (Life Technologies) and associated software, we were able to locate our beads and cells using side scatter (SSC) and front scatter (FSC) characteristics. The beads are smaller and have a more complex internal core than the THP-1 cells. The bead's complex internal core is made up of two fluorescent dyes that can be detected on the BL3 channel of the flow cytometer. To locate our ligated and potentially phagocytosed beads, we gated the THP-1 cells and analyzed the gated region for the BL3 channel. We compared the number of beads (positive signal in BL3) contained within our THP-1 cells to the total amount of beads in the system to determine the percentage of beads ligated/phagocytosed. The percentage of ligated/phagocytosed beads, which reflects the ability of domain-coated beads to be ligated/phagocytosed, were compared for statistical significance to the control by a two-tailed T. Test with two sample equal variance and a 95% confidence interval using both Microsoft Excel and Bio-Plex Manager 5.0 (\* =  $P \leq 0.05$ , \*\* =  $P \leq 0.01$ , \*\*\* =  $P \leq 0.001$ , \*\*\*\* =  $P \leq 0.0001$ ). All ligation experiments were conducted in duplicate and repeated at least once. All graphical error bars are Standard Error of Means (SEM).

*PfEMP1::THP-1 cytokine and chemokine analysis and statistical comparison*

Utilizing the same process as Bio-Plex bead coupling, HAE and DBL2 $\delta$ <sub>PFL 2665c</sub> were immobilized on the surface of a 96-well flat bottom plate through Goat anti-GFP targeted attachment.  $4.0 \times 10^5$  THP-1 cells were added to each well and incubated at 37°C for 0, 12, and 24 hours. The supernatants were collected and analyzed using Bio-Plex Pro Human Cytokine kits (BioRad Cat# 171304090M and Cat# 171-AL003M) testing for the presence of IL-1 $\alpha$ , IL-1 $\beta$ , IL-2, IL-6, IL-8, IL-10, IL-12 (p40), IL-12 (p70), IL-13, IL-19, IL-20, IL-22, IL-26, IL-27, IL28a, IL29, IFN- $\gamma$ , MCP-1, MIP-1 $\alpha$ , and TNF- $\alpha$ . 4 parameter logistic (4PL) or 5 parameter logistic (5PL) standard curves for each cytokine/chemokine were created using the provided standards with the concentration on the x-axis and the MFI on the y-axis. Unknown sample concentrations were determined by fitting the MFI values to the standard curves using the Bio-Plex Manager 5.0 software and confirmed by MyCurveFit online-based application. All samples were analyzed with a one-way ANOVA followed by a two-tailed T. Test with two sample equal variance and a 95% confidence interval using both Microsoft Excel and Bio-Plex Manager 5.0 (\* =  $P \leq 0.05$ , \*\* =  $P \leq 0.01$ , \*\*\* =  $P \leq 0.001$ , \*\*\*\* =  $P \leq 0.0001$ ). Only statistical significant experimental values compared to the HAE control are reported. All graphical error bars are Standard Error of Means (SEM).

#### THP-1::DBL2 $\delta$ <sub>PFL 2665c</sub> global gene expression analysis

Utilizing the same process as Bio-Plex bead coupling, HAE (control) and DBL2 $\delta$ <sub>PFL 2665c</sub> were immobilized on the surface of a 96-well flat bottom plate through Goat anti-GFP targeted attachment. Surface-immobilization restricts the THP-1 cells to ligation triggered cell signaling; therefore, phagocytosis does not take place in this model.

4.0x10<sup>5</sup> THP-1 cells were added to each well and incubated at 37°C for 3 hours. The cells will be seeded in triplicate, three times for HAE and DBL2δ<sub>PFL 2665c</sub>. The cells were gently scraped, collected, and RNA was prepared using the E.Z.N.A. Blood RNA Kit I (Omega Bio-tek, Cat# R6814), following the manufacturer's protocol. The RNA was submitted for high-throughput RNA sequencing (RNA<sub>Seq</sub>) to Novogene Co. Ltd. (Sacramento, CA.). The results were received in Microsoft Excel format by fragments per kilobase million (FPKM).

## Results

### BLASTp protein sequence similarity analysis

The complete DBL2δ domain sequence coded by the PFL 2665c *var* gene served as the BLASTp search query to determine a small subset of DBL2δ containing PfEMP1 proteins from different *var* genes that are similar in overall protein structure (Figure 6A). The first result from BLASTp analysis was a direct match to the DBL2δ protein sequence from the PFL 2665c *var* gene, containing two RGD motifs. Aligning the sequences produced a query cover of 100%, identical value of 100%, and an E-value of 0.0 (Figure 6B). The second result from BLASTp analysis corresponded to the DBL2δ protein sequence from the PF10 0406 *var* gene, not containing an RGD motif. Aligning this sequence with the original query produced a query cover of 98%, an identical value of 43%, and an E-value of 5e-119 (Figure 6C). The third result from BLASTp analysis corresponded to the DBL2δ protein sequence from the PFD 1015c *var* gene, also not containing an RGD motif. Aligning this sequence with the original query produced a query cover of 100%, an identical value of 43%, and an E-value of 1e-102 (Figure 6D).



**Figure 6. BLASTp Sequence Alignment for PfEMP1s targeting Integrin  $\alpha$ V $\beta$ 3:** **A.** The original query consisting of the DBL2 $\delta$  protein sequence (amino acids 1-527) from the PFL 2665c gene compared to: **B.** DBL2 $\delta$ <sub>PFL 2665c</sub>, **C.** DBL2 $\delta$ <sub>PF10 0406</sub>, & **D.** DBL2 $\delta$ <sub>PF10 1015c</sub>. The top line is the original query sequence, the second line lists which amino acids are shared between each sequence, and the third line is the sequence from BLASTp query results.

50

Gene	NCBI Reference Sequence	Classification Group	Query Cover	E value	Identical	Experimental Construct
PFL 2665c	XP_001350935.1	B	100%	0.0	100%	DBL2δ CIDR2β PFL 2665c
PF10 0406	XP_001351517.1	B	98%	5e-119	43%	DBL2δ CIDR2β PF10 0406
PFD 1015c	XP_001351517.1	C	100%	1e-102	43%	DBL2δ CIDR2β PFD 1015c

**Table 2: Summary of DBL2δ BLASTp Sequence Analysis.** The DBL2δ protein sequence from the PFL 2665c *var* gene was used as the original query. Genes showing the most sequence similarity, determined by E-values closest to zero, were chosen for further analysis.

*Overall sequence similarity to DBL2β<sub>PF11 0521</sub> does not determine integrin αVβ3 binding*

HisAdEx (HAE, control), DBL2δ<sub>PFD 1015c</sub>, DBL2δ<sub>PF10 0406</sub>, and DBL2δ<sub>PFL 2665c</sub> coated Bio-Plex beads, pre-incubated with PBS, showed mean fluorescent intensity (MFI) values of bound integrin αVβ3 to be  $475.33 \pm 24.33$ ,  $231.5 \pm 16.23$ ,  $311 \pm 18.45$ , and  $792.5 \pm 83.53$  respectively. Control, DBL2δ<sub>PFD 1015c</sub>, DBL2δ<sub>PF10 0406</sub>, and DBL2δ<sub>PFL 2665c</sub> coated Bio-Plex beads incubated with integrin αVβ3, which was pre-incubated with anti-β1 antibodies, showed MFI values of  $553.17 \pm 13.45$ ,  $326.5 \pm 7.78$ ,  $415.83 \pm 14.42$ , and  $593.33 \pm 44.60$ , respectively. Control, DBL2δ<sub>PFD 1015c</sub>, DBL2δ<sub>PF10 0406</sub>, and DBL2δ<sub>PFL 2665c</sub> coated Bio-Plex beads incubated with integrin αVβ3, which was pre-incubated with anti-αVβ3 antibodies, showed MFI values of  $378.5 \pm 4.33$ ,  $190.17 \pm 6.19$ ,  $219.17 \pm 5.09$ , and  $423.33 \pm 10.58$ , respectively. Control, DBL2δ<sub>PFD 1015c</sub>, DBL2δ<sub>PF10 0406</sub>, and DBL2δ<sub>PFL 2665c</sub> coated Bio-Plex beads, pre-incubated with a RGD inhibitor peptide (RGD-IP), showed MFI values of  $330.17 \pm 9.06$ ,  $153.5 \pm 7.01$ ,  $189.5 \pm 9.37$ , and  $394.67 \pm 6.23$ , respectively (Figure 7A). DBL2δ<sub>PFL 2665c</sub> was the only domain with a statistically significant amount of bound integrin αVβ3 detected compared to the control ( $P \leq 0.05$ ).

Figure 7B). Additionally, pre-incubation with either anti- $\alpha$ V $\beta$ 3 antibody ( $P \leq 0.05$ ) or RGD-IP ( $P \leq 0.01$ ) significantly reduced the amount of bound integrin  $\alpha$ V $\beta$ 3 (Figure 7C).

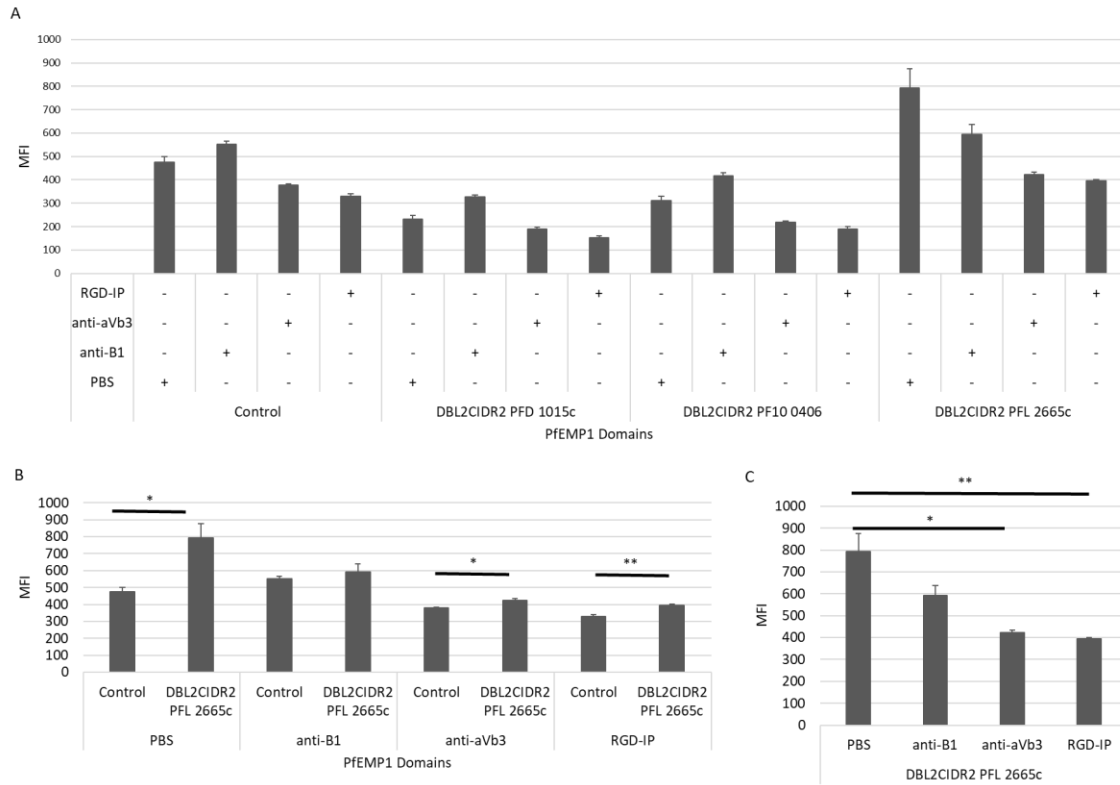


**Figure 7. Integrin  $\alpha$ V $\beta$ 3 Bound to PfEMP1 Domains:** MFI of integrin  $\alpha$ V $\beta$ 3 pre-incubation with PBS, anti-integrin  $\alpha$ V $\beta$ 3 monoclonal antibody, anti- $\beta$ 1 monoclonal antibody, or a RGD inhibitor peptide (RGD-IP) bound to **A.** HAE, DBL2 $\delta$ PFD 1015c, DBL2 $\delta$ PFD 10406, and DBL2 $\delta$ PFL 2665c **B.** HAE and DBL2 $\delta$ PFL 2665c **C.** DBL2 $\delta$ PFL 2665c. Error bars are SEM. Asterisks indicate P-value from T. Test. (\* =  $P \leq 0.05$ , \*\* =  $P \leq 0.01$ , \*\*\* =  $P \leq 0.001$ , \*\*\*\* =  $P \leq 0.0001$ ).

Therefore, compared to the control, there was no binding between integrin  $\alpha$ V $\beta$ 3 and the two PfEMP1 constructs not containing RGD motifs, DBL2 $\delta$ PFD 1015c and DBL2 $\delta$ PFD 10406. The beads that those domains were attached to were checked for functionality. When the beads in question were coated with DBL2 $\delta$ PFL 2665c instead of the other domains, there was comparable amount of bound integrin  $\alpha$ V $\beta$ 3, similar to the

results reported in Figure 9A for DBL2 $\delta$ <sub>PFL 2665c</sub> (Data not shown). Therefore, the beads were ruled out as a contributor to integrin  $\alpha$ V $\beta$ 3 not binding to DBL2 $\delta$ <sub>PFD 1015c</sub> and DBL2 $\delta$ <sub>PF10 0406</sub>. DBL2 $\delta$ <sub>PFD 1015c</sub> and DBL2 $\delta$ <sub>PF10 0406</sub> were not included in future experiments. Therefore, integrin  $\alpha$ V $\beta$ 3 binding ability of DBL2 $\delta$ <sub>PFL 2665c</sub> was compared to other RGD-containing DBL2 $\delta$  PfEMP1 constructs and is addressed in the Chapter III: Integrin Studies Discussion section (16).

*Equilibrium constant ( $K_D$ ): Strong avidity of integrin  $\alpha$ V $\beta$ 3 toward DBL2 $\delta$ <sub>PFL 2665c</sub>*

Bio-Plex analysis demonstrated that there was a statistically significant amount of bound integrin  $\alpha$ V $\beta$ 3 to DBL2 $\delta$ <sub>PFL 2665c</sub>, when compared to the control (Figure 7B). To determine the avidity, via calculated equilibrium constant ( $K_D$ ), of integrin  $\alpha$ V $\beta$ 3 toward DBL2 $\delta$ <sub>PFL 2665c</sub>, the change in MFI of bound integrin  $\alpha$ V $\beta$ 3 was compared to change in time to determine the velocity of binding for 12.0 $\mu$ g/ml, 6.0 $\mu$ g/ml, and 3.0 $\mu$ g/ml of recombinant integrin  $\alpha$ V $\beta$ 3. After plotting the inverse velocities ( $1/V = \Delta\text{Time}/\Delta\text{MFI}$ ) against the corresponding inverse concentrations ( $1/C$ ) on a Lineweaver-Burk double reciprocal plot, the  $K_D$  of integrin  $\alpha$ V $\beta$ 3 toward DBL2 $\delta$ <sub>PFL 2665c</sub> was found to be 62.2nM (Figure 8).

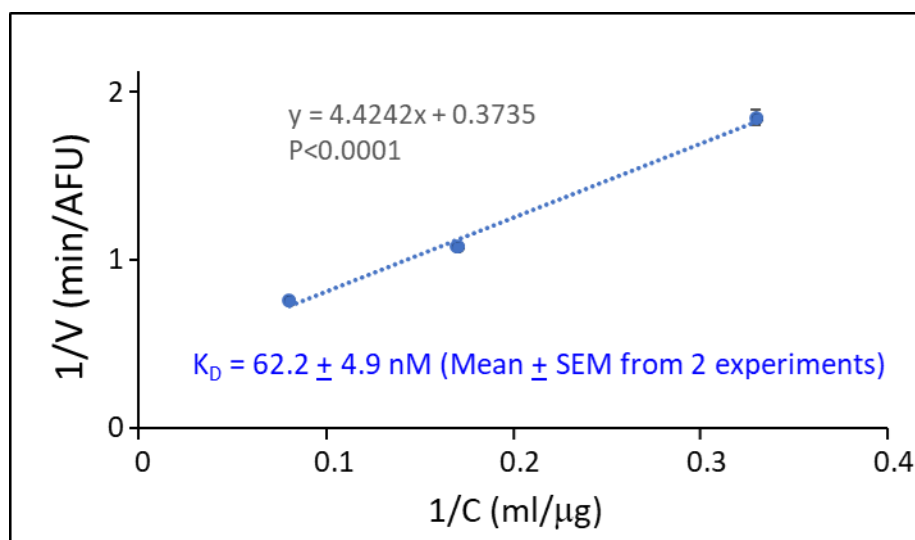


**Figure 8. Avidity of integrin  $\alpha V\beta 3$  for DBL2 $\delta$ PFL 2665c:** The inverse of the integrin  $\alpha V\beta 3$  concentrations (12.0 $\mu$ g/ml, 6.0 $\mu$ g/ml, and 3.0 $\mu$ g/ml) is on the x-axis and the inverse of the average velocities is on the y-axis.  $K_D$  value is derived where the x-intercept =  $1/-K_D$ . Error bars are SEM. Adapted from (16).

#### DBL2 $\delta$ PFL 2665c coated beads ligated integrin $\alpha V\beta 3$ on THP-1 cells

The previous sections have shown that recombinant integrin  $\alpha V\beta 3$  binds strongly to DBL2 $\delta$ PFL 2665c. To determine if this direct-binding ability translates to ability to ligate to integrin  $\alpha V\beta 3$  on monocyte-like THP-1 cells, HAE (control) and DBL2 $\delta$ PFL 2665c coated beads were incubated with monocyte-like THP-1 cells. The percentage of control beads ligated by THP-1 cells when pre-incubated with PBS was 7.94%  $\pm$  1.59, with RGD-IP was 17.13%  $\pm$  2.39, with anti-integrin  $\beta 1$  was 8.17%  $\pm$  0.33, and with anti-integrin  $\alpha V\beta 3$  was 10.46%  $\pm$  1.92 (Figure 9A). The percentage of DBL2 $\delta$ PFL 2665c coated beads ligated by THP-1 cells when pre-incubated with PBS was 10.18%  $\pm$  0.78, with RGD-IP was 7.01%  $\pm$  0.60, with anti-integrin  $\beta 1$  was 5.31%  $\pm$  0.06, and with anti-integrin  $\alpha V\beta 3$  was 8.24%  $\pm$  3.64 (Figure 9B). Although not statistically significant, the DBL2 $\delta$ PFL 2665c coated beads are ligated by THP-1 cells 30% more than the control beads over a 2-hour

period. When adjusted for the control, ligation through the integrin  $\alpha V\beta 3::DBL2\delta_{PFL\ 2665c}$  interaction was 100% inhibited by RGD-IP, anti-integrin  $\beta 1$ , and anti-integrin  $\alpha V\beta 3$ .

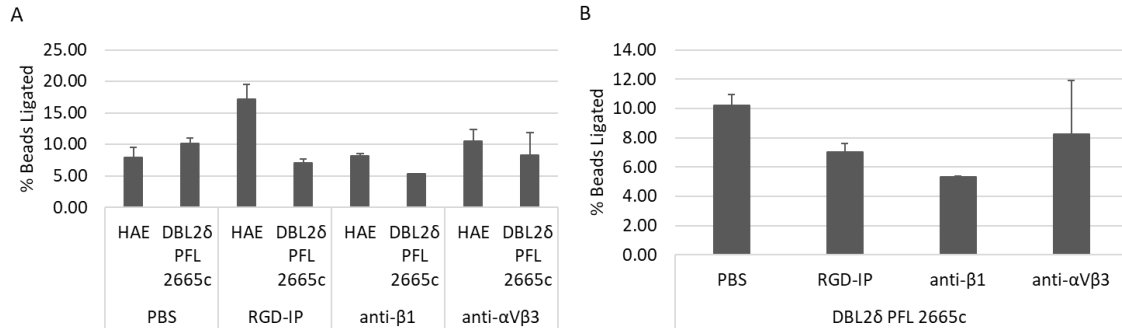


**Figure 9. Percentage of DBL2 $\delta$ PFL 2665c coated beads ligated by THP-1:** **A.** The percentage of control and DBL2 $\delta$ PFL 2665c coated beads ligated by THP-1 cells pre-incubated PBS, anti-integrin  $\alpha V\beta 3$  monoclonal antibody, anti- $\beta 1$  monoclonal antibody, or a RGD inhibitor peptide (RGD-IP). **B.** The percentage of DBL2 $\delta$ PFL 2665c coated beads ligated by THP-1 cells pre-incubated with PBS, anti- $\alpha V\beta 3$ , anti- $\beta 1$ , or RGD-IP. Error bars are SEM.

### THP-1 cell ligation to surface-immobilized DBL2 $\delta$ PFL 2665c produces anti-inflammatory effects

THP-1 cells were incubated for 0, 12, and 24 hours in a 48 well plate with empty wells, HAE (control) surface-immobilized wells, and DBL2 $\beta 3_{PFL11\ 0521}$  surface-immobilized wells. The supernatants were collected and tested for the production of IL-1ra, IL-1 $\beta$ , IL-2, IL-6, IL-8, IL-10, IL-12 (p40), IL-12 (p70), IL-13, IL-19, IL-20, IL-22, IL-26, IL-27, IL28a, IL29, IFN- $\gamma$ , MCP-1, MIP-1 $\alpha$ , and TNF- $\alpha$ . Only detected cytokines and statistically significant reductions or increases in the production of cytokines were reported.

THP-1 cells incubated in DBL2 $\delta$ PFL 2665c coated wells for 12 hours produced more IL-1ra ( $6488.75 \pm 271.83$  pg/ml) than THP-1 cells alone ( $2903.33 \pm 133.28$  pg/ml) and

significantly more than control incubated THP-1 cells ( $4850.39 \pm 256.30$  pg/ml,  $P \leq 0.05$ , Figure 10A). THP-1 cells incubated for 24 hours in DBL2 $\delta$ <sub>PFL 2665c</sub> coated wells produced less IL-1 $\beta$  ( $6.65 \pm 0.39$  pg/ml) than THP-1 cells alone ( $9.74 \pm 0.36$  pg/ml) and significantly less than control incubated THP-1 cells ( $13.89 \pm 0.38$  pg/ml,  $P \leq 0.01$ , Figure 10B). There was also a reduction in IL-8 and MCP-1 after 24 hours; however, the reduction was not statistically significant compared to the control.

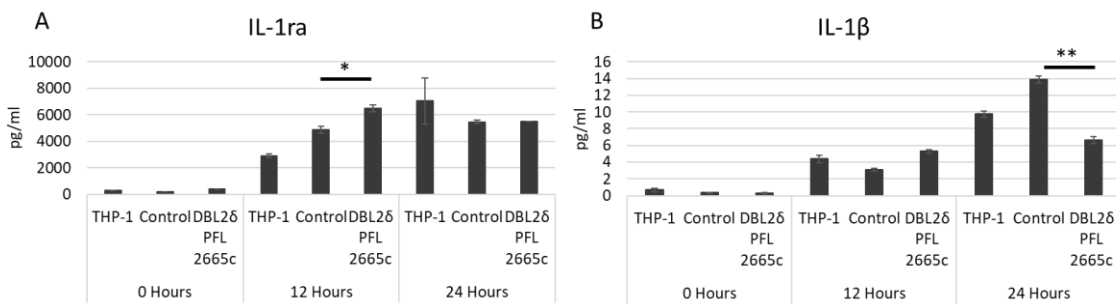


**Figure 10. Cytokine/Chemokine production from integrin  $\alpha V\beta 3::$ DBL2 $\delta$ <sub>PFL 2665c</sub> ligation:** The amount of **A.** IL-1ra and **B.** IL-1 $\beta$  produced after 0, 12, 24 hours of incubation in empty, HAE coated, or DBL2 $\delta$ <sub>PFL 2665c</sub> coated wells. All samples were analyzed with a one-way ANOVA followed by a two-tailed T. Test with two sample equal variance and a 95% confidence (\* =  $P \leq 0.05$ , \*\* =  $P \leq 0.01$ ). Error bars are SEM.

### THP-1 cell ligation to surface-immobilized DBL2 $\delta$ <sub>PFL 2665c</sub> downregulates inflammatory gene expression

The study demonstrated an extremely high level of reproducibility and precision based on Pearson r Correlation between all samples ( $R^2 \geq 0.991$ , Figure 11A). Cluster analysis of differentially expressed genes (DEG) demonstrated that multiple pathways for the pro-inflammatory response were significantly downregulated in THP-1 cells, when incubated with DBL2 $\delta$ <sub>PFL 2665c</sub> compared to HAE (Figure 11B). Gene Ontology (GO) analysis determined that many of those pathways are involved in the immune response

and that the pathways included a substantial number of DEG per pathway (Figure 11C). Further analysis of the pathways determined that the downregulation of specific genes producing pro-inflammatory cytokines/chemokines (CSF-1, TNF, CXCL10, MIP-3a/CCL20, MIP-1 $\beta$ /CCL4, MCP-1/CCL2, IL-1 $\beta$ , and IL-8), adhesion molecules (ICAM-1), and transcription factors (EGR1, EGR2, NF $\kappa$ B1, and NF $\kappa$ B2) was statistically significant. This is a significantly new data set and further analysis of the pathways and genes involved should be continued.



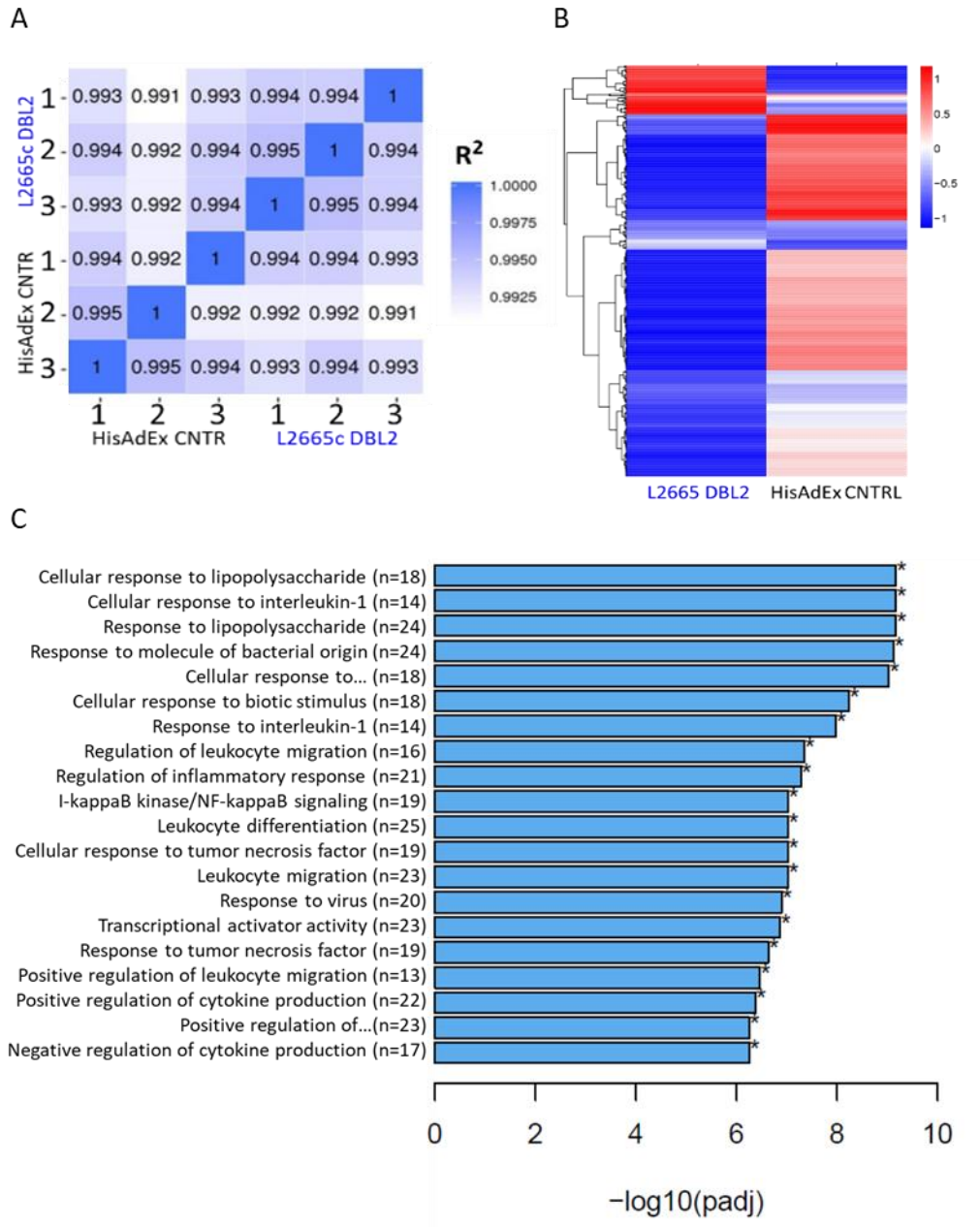


**Figure 11. RNA<sub>Seq</sub> Analysis from THP-1 ligation to HAE and DBL2 $\delta$ <sub>PFL 2665c</sub>: A.** Pearson correlation analysis of all samples **B.** Cluster analysis of differentially expressed genes (DEG) **C.** Genetic Ontology analysis showing downregulated pathways and number of associated DEG (n).

## Discussion

Similar to how pattern recognition receptors (PRRs) on immune cells recognize conserved pathogen associated molecular patterns (PAMPs) unique to each pathogen, integrins recognize distinct protein sequence patterns within various ligands to facilitate binding. One of the most commonly recognized sequences is the arginine-glycine-aspartic acid (RGD) sequence. Collagen, laminin, viruses, and *Plasmodium falciparum* iRBCs can be recognized by integrins through conserved RGD sequences, for cell adhesion. Integrin  $\alpha V\beta 3$  is a phagocytic receptor that recognizes RGD sequences (92); therefore, we interacted integrin  $\alpha V\beta 3$  with RGD-containing and non-RGD-containing PfEMP1 protein constructs from the 3D7 strain of *P. falciparum* to determine binding ability. Of the PfEMP1 proteins tested, only tandem construct DBL2 $\delta$ CIDR2 $\beta$ <sub>PFL 2665c</sub> had a statistically significant amount of bound integrin  $\alpha V\beta 3$  ( $p \leq 0.001$ , Figure 12A). We further broke down the DBL2 $\delta$ CIDR2 $\beta$ <sub>PFL 2665c</sub> protein construct from a tandem construct of DBL2 $\delta$  and CIDR2 $\beta$  to a single domain containing only DBL2 $\delta$  and interacted it with integrin  $\alpha V\beta 3$ . The amount of bound Integrin  $\alpha V\beta 3$  was higher for the single DBL2 $\delta$ <sub>PFL 2665c</sub> domain compared to the tandem construct and the integrin  $\alpha V\beta 3$ ::DBL2 $\delta$ <sub>PFL 2665c</sub> interaction was significantly inhibited by pre-incubation with an RGD inhibitory peptide (RGD-IP,  $p \leq 0.001$ , Figure 12B). These results were the first experimental demonstration of binding between a specific PfEMP1 domain and integrin, which resulted in our recent publication (16).

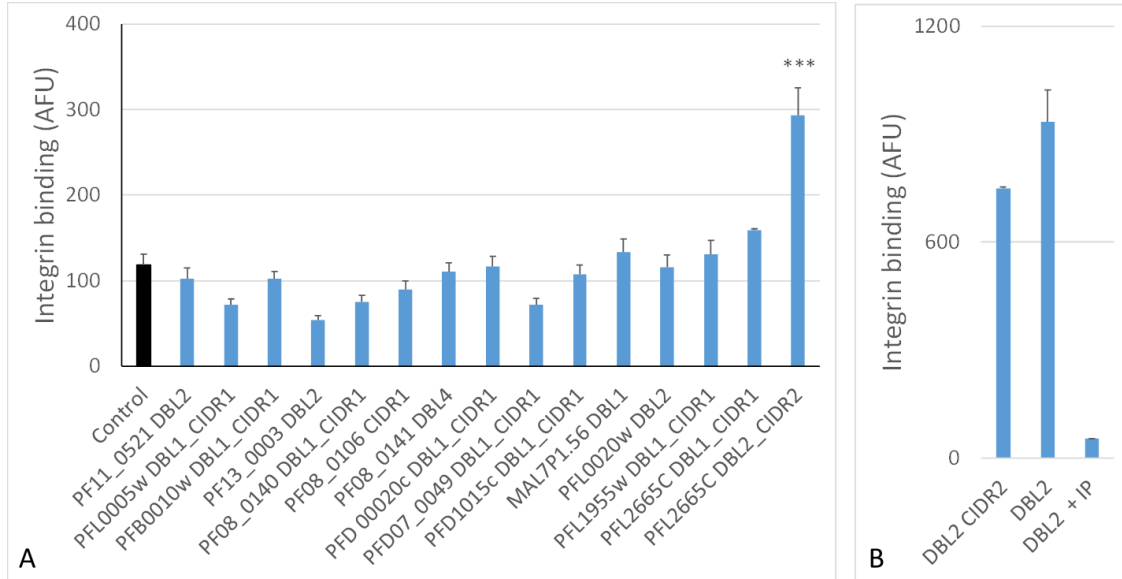


**Figure 12. Integrin  $\alpha$ V $\beta$ 3 binding to various PfEMP1 proteins:** **A.** Bio-Plex immobilized PfEMP1 tandem constructs were tested for ability to bind to integrin  $\alpha$ V $\beta$ 3. **B.** The tandem (DBL2 $\delta$ C1DR2 $\beta$ <sub>PFL 2665c</sub>) and single (DBL2 $\delta$  $\beta$ <sub>PFL 2665c</sub>) construct from the PFL 2665c gene were test for binding ability to integrin  $\alpha$ V $\beta$ 3 with or without RGD-IP. Statistical significance is expressed as P-value from T. Test. \*\*\* =  $P \leq 0.001$ . Error bars are SEM. Adapted from (16).

In further experiments, we were able to significantly inhibit the integrin  $\alpha$ V $\beta$ 3::DBL2 $\delta$ <sub>PFL 2665c</sub> interaction by pre-incubation with anti-integrin  $\alpha$ V $\beta$ 3 antibodies ( $p \leq 0.05$ , Figure 7C). The single DBL2 $\delta$ <sub>PFL 2665c</sub> protein domain possesses two RGD motifs and, therefore, was expected to bind to integrin  $\alpha$ V $\beta$ 3. We hypothesized that simply possessing a single RGD motif would ensure the ability to bind to integrin  $\alpha$ V $\beta$ 3. Interestingly, in addition to DBL2 $\delta$ <sub>PFL 2665c</sub>, all other RGD-containing PfEMP1 constructs in our limited set showed a significant amount of bound integrin  $\alpha$ V $\beta$ 3 (Figure 13).

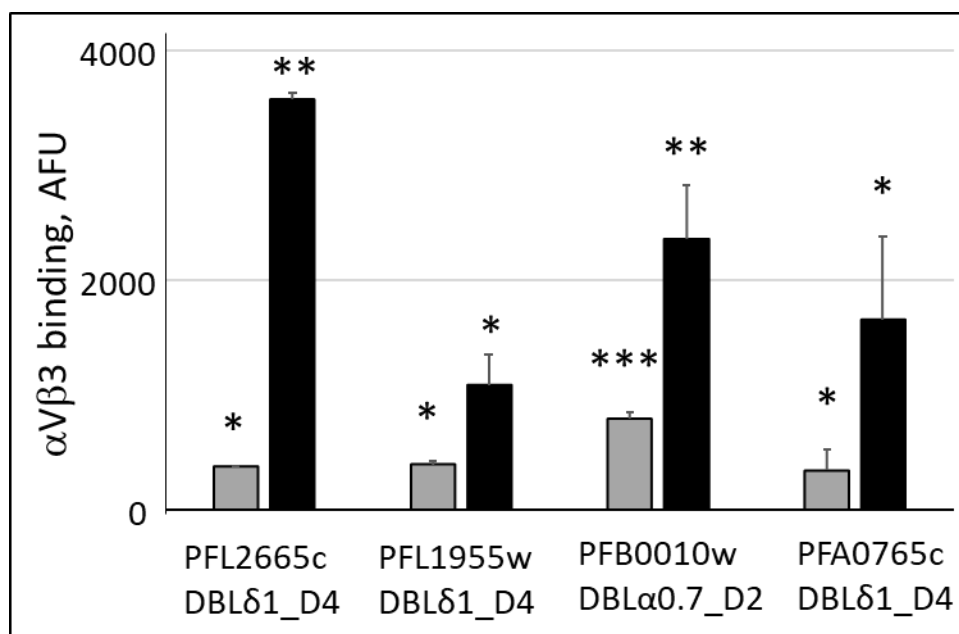


**Figure 13. Integrin  $\alpha$ V $\beta$ 3 binding to various RGD-containing PfEMP1 proteins:** Gray bars, 1 mg/ml, black bars, 5 mg/ml. AFU, Arbitrary fluorescence units. Control value for His AdEx construct was subtracted from binding of domain constructs. Bars represent means of duplicate measurements. Error bars indicate Standard Deviations (SD). Differences in binding between each domain and control construct for each concentration were calculated by one-way ANOVA using Holm-Sidak's multiple comparisons tests. (\* =  $P \leq 0.05$ , \*\* =  $P \leq 0.01$ , \*\*\* =  $P \leq 0.001$ , \*\*\*\* =  $P \leq 0.0001$ ). These experiments were repeated at least once with similar qualitative results. Adapted from (16).

The results demonstrate that possessing a single RGD motif was sufficient for a PfEMP1::integrin  $\alpha$ V $\beta$ 3 interaction to occur in our limited set. However, DBL2 $\delta$ <sub>PFL 2665c</sub> was by far the strongest integrin  $\alpha$ V $\beta$ 3 binding PfEMP1 and the location of the two RGD sequences within the loops of the predicted secondary structure of DBL2 $\delta$ <sub>PFL 2665c</sub> might play an important role in the ability to strongly bind to integrin  $\alpha$ V $\beta$ 3 (16).

Since the presence of an RGD motif translates into integrin  $\alpha$ V $\beta$ 3 binding, we wanted to determine if the overall protein sequence similarities between PfEMP1 protein constructs contributes to the PfEMP1s ability to bind to integrin  $\alpha$ V $\beta$ 3 or if binding is exclusively dependent on the RGD motif. The complete DBL2 $\delta$  domain sequence coded

by the PFL 2665c *var* gene served as a NIH-BLASTp search query and determined the DBL2 $\delta$ <sub>PF10 0406</sub> (E-value = 5e-119) and DBL2 $\delta$ <sub>PF10 1015c</sub> (E-value = 1e-102) PfEMP1 proteins to be the most closely related, although neither PfEMP1 protein contains a RGD motif (Table 2). Both DBL2 $\delta$ <sub>PF10 0406</sub> and DBL2 $\delta$ <sub>PF10 1015c</sub> did not show the ability to bind to integrin  $\alpha$ V $\beta$ 3 and were excluded from further experimentation. In line with our predicted hypothesis, sequence similarity toward DBL2 $\delta$ <sub>PFL 2665c</sub> did not translate into PfEMP1 ability to bind integrin  $\alpha$ V $\beta$ 3. However, possessing a single RGD motif resulted in integrin  $\alpha$ V $\beta$ 3 binding in our limited set.

The avidity of the specific integrin  $\alpha$ V $\beta$ 3::DBL2 $\delta$ <sub>PFL 2665c</sub> interaction was determined by calculating the equilibrium constant ( $K_D$ ) of integrin  $\alpha$ V $\beta$ 3 toward DBL2 $\delta$ <sub>PFL 2665c</sub>. The  $K_D$  of integrin  $\alpha$ V $\beta$ 3 toward the PfEMP1 protein DBL2 $\delta$ <sub>PFL 2665c</sub> was calculated to be 62.2nM. A 62.2nM concentration of integrin  $\alpha$ V $\beta$ 3 is low and signifies a moderate avidity of integrin  $\alpha$ V $\beta$ 3 toward DBL2 $\delta$ <sub>PFL 2665c</sub>. Integrins are involved in cell migration, which involves constantly breaking bonds, and have been widely documented as low affinity receptors, which is comparable to our calculated  $K_D$  (94). Therefore, it is understandable that the integrin  $\alpha$ V $\beta$ 3::DBL2 $\delta$ <sub>PFL 2665c</sub> interaction ( $K_D$  = 62.2nM) would not be as strong as the ICAM-1::DBL2 $\beta$ <sub>PF11 0521</sub> interaction ( $K_D$  = 7.62nM), characterized in Chapter II: ICAM-1 Studies.

Additionally, we sought to determine if integrin  $\alpha$ V $\beta$ 3 recognizing the RGD motif of DBL2 $\delta$ <sub>PFL 2665c</sub> induces ligation by monocyte-like THP-1 cells, similar to how integrin  $\alpha$ V $\beta$ 3 can recognize RGD motifs on apoptotic cells by macrophage (91). Since we wanted to determine the immune response in naïve hosts, those who suffer the highest mortalities, we chose non-stimulated THP-1 cells to simulate a circulating monocyte that

would encounter a PfEMP1-expressing iRBC in the vasculature. In our study, the percentage of DBL2 $\delta$ <sub>PFL 2665c</sub> coated beads ligated by THP-1 cells was slightly elevated compared to the control, but the value was not statistically significant (Figure 9A). Pre-incubation with RGD-IP, anti-integrin  $\beta$ 1 antibody, and anti-integrin  $\alpha$ V $\beta$ 3 antibody all reduced the percentage of DBL2 $\delta$ <sub>PFL 2665c</sub> coated beads ligated to THP-1 cells by 100%, when adjusted for the background control. Since RGD-IP specifically targets RGD motifs and anti-integrin  $\alpha$ V $\beta$ 3 antibody targets integrin  $\alpha$ V $\beta$ 3, they are both expected to inhibit the integrin  $\alpha$ V $\beta$ 3::DBL2 $\delta$ <sub>PFL 2665c</sub> interaction. Unexpectedly, anti-integrin  $\beta$ 1 antibody, which does not target integrin  $\alpha$ V $\beta$ 3, also inhibited ligation to the DBL2 $\delta$ <sub>PFL 2665c</sub> coated beads. It is known that other integrins play a role in ligation and phagocytosis (92). For example, integrin  $\alpha$ 2 $\beta$ 1 has been shown to ligate and phagocytose collagen-coated beads and ligation/phagocytosis was inhibited by integrin  $\beta$ 1 targeted antibodies (128). Therefore, since anti-integrin  $\beta$ 1 antibodies inhibited PfEMP1 mediated ligation to THP-1 cells in our study,  $\beta$ 1-containing integrins, like integrin  $\alpha$ 2 $\beta$ 1, might indirectly contribute to PfEMP1 mediated ligation and possibly phagocytosis by non-stimulated THP-1 cells.

Although the ability of DBL2 $\delta$ <sub>PFL 2665c</sub> to induce ligation and, potentially phagocytosis, by THP-1 cells was not statistically significant, it does not mean that cell signaling isn't taking place upon ligation. To determine if ligation and subsequent cell signaling is resulting in an immune response, THP-1 cells were incubated with and without DBL2 $\delta$ <sub>PFL 2665c</sub> ligation, supernatants were collected, and the supernatants were analyzed for the presence of pro- and anti-inflammatory cytokine/chemokine production. It is worth noting that there was a detected increase in production of cytokines over time

from our control THP-1 cells. Possible causes and solutions were discussed in Chapter II: ICAM-1 Studies – Discussion. After 12 hours of incubation with DBL2 $\delta$ <sub>PFL 2665c</sub>, THP-1 cells produced more IL-1 $\alpha$  than production by THP-1 cells alone and significantly more IL-1 $\alpha$  than the control. Additionally, after 24 hours of incubation with DBL2 $\delta$ <sub>PFL 2665c</sub>, THP-1 cells produced less IL-1 $\beta$ , compared to production by THP-1 cells alone and significantly less than the control. Ligation through DBL2 $\delta$ <sub>PFL 2665c</sub> contributes to an anti-inflammatory immune response by blocking IL-1 $\alpha$  signaling through the production of IL-1 $\alpha$  and reduces the efficiency of available IL-1 $\alpha$  by reducing the production of its ligand, IL-1 $\beta$ . Although not statistically significant, there was a reduction in both MCP-1 and IL-8 resulting from DBL2 $\delta$ <sub>PFL 2665c</sub>.

This method assumes that there are enough THP-1::DBL2 $\delta$ <sub>PFL 2665c</sub> interactions to produce detectable amounts of secreted cytokines in the supernatant. Clearly each THP-1 cell would not be involved in integrin:surface immobilized PfEMP1 binding. Each non-engaged cell would produce a response similar to the cells in the control well. For example, if 25% of the THP-1 cells were able to interact with DBL2 $\delta$ <sub>PFL 2665c</sub>, most of the cells would behave like our control populations. Another complementary method, which detects changes at the gene level instead of at the protein level (cytokines), would be to look at the differentially expressed genes (DEG) from THP-1 cells interacting with DBL2 $\delta$ <sub>PFL 2665c</sub>.

We compared the DEG from our THP-1 cells incubated with surface-immobilized DBL2 $\delta$ <sub>PFL 2665c</sub> to THP-1 cells incubated with surface-immobilized control, after 3 hours of incubation. Gene Ontology analysis determined that the downregulated genes would normally be active in pathways that regulate cytokine production, leukocyte migration,

NF- $\kappa$ B signaling, response to interleukin-1, etc. The results showed that DBL2 $\delta_{\text{PFL 2665c}}$  ligation led to the downregulation of many important immune response modulating pathways. More specifically, in regard to cytokine/chemokine gene expression, there was a downregulation in the mRNA levels of IL-1 $\beta$  ( $P=0.00091$ ,  $\text{P}_{\text{adj}}=0.068$ ), MCP-1 ( $P=5.11\text{E-}12$ ,  $\text{P}_{\text{adj}}=2.71\text{E-}09$ ), and IL-8 ( $P=5.11\text{E-}12$ ,  $\text{P}_{\text{adj}}=2.71\text{E-}09$ ), which aligns with a decreased production of the same cytokines, at the protein level, after 24 hours of ligation with DBL2 $\delta_{\text{PFL 2665c}}$ , determined from our cytokine analysis of the THP-1 cell supernatants.

In conclusion, our study sought to determine if overall protein sequence similarity toward the integrin  $\alpha\text{V}\beta 3$ -binding DBL2 $\delta_{\text{PFL 2665c}}$  protein construct plays a role in integrin  $\alpha\text{V}\beta 3$  binding strength and avidity using PfEMP1-coated Bio-Plex beads. Using our bead-based iRBC model expressing one target PfEMP1 protein at a time, we determined that overall sequence similarity toward DBL2 $\delta_{\text{PFL 2665c}}$  did not result in ability to bind to integrin  $\alpha\text{V}\beta 3$ ; however, we did confirm that the presence of an RGD motif was a key determinate of integrin  $\alpha\text{V}\beta 3$  binding. Confirming the specific interaction between PfEMP1 proteins and integrins is important for further studies at the molecular level. Therefore, we wanted to understand if immune cell interaction with DBL2 $\delta_{\text{PFL 2665c}}$  would contribute to a pro-inflammatory immune response. Through THP-1 cell ligation, cytokine production, and DEG analysis we found that integrin  $\alpha\text{V}\beta 3::\text{DBL2}\delta_{\text{PFL 2665c}}$  ligation using THP-1 cells resulted in the downregulation of important genes needed for the production of pro-inflammatory cytokines, which resulted in a lower concentration of pro-inflammatory cytokines being produced and released into the cell supernatant. The presence of an anti-inflammatory response may signal that the malaria parasite is



attempting to curb the immune response through specific receptor interactions. However, if integrin  $\alpha V\beta 3$  does not lead to a robust immune response from immune cells, the information reported is also important for understanding the interaction between immune cell integrins and iRBC. For example, the specificity of cell surface receptors toward the RGD motif of PfEMP1 proteins, instead of to the whole PfEMP1 protein sequence, makes it difficult to therapeutically target effects of integrin binding iRBC on immune cells, if necessary by RGD-like peptides, since the RGD motif can be found on many naturally occurring cell surface receptors. However, anti-adhesion small molecule drugs may still interfere with these interactions by binding to conserved pockets of integrin-binding PfEMP1 domains, as was the case for anti-adhesion drugs specific for ICAM-1::PfEMP1 domain interactions active against heterologous domains (125).

## CHAPTER IV: CD36 STUDIES

### **Abstract**

CD36 is a cell surface class B scavenger receptor found on various cell types. During the innate immune response, scavenger receptors act as PRRs to bind to a wide array of PAMPs. Immune cell signaling through CD36 ligation activates the transcription factors NF- $\kappa$ B, JNK, MAPK, and TRAF6 leading to cytokine production, inflammation, oxidative stress, and apoptosis. Since CD36 is abundantly expressed on various cell types and ligation contributes to a vast array of cell signaling functions, it is no surprise that CD36 plays a major role in malaria pathology. The CD36 receptor offers binding sites for malarial PfEMP1 proteins throughout the vascular endothelium to help facilitate iRBC sequestration. As malarial research progresses, there has been great progress in pinpointing specific functional groups that bind to human cell surface receptors. Specifically, the CIDR1 $\alpha$  functional group from the PF08 0106 *var* gene has an affinity for scavenger receptor CD36. Interestingly, the immune consequences of individual PfEMP1::CD36 interactions have not been extensively researched. In this study, we examine the effects of PfEMP1 protein sequence similarity, toward the CIDR1 $\alpha$ <sub>PF08 0106</sub> protein construct, on CD36 binding strength and avidity. Additionally, we examine if CIDR1 $\alpha$ <sub>PF08 0106</sub>::CD36 ligation will induce cytokine/chemokine release by monocyte-like THP-1 cells. Overall protein sequence similarity toward the strong CD36 binding

CIDR1 $\alpha$ <sub>PF08 0106</sub> PfEMP1 protein was correlated with CD36-binding strength and ability to bind to monocyte-like THP-1 cells. However, surface-immobilized CIDR1 $\alpha$ <sub>PF08 0106</sub> ligation to THP-1 cells produced mainly anti-inflammatory effects.

## **Introduction**

Scavenger receptors play an important role in recognition and immune clearance of endogenous proteins, exogenous proteins, and pathogens. Cluster of Differentiation 36 (CD36) is a class B scavenger receptor found on various cell types including platelets, red blood cells, mononuclear phagocytes, endothelial cells, hepatocytes, etc. CD36 is an integral membrane glycoprotein, which consists of an extracellular region for ligand binding, two transmembrane regions, and two cytoplasmic regions. The extracellular region binds to oxidized low-density lipoproteins (ox-LDL) produced by endogenous and exogenous pathways of cholesterol metabolism, long chain fatty acids, and various other ligands through pathogen-associated molecular patterns (PAMPs) (96). The cytoplasmic tail region is associated with Src-family tyrosine kinases for signal transduction and cell signaling (97). More specifically, CD36 is directly associated with Fyn, Lyn, and Yes tyrosine kinases (98, 99). Src-family tyrosine kinase signaling regulates cell adhesion, spreading, migration, growth, maturation, differentiation, apoptosis, and gene transfection (100).

On monocyte/macrophage, CD36 will bind and endocytose ox-LDL in a caveolae- independent lipid raft pathway (101). Ox-LDL promotes differentiation of monocytes to macrophage and increases further uptake of ox-LDL (102). In the arterial wall, accumulation of ox-LDL within macrophage further differentiate the cells into foam

cells. Due to the accumulation of ox-LDL, foam cells release the IL-1 $\beta$  pro-inflammatory precursor protein (pro-IL-1 $\beta$ ) and activate the NLRP3 inflammasome, including caspase-1 (103). Caspase-1 cleaves pro-IL-1 $\beta$  to produce the IL-1 $\beta$  pro-inflammatory cytokine, which is an active participant in the initiation and progression of atherosclerosis. IL-1 $\beta$  increases the expression of vascular adhesion molecule 1 (VCAM-1), which aids in monocyte rolling to the site of foam cells (104, 105), and monocyte chemoattractant protein 1 (MCP-1), which aids in immune cell infiltration through vessel walls and lesion formation (104, 106).

During the innate immune response, scavenger receptors act as pattern recognition receptors (PRRs) to bind to a wide array of PAMPs. For example, CD36 recognizes gram-positive and gram-negative bacteria, phagocytoses the pathogens, and presents it to internal toll-like receptors (TLRs) to initiate inflammatory pathogen-clearing signals within the cell (107). More specifically, TLR4, on the surface of phagocytes, co-localizes with CD36 when bound to gram-negative *Escherichia coli*. Signaling through TLR4/CD36 activates the transcription factors nuclear factor-kappa B (NF- $\kappa$ B), c-Jun N-terminal kinase (JNK), mitogen-activated protein kinase (MAPK), and tumor necrosis factor receptor-associated factor 6 (TRAF6) leading to cytokine production, inflammation, oxidative stress, and apoptosis (97, 108). Independent of TLR co-localization, ligation of CD36 to lipoteichoic acid (LTA), from the gram-positive bacterial *Staphylococcus aureas*, activates the JNK signaling pathway leading to phagocytosis and an interleukin-8 (IL-8) mediated inflammatory response (109).

On various tissues of the host, the ever-present CD36 receptor offers malarial PfEMP1 binding sites throughout the vascular endothelium (110). It is predicted that

approximately 85% of PfEMP1 proteins contain domains that are able to bind to CD36 (111, 112). Since CD36 is abundantly expressed on various cell types and ligation contributes to a vast array of cell signaling functions, it is no surprise that CD36 plays a major role in malaria pathology.

Endothelial cell surface bound CD36 ligation results in phosphorylation and activation of src-family kinases involved in the extracellular signal-regulated kinase 1/2 (ERK 1/2) and p38 mitogen-activated protein kinase (MAPK) pathways in both *in vitro* studies using recombinant PfEMP1 protein, and *in vivo* studies using parasite isolates (113). Furthermore, blockage of Src kinase phosphorylation using inhibitory molecule PP1 reduced sequestration of iRBC to the endothelium *in vitro* and *in vivo* using human dermal microvascular endothelial cell (HDMEC) monolayers and a Human/SCID mouse model, respectively (113). As mentioned earlier, the expression of CD36 is not exclusive to endothelial cells and CD36 ligation to malaria proteins has varying effects on immune cells as well.

In dendritic cells, CD36-adherent iRBC, from the 3D7 strain, were phagocytosed at a higher rate than CD36-nonadherent iRBC. Additionally, blocking the CD36 receptor on dendritic cells using a Human anti-CD36 antibody reduced the uptake of CD36-adherent iRBC (114). After incubating dendritic cells with CD36 adherent iRBC for 24 hours, analysis of the supernatants showed that the dendritic cells were producing and secreting the pro-inflammatory tumor necrosis factor  $\alpha$  (TNF- $\alpha$ ) and interleukin-12 (IL-12) cytokines (114). TNF- $\alpha$  is an endogenous pyrogen that causes inflammation, induces a fever, and promotes apoptotic cell death. IL-12 stimulates T cells and natural killer (NK) cells to produce interferon  $\gamma$  (IFN $\gamma$ ) and TNF- $\alpha$ , thus increasing the cytotoxic

ability of NK cells. Furthermore, IL-12 is the key mediator of naïve T cell differentiation into Type 1 T Helper (Th1) cells, which increases the cell-mediated immune response opposed to the humoral immune response. Since the cell-mediated response typically targets intracellular pathogens and the humoral immune response typically targets extracellular parasites, dendritic cell signaling through CD36 further contributes to inflammation instead of antibody formation towards the malaria parasite. Additionally, co-culturing dendritic cells with CD36-adherent iRBC activated NK cells and T cells to increase production of IFN $\gamma$  compared to wildtype controls, demonstrating the importance of CD36 ligation in phagocytosis, antigen presentation, and the inflammatory response (114).

When non-opsonized iRBCs, from the ITG malarial clone, were incubated with macrophage derived from isolated human monocytes, a significant amount of macrophage phagocytosed the iRBC. Additionally, pre-incubation with anti-CD36 antibodies significantly inhibited phagocytosis, while anti-ICAM, anti-thrombospondin, anti-integrin  $\alpha$ V $\beta$ 3, and anti-platelet/endothelial cell adhesion molecule 1 antibodies did not inhibit phagocytosis of the ITG iRBC by macrophage derived from human monocytes. Unlike the before mentioned DC, in this case the macrophage did not release TNF- $\alpha$  (17).

PfEMP1 proteins consist of an intracellular, transmembrane, and an extracellular region. The extracellular portion of each PfEMP1 can be constructed using various combinations of functional domains (DBL and CIDR regions). As malarial research progresses, there has been achievements in pinpointing specific functional domain subclasses that bind to human cell surface receptors. Specifically, several subclasses of the

CIDR1 $\alpha$ 0 functional domain have an affinity for scavenger receptor CD36 (19). To determine if various PfEMP1 proteins containing a CIDR1 $\alpha$  functional domain bind to CD36 equally, we expressed 8 PfEMP1 proteins from 8 different *var* genes. Each PfEMP1 protein, containing a CIDR1 $\alpha$  functional group, was coupled to Bio-Plex beads for experimentation. 6 of the 8 PfEMP1 proteins had varying amounts of bound CD36 molecules based on MFI of fluorescently labeled CD36. The highest MFI recorded was for the CIDR1 $\alpha$  domain from the PF08 0106 *var* gene and it was significantly ( $P \leq 0.01$ ) higher than the second highest MFI recorded from CIDR1 $\alpha$  PFB0010w (Figure 14). Since CIDR1 $\alpha$ PF08 0106 had significantly more bound CD36 compared to the other domains that were incubated under the same conditions, CIDR1 $\alpha$ PF08 0106 serves as our reference point for our CD36 studies.

In this study, we determine if protein sequence similarity toward the CIDR1 $\alpha$ PF08 0106 protein construct plays a role in CD36 binding strength and avidity using PfEMP1-coated Bio-Plex beads. Additionally, we determine if CD36::CIDR1 $\alpha$ PF08 0106 ligation will induce cytokine/chemokine release by monocyte-like THP-1 cells. Since CD36 interactions with iRBCs have various signaling mechanisms leading to different downstream cellular functions (17, 114), it is predicted that multiple PfEMP1 proteins will bind to CD36, as each PfEMP1 might induce a different internal cell signal following ligation. We hypothesize that sequence similarity toward the strong CD36 binding CIDR1 $\alpha$ PF08 0106 domain will result in better ability to bind to CD36. It is predicted that ligation through CD36 will induce production of inflammatory cytokines/chemokines by THP-1 cells.

## Materials and Methods

### THP-1 Culture

THP-1 cells, kindly provided by Dr. Yoshimi Shibata from Florida Atlantic University, were cultured in RPMI 1640 growth medium, supplemented with 25 $\mu$ g/ml gentamicin sulfate, 0.125 $\mu$ g/ml Amphotericin B, and 10% heat-inactivated FBS. The cells were cultured below 5X10<sup>5</sup>cells/ml in order to maintain an unstimulated, nonadherent monocyte population to simulate naïve host immune cells for cytokine analysis.

For interaction with surface-immobilized PfEMP1 proteins, THP-1 cells were incubated with Goat IgG (Jackson Laboratories, Cat# 005-000-002) to block the cells from interacting with our PfEMP1 capture antibody, Goat anti-GFP (Rockland, Cat# 600-101-215). Antibiotic and anti-fungal additives were withheld from the media for all experiments requiring binding.

### Plasmids coding for PfEMP1 domains

PfEMP1 plasmids were created previously using the methods described in (120). Briefly, all PfEMP1 domains were cloned into the pHisAdEx vector, expressed by COS-7 cells, harvested, and immobilized on either COOH Bio-Plex beads (BioRad, Cat# 1715060##) or individual wells of a 48 well plate. Immobilization steps are mentioned in subsequent corresponding sections below. The pHisAdEx vector without inserted malarial DNA was used as the control in all PfEMP1 experiments. This plasmid contains a 54kDA malaria-irrelevant protein fragment that is a part of all PfEMP1 domain-containing constructs and thus is a perfect control for all recombinant PfEMP1 domains tested.





coupled beads were washed and stored at -80°C in 1xPBS with 0.1% BSA, 0.02% Tween-20, 0.05% sodium azide, and 15% glycerol until experimentation, but no longer than 1 month. The solution was switched to 1x TBS, 0.05% tween-20, and 0.1% BSA Fraction V for binding experiments. Our initial experimental group of HAE, CIDR1 $\alpha$ <sub>PFL0005w</sub>, CIDR1 $\alpha$ <sub>PFB0010w</sub>, CIDR1 $\alpha$ <sub>PF08 0140</sub>, CIDR1 $\alpha$ <sub>PF00020c</sub>, CIDR1 $\alpha$ <sub>PF01015c</sub>, CIDR1 $\alpha$ <sub>PFL1955w</sub>, CIDR1 $\alpha$ <sub>PFL2665c</sub>, and CIDR1 $\alpha$ <sub>PF08 0106</sub> coupled Bio-Plex beads were incubated with 2 $\mu$ g/ml of recombinant human CD36-FC (R&D Systems, Cat# 1955-CD-050) for 1 hour with shaking at room temperature. Any unbound CD36 was washed out of the system through vacuum filtration and then the beads were incubated with a 1:250 dilution of Goat anti-human IgG-Phycoerythrin (R&D Systems, Cat# 109-116-170) with shaking at room temperature, to target bound CD36 through the FC portion of the recombinant protein.

Our final experimental group of HAE, CIDR1 $\alpha$ <sub>PF07 0049</sub>, CIDR1 $\alpha$ <sub>MAL7P1.56</sub>, and CIDR1 $\alpha$ <sub>PF08 0106</sub> PfEMP1 proteins were expressed as GFP-fusion proteins by COS-7 cells and attached to anti-GFP coated COOH Bio-Plex beads. To determine binding ability and specificity to CD36, 2 $\mu$ g/ml of recombinant CD36-FC was incubated with PBS, 5 $\mu$ g/ml anti-CD36 monoclonal antibody (Abcam, Cat# ab17044), or 5 $\mu$ g/ml anti-ICAM-1 monoclonal antibody (Invitrogen, Cat# MA5407) for 1 hour with shaking at room temperature. Following pre-incubation with blocking agents, the CD36 recombinant proteins were incubated with HAE, CIDR1 $\alpha$ <sub>PF07 0049</sub>, CIDR1 $\alpha$ <sub>MAL7P1.56</sub>, and CIDR1 $\alpha$ <sub>PF08 0106</sub> coated beads for 1 hour with shaking at room temperature. Any unbound CD36 was washed out of the system through vacuum filtration and then the beads were incubated

with a 1:250 dilution of Goat anti-human IgG-PE with shaking at room temperature, to target bound CD36 through the FC portion of the recombinant protein.

Mean fluorescent intensity (MFI) of bound fluorescently-labeled CD36 was determined by the Bio-Plex 200 suspension array system (BioRad) using Bio-Plex Manager Software 5.0. All binding experiments were conducted in triplicate and repeated at least once. MFI values were compared for statistical significance to the control by a two-tailed T. Test with two sample equal variance and a 95% confidence interval using both Microsoft Excel and Bio-Plex Manager 5.0 (\* =  $P \leq 0.05$ , \*\* =  $P \leq 0.01$ , \*\*\* =  $P \leq 0.001$ , \*\*\*\* =  $P \leq 0.0001$ ). All graphical error bars are Standard Error of Means (SEM). The MFI values were compared to E-values using Pearson's r correlation coefficient calculations ( $r < 0.5$  = weak correlation,  $0.5 < r < 0.7$  = moderate correlation,  $0.7 < r$  = strong correlation).

#### *Bead-based equilibrium constant ( $K_D$ ) analysis*

Various concentrations of recombinant CD36-FC (3.0 $\mu$ g/ml, 1.0 $\mu$ g/ml, and 0.3 $\mu$ g/ml) were incubated with a 1:250 dilution of Goat anti-human IgG-PE, to fluorescently label the CD36 receptor. Following fluorescent labeling, the various concentrations of CD36 were incubated with HAE, CIDR1 $\alpha$ <sub>PF07 0049</sub>, CIDR1 $\alpha$ <sub>MAL7P1.56</sub>, and CIDR1 $\alpha$ <sub>PF08 0106</sub> coated Bio-Plex beads for 0, 5, 10, and 15 minutes. The change in MFI of bound fluorescently labeled ICAM-1 was compared to change in time to determine the velocity of binding for 3.0 $\mu$ g/ml, 1.0 $\mu$ g/ml, and 0.3 $\mu$ g/ml of recombinant CD36. The inverse velocities ( $1/V = \Delta\text{Time}/\Delta\text{MFI}$ ) were plotted against their corresponding inverse concentrations ( $1/C$ ) on a Lineweaver-Burk double reciprocal

scatter plot. On a Lineweaver-Burk plot, the x-intercept of the linear line of best fit equals  $1/K_D$ , where  $K_D$  represents the equilibrium dissociation constant. In this case, the equilibrium constant signifies the concentration of CD36 where 50% of CD36 is bound to the PfEMP1 receptor and 50% of CD36 is not bound to the PfEMP1 receptor. Mean fluorescent intensity (MFI) of bound fluorescently-labeled CD36 was determined by the Bio-Plex 200 suspension array system using Bio-Plex Manager Software 5.0. All  $K_D$  experiments were plotted using Microsoft Excel and conducted in duplicate with at least one repetition. All graphical error bars are Standard Error of Means (SEM). The  $K_D$  values were compared to E-values using Pearson's r correlation coefficient calculations ( $r < 0.5$  = weak correlation,  $0.5 < r < 0.7$  = moderate correlation,  $0.7 < r$  = strong correlation).

#### THP-1: Bead-based ligation analysis and statistical comparison

THP-1 cells were incubated with PBS, 10  $\mu\text{g/ml}$  of anti-CD36 monoclonal antibody, or 10  $\mu\text{g/ml}$  of anti-ICAM-1 monoclonal antibody for 30 minutes at 37°C with shaking. The cells were washed and then incubate with either HAE, CIDR1 $\alpha_{\text{PF07 0049}}$ , CIDR1 $\alpha_{\text{MAL7P1.56}}$ , or CIDR1 $\alpha_{\text{PF08 0106}}$  coated beads, at a 1:20 ratio of Beads:THP-1 cells, for 2 hours with shaking at 0°C and 37°C. The 0°C samples were used as a ligation control (no phagocytosis taking place) and the results at 0°C were subtracted as background from the 37°C samples. Others have confirmed phagocytosis takes place at 37°C, but not at 0°C by confocal microscopy also using THP-1 cells and PfEMP1-coated fluorescent beads (137). Therefore, reported values adjusted for the control signify ligation and possibly phagocytosis, further analysis is needed to confirm phagocytosis.

Using the Attune NXT acoustic focusing flow cytometer (Life Technologies) and associated software, we were able to locate our beads and cells using side scatter (SSC) and front scatter (FSC) characteristics. The beads are smaller and have a more complex internal core than the THP-1 cells. The bead's complex internal core is made up of two fluorescent dyes that can be detected on the BL3 channel of the flow cytometer. To locate our phagocytosed beads, we gated the THP-1 cells and analyzed the gated region for the BL3 channel. We compared the number of beads (positive signal in BL3) contained within our THP-1 cells to the total amount of beads in the system to determine the percentage of beads ligated and possibly phagocytosed. The percentage of ligated/phagocytosed beads, which reflects the ability of domain-coated beads to be ligated/phagocytosed, were compared for statistical significance to the control by a two-tailed T. Test with two sample equal variance and a 95% confidence interval using both Microsoft Excel and Bio-Plex Manager 5.0 (\* =  $P \leq 0.05$ , \*\* =  $P \leq 0.01$ , \*\*\* =  $P \leq 0.001$ , \*\*\*\* =  $P \leq 0.0001$ ). All ligation experiments were conducted in duplicate with at least one repetition. All graphical error bars are Standard Error of Means (SEM). The percentage of beads ligated/phagocytosed was compared to  $K_D$  value and E-value using Pearson's r correlation coefficient calculations ( $r < 0.5$  = weak correlation,  $0.5 < r < 0.7$  = moderate correlation,  $0.7 < r$  = strong correlation).

#### *PfEMP1::THP-1 cytokine and chemokine analysis and statistical comparison*

Utilizing the same process as Bio-Plex bead coupling, HAE, CIDR1 $\alpha$ <sub>PF07 0049</sub>, CIDR1 $\alpha$ <sub>MAL7P1.56</sub>, and CIDR1 $\alpha$ <sub>PF08 0106</sub> were immobilized on the surface of a 96-well flat bottom plate through Goat anti-GFP targeted attachment.  $4.0 \times 10^5$  THP-1 cells were

added to each well and incubated at 37°C for 0, 12, and 24 hours. The supernatants were collected and analyzed using Bio-Plex Pro Human Cytokine kits (BioRad, Cat# 171304090M and Cat# 171-AL003M) testing for the presence of IL-1 $\alpha$ , IL-1 $\beta$ , IL-2, IL-6, IL-8, IL-10, IL-12 (p40), IL-12 (p70), IL-13, IL-19, IL-20, IL-22, IL-26, IL-27, IL28a, IL29, IFN- $\gamma$ , MCP-1, MIP-1 $\alpha$ , and TNF- $\alpha$ . 4 parameter logistic (4PL) or 5 parameter logistic (5PL) standard curves for each cytokine/chemokine were created using the provided standards with the concentration on the x-axis and the MFI on the y-axis. Unknown sample concentrations were determined by fitting the MFI values to the standard curves using the Bio-Plex Manager 5.0 software and confirmed by MyCurveFit online-based application. All samples were analyzed with a one-way ANOVA followed by a two-tailed T. Test with two sample equal variance and a 95% confidence interval using both Microsoft Excel and Bio-Plex Manager 5.0 (\* =  $P \leq 0.05$ , \*\* =  $P \leq 0.01$ , \*\*\* =  $P \leq 0.001$ , \*\*\*\* =  $P \leq 0.0001$ ). Only statistically significant experimental values compared to the HAE control are reported. All graphical error bars are Standard Error of Means (SEM).

#### THP-1::CIDR1 $\alpha$ <sub>PF08 0106</sub> global gene expression analysis

Utilizing the same process as Bio-Plex bead coupling, HAE (control) and CIDR1 $\alpha$ <sub>PF08 0106</sub> were immobilized on the surface of a 96-well flat bottom plate through Goat anti-GFP targeted attachment. Surface-immobilization restricts the THP-1 cells to ligation triggered cell signaling; therefore, phagocytosis does not take place in this model.  $4.0 \times 10^5$  THP-1 cells were added to each well and incubated at 37°C for 3 hours. The cells were seeded in triplicate, repeated three times for HAE and CIDR1 $\alpha$ <sub>PF08 0106</sub>. The cells

were gently scraped, collected, and RNA was prepared using the E.Z.N.A. Blood RNA Kit I (Omega Bio-tek, Cat# R6814), following the manufacturer's protocol. The RNA was submitted for high-throughput RNA sequencing (RNA<sub>seq</sub>) to Novogene Co. Ltd. (Sacramento, CA.). The results were received in Microsoft Excel format by fragments per kilobase million (FPKM).

## Results

### Survey of CIDR1 $\alpha$ containing PfEMP1 domains for CD36 binding ability

HisAdEx (HAE, control), CIDR1 $\alpha$ <sub>PFL0005w</sub>, CIDR1 $\alpha$ <sub>PFB0010w</sub>, CIDR1 $\alpha$ <sub>PF08\_0140</sub>, CIDR1 $\alpha$ <sub>PDF0020C</sub>, CIDR1 $\alpha$ <sub>PDF1015c</sub>, CIDR1 $\alpha$ <sub>PFL1955w</sub>, CIDR1 $\alpha$ <sub>PFL2665c</sub>, and CIDR1 $\alpha$ <sub>PF08\_0106</sub> coated Bio-Plex beads were incubated with recombinant human CD36-FC receptor, washed twice, and then incubated with anti-human IgG-PE antibody for detection by the Bio-Plex 200 suspension array analysis. CD36 was detected bound to 6 of the 8 PfEMP1 proteins compared to the control. The mean fluorescent intensity (MFI) from CD36 bound to HAE was  $309.33 \pm 26.32$ , CIDR1 $\alpha$ <sub>PFL0005w</sub> was  $401.17 \pm 40.80$ , CIDR1 $\alpha$ <sub>PFB0010w</sub> was  $1536.25 \pm 197.41$ , CIDR1 $\alpha$ <sub>PF08\_0140</sub> was  $231.83 \pm 11.97$ , CIDR1 $\alpha$ <sub>PDF0020C</sub> was  $298.58 \pm 30.55$ , CIDR1 $\alpha$ <sub>PDF1015c</sub> was  $403.33 \pm 20.09$ , CIDR1 $\alpha$ <sub>PFL1955w</sub> was  $1140.50 \pm 109.01$ , CIDR1 $\alpha$ <sub>PFL2665c</sub> was  $468.33 \pm 28.47$ , and CIDR1 $\alpha$ <sub>PF08\_0106</sub> was  $8836.00 \pm 1318.43$  (Figure 14).

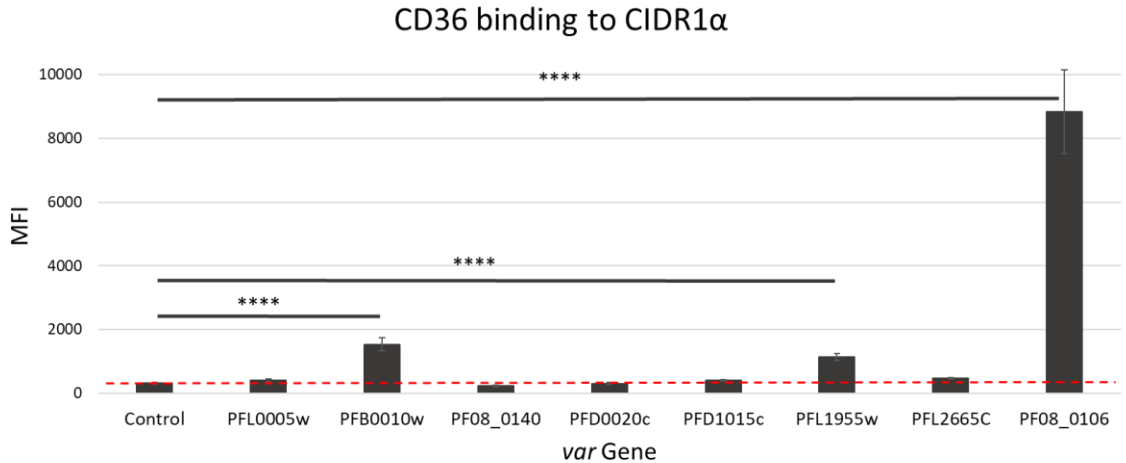


**Figure 14. Survey of CIDR1 $\alpha$  containing PfEMP1 proteins for CD36 binding.** 8 Bio-Plex bead bound PfEMP1 proteins, each containing a CIDR1 $\alpha$  functional group, and 1 control (HisAdEx) were incubated with recombinant human CD36-FC. The mean fluorescent intensity (MFI) of bound CD36-IgG-PE was used to compare binding ability. Error bars are SEM. Asterisks indicate P-value from Student *t* test. \*\*\*\* =  $P \leq 0.0001$ .

#### BLASTp protein sequence similarity analysis

Our original population of 8 PfEMP1 proteins, each containing a CIDR1 $\alpha$  functional unit, determined that multiple *var* genes can produce CD36 binding PfEMP1 proteins, but with varying abilities. Since there are ~60 *var* genes, which are capable of producing PfEMP1 proteins containing CIDR1 $\alpha$  functional groups, trial and error is not an efficient strategy to determine PfEMP1 proteins that bind CD36 as strong as CIDR1 $\alpha$ <sub>PF08 0106</sub>. Deeper analysis of the protein structure of CIDR1 $\alpha$ <sub>PF08 0106</sub> to look for similarities might shed light on binding ability of other PfEMP1 proteins. Therefore, the complete CIDR1 $\alpha$  domain sequence coded by the PF08 0106 *var* gene served as the BLASTp search query to determine a small subset of CIDR1 $\alpha$  containing PfEMP1 proteins from other *var* genes that are similar in protein structure (Figure 15A). The first result from BLASTp analysis was a direct match to the CIDR1 $\alpha$  protein sequence from



the PF08 0106 *var* gene. Aligning the sequences produced a query cover of 100%, identical value of 100% and an E-value of 0.0 (Figure 15B). The second result from BLASTp analysis corresponded to the CIDR1 $\alpha$  protein sequence from the MAL7P1.56 *var* gene. Aligning this sequence with the original query produced a query cover of 79%, an identical value of 49%, and an E-value of 5e-103 (Figure 15C). The third result from BLASTp analysis corresponded to the CIDR1 $\alpha$  protein sequence from the PF07 0049 *var* gene. Aligning this sequence with the original query produced a query cover of 98%, an identical value of 47%, and an E-value of 1e-100 (Figure 15D).

C

Original Query

Score	Expect	Method	Identities	Positives	Gaps
Query 1	RKTRAAITKYGVEKTFKLEKESDYGVDFVLEKLSKDECEKVDDEGGKINFAEKHD				60
Query 61	NNNNIEKGT FYRSYQCPFCYCMGGSGVQKMEKNGKNTSGKLYEPGDAGETPIKI				120
Query 121	LKSGENDDIKQIDDFCKTEDESLAAAMCYKHDEVQKVRGEEEDDEEDYVYGA				180
Query 181	AGGLCILNKKGKEGKEKKSEPEQFQTFNFTYVWALMISQIVWRKIKKCLE				240
Query 241	NGKTMCKRNGCNDICDFESVWQKQKKEWPKIKHFGQKDIQKGTGMDPFLYYLK				300
Query 301	LQFEEVSEKSGTGDEDAKGRGKIDEMFDGQKQIDVASNETTIDIMPLEEKDATK				360
Query 361	CKDQCKQRPAGGAGDVSDTVSPDRPTPGTDGHDSEDEEEEEEDDEHDPDQK				420
Query 421	GTEENVEITVEDQVEEKAKNITDQGEKEENOGGETTITDQDGNPCDVIQKLFQ				480
Query 481	DNLT 484				

D

XP\_001349036.1: MAL7P1.56

Score	Expect	Method	Identities	Positives	Gaps
337 bits(863)	Se-103	Compositional matrix adjust.	213/439(49%)	274/439(62%)	76/439(17%)
Query 1	KYKRA---TIKYGVEKTFKLEKESDYGVDFVLEKLSKDECEKVDDEGGKINFAEKHD				55
Query 41	RYKRA---TYKVEKTFKLEKESDYGVDFVLEKLSKDECEKVDDEGGKINFAEKHD				55
Query 56	---AKHNNNNNDKGT FYRSYQCPFCYCMGGSGVQKMEKNGKNTSGKLYEPGDAGETPIKI				92
Query 481	KISSASVPGGNDVAASGDEGKSGADSNK-----ITYSEYQCPFCYCMGGSGS				536
Query 93	E-WKGN---DNCTSGLYEPGDAGETPIKISGENDDIKQIDDFCKTEDESLAAAMCYKHDEVQKVRGEEEDDEEDYVYGA				143
Query 537	GWEKGTGNTGKLYEPGDAGETPIKISGENDDIKQIDDFCKTEDESLAAAMCYKHDEVQKVRGEEEDDEEDYVYGA				596
Query 144	---DNLTGKLYEPGDAGETPIKISGENDDIKQIDDFCKTEDESLAAAMCYKHDEVQKVRGEEEDDEEDYVYGA				194
Query 537	GGGGNNNDKGT FYRSYQCPFCYCMGGSGVQKMEKNGKNTSGKLYEPGDAGETPIKI				649
Query 195	EKEKSGKELEKQKTFNFTYVWALMISQIVWRKIKKCLENGKNGKNTSGKLYEPGDAGETPIKI				225
Query 650	NGKVMH-----QKIT DFTF VYVWALMISQIVWRKIKKCLENGKNGKNTSGKLYEPGDAGETPIKI				703
Query 255	CDCEFSVWQKQKKEWPKIKHFGQKDIQKGTGMDPFLYYLKQFEEVSEKSGTGDEDAKGRGKIDEMFDGQKQIDVASNETTIDIMPLEEKDATK				712
Query 704	CDCEFSVWQKQKKEWPKIKHFGQKDIQKGTGMDPFLYYLKQFEEVSEKSGTGDEDAKGRGKIDEMFDGQKQIDVASNETTIDIMPLEEKDATK				712
Query 764	ENNSNPNDKGT FYRSYQCPFCYCMGGSGVQKMEKNGKNTSGKLYEPGDAGETPIKI				823
Query 366	EKRPAGGAGDVSDTVSPDRPTPGTDGHDSEDEEEEEEDDEHDPDQK				384
Query 824	---PFQELARSATQV 838				

B

XP\_001349437.1: PF08 0106

Score	Expect	Method	Identities	Positives	Gaps
970 bits(2508)	0.0	Compositional matrix adjust.	484/484(100%)	484/484(100%)	0/484(0%)
Query 1	RKTRAAITKYGVEKTFKLEKESDYGVDFVLEKLSKDECEKVDDEGGKINFAEKHD				60
Query 413	RKTRAAITKYGVEKTFKLEKESDYGVDFVLEKLSKDECEKVDDEGGKINFAEKHD				472
Query 413	NNNNIEKGT FYRSYQCPFCYCMGGSGVQKMEKNGKNTSGKLYEPGDAGETPIKI				120
Query 413	NNNNIEKGT FYRSYQCPFCYCMGGSGVQKMEKNGKNTSGKLYEPGDAGETPIKI				120
Query 413	NNNNIEKGT FYRSYQCPFCYCMGGSGVQKMEKNGKNTSGKLYEPGDAGETPIKI				120
Query 121	LKSGENDDIKQIDDFCKTEDESLAAAMCYKHDEVQKVRGEEEDDEEDYVYGA				180
Query 121	LKSGENDDIKQIDDFCKTEDESLAAAMCYKHDEVQKVRGEEEDDEEDYVYGA				180
Query 121	LKSGENDDIKQIDDFCKTEDESLAAAMCYKHDEVQKVRGEEEDDEEDYVYGA				180
Query 181	AGGLCILNKKGKEGKEKKSEPEQFQTFNFTYVWALMISQIVWRKIKKCLE				240
Query 181	AGGLCILNKKGKEGKEKKSEPEQFQTFNFTYVWALMISQIVWRKIKKCLE				240
Query 181	AGGLCILNKKGKEGKEKKSEPEQFQTFNFTYVWALMISQIVWRKIKKCLE				240
Query 241	NGKTMCKRNGCNDICDFESVWQKQKKEWPKIKHFGQKDIQKGTGMDPFLYYLK				300
Query 241	NGKTMCKRNGCNDICDFESVWQKQKKEWPKIKHFGQKDIQKGTGMDPFLYYLK				300
Query 241	NGKTMCKRNGCNDICDFESVWQKQKKEWPKIKHFGQKDIQKGTGMDPFLYYLK				300
Query 301	LQFEEVSEKSGTGDEDAKGRGKIDEMFDGQKQIDVASNETTIDIMPLEEKDATK				360
Query 301	LQFEEVSEKSGTGDEDAKGRGKIDEMFDGQKQIDVASNETTIDIMPLEEKDATK				360
Query 301	LQFEEVSEKSGTGDEDAKGRGKIDEMFDGQKQIDVASNETTIDIMPLEEKDATK				360
Query 361	CKDQCKQRPAGGAGDVSDTVSPDRPTPGTDGHDSEDEEEEEEDDEHDPDQK				420
Query 361	CKDQCKQRPAGGAGDVSDTVSPDRPTPGTDGHDSEDEEEEEEDDEHDPDQK				420
Query 361	CKDQCKQRPAGGAGDVSDTVSPDRPTPGTDGHDSEDEEEEEEDDEHDPDQK				420
Query 421	GTEENVEITVEDQVEEKAKNITDQGEKEENOGGETTITDQDGNPCDVIQKLFQ				482
Query 421	GTEENVEITVEDQVEEKAKNITDQGEKEENOGGETTITDQDGNPCDVIQKLFQ				482
Query 421	GTEENVEITVEDQVEEKAKNITDQGEKEENOGGETTITDQDGNPCDVIQKLFQ				482
Query 481	DNLT 484				
Query 481	DNLT 484				

**Figure 15: BLASTp Sequence Alignment for PfEMP1s targeting CD36:** **A.** The original query consisting of the CIDR1 $\alpha$  protein sequence (amino acids 1-484) from the PF08 0106 gene, which is compared to: **B.** CIDR1 $\alpha$ <sub>PF08 0106</sub>, **C.** CIDR1 $\alpha$ <sub>MAL7P1.56</sub>, & **D.** CIDR1 $\alpha$ <sub>PF07 0049</sub>. The top line is the original query sequence, the second line lists which amino acids are shared between each sequence, and the third line is the sequence from BLASTp query results.

The genes are closely related, with MAL7P1.56 and PF07 0049 belonging to *var* gene subgroup C and PF08 0106 belonging to intermediate subgroup B/C (Table 3). Group B genes are located near the telomere with transcription proceeding towards the centromere. Group C genes are located in the centromere with transcription also taking place near the centromere. Group B/C genes share qualities from each group and have been described as a transitional state between the two separate subclasses (58).

Gene	NCBI Reference Sequence	Classification Group	Query Cover	E value	Identical	Experimental Construct
PF08 0106	XP_001349437.1	B/C	100%	0.0	100%	CIDR1 $\alpha$ PF08 0106
MAL7P1.56	XP_001349036.1	C	79%	5e-103	49%	CIDR1 $\alpha$ MAL7P1.56
PF07 0049	XP_001349031.1	C	98%	1e-100	47%	CIDR1 $\alpha$ PF07 0049

**Table 3: Summary of CIDR1 $\alpha$  BLASTp Sequence Analysis.** The CIDR1 $\alpha$  protein sequence from the PF08 0106 *var* gene was used as the original query. Genes showing the most sequence similarity, determined by E-values closest to zero, were chosen for further analysis.

*PfEMP1 Degree and specificity of binding to CD36 is correlated with E-value*

Control, CIDR1 $\alpha$ <sub>PF07 0049</sub>, CIDR1 $\alpha$ <sub>MAL7P1.56</sub>, and CIDR1 $\alpha$ <sub>PF08 0106</sub> coated Bio-Plex beads pre-incubated with PBS, showed mean fluorescent intensity (MFI) values of bound CD36 to be  $401 \pm 8.98$ ,  $937.88 \pm 24.79$ ,  $4022.13 \pm 67.88$ , and  $5702.63 \pm 112.73$ , respectively. Control, CIDR1 $\alpha$ <sub>PF07 0049</sub>, CIDR1 $\alpha$ <sub>MAL7P1.56</sub>, and CIDR1 $\alpha$ <sub>PF08 0106</sub> coated Bio-Plex beads, pre-incubated with anti-ICAM-1 monoclonal antibodies, showed MFI values of  $387.63 \pm 11.65$ ,  $834.13 \pm 12.47$ ,  $3512.13 \pm 85.60$ ,  $5047.63 \pm 88.33$ , respectively. Control, CIDR1 $\alpha$ <sub>PF07 0049</sub>, CIDR1 $\alpha$ <sub>MAL7P1.56</sub>, and CIDR1 $\alpha$ <sub>PF08 0106</sub> coated Bio-Plex beads,

pre-incubated with anti-CD36 monoclonal antibodies, showed MFI values of  $352.50 \pm 8.17$ ,  $808.25 \pm 14.37$ ,  $115.25 \pm 1.70$ ,  $117.50 \pm 3.23$ , respectively (Figure 16A). When compared to the control, there was significantly more CD36 bound to CIDR1 $\alpha_{\text{PF07 0049}}$  ( $P \leq 0.0001$ ), CIDR1 $\alpha_{\text{MAL7P1.56}}$  ( $P \leq 0.0001$ ), and CIDR1 $\alpha_{\text{PF08 0106}}$  ( $P \leq 0.0001$ , Figure 16B). Pre-incubation with anti-CD36 antibody showed reductions of 13.82% for CIDR1 $\alpha_{\text{PF07 0049}}$  ( $P \leq 0.01$ ), 97.13% for CIDR1 $\alpha_{\text{MAL7P1.56}}$  ( $P \leq 0.0001$ ), and 97.94% for CIDR1 $\alpha_{\text{PF08 0106}}$  ( $P \leq 0.0001$ , Figure 16C).

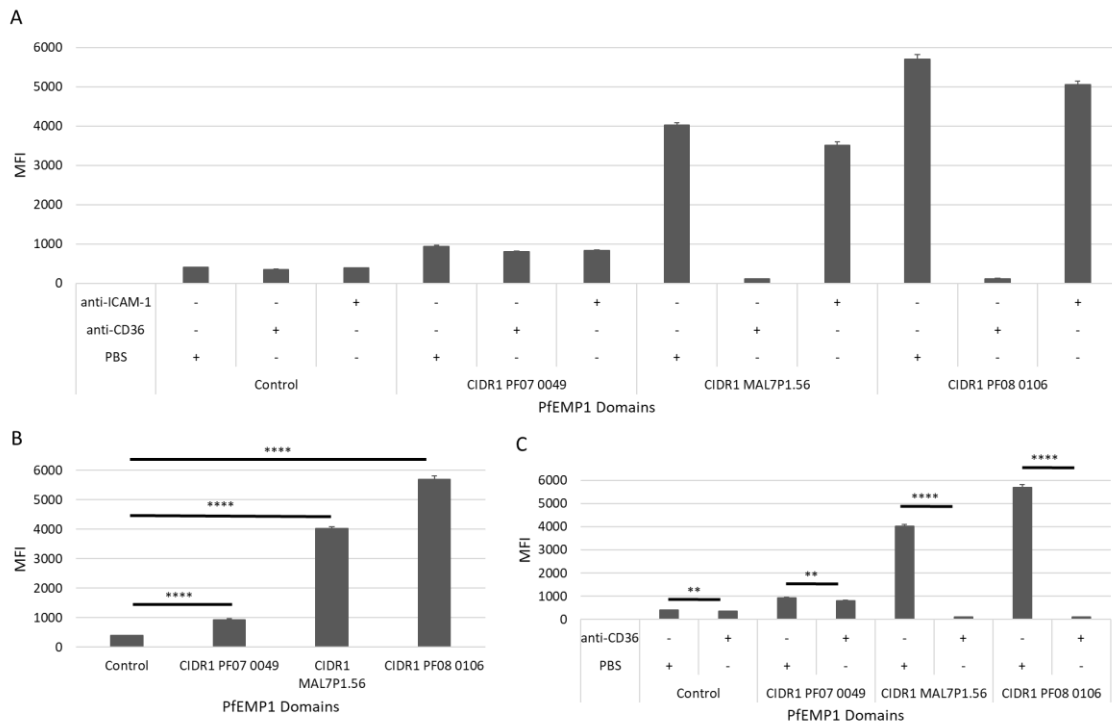


**Figure 16. CD36 Bound to PfEMP1 Domains: A.** CD36 bound to HAE (Control), CIDR1 $\alpha_{\text{PF07 0049}}$ , CIDR1 $\alpha_{\text{MAL7P1.56}}$ , and CIDR1 $\alpha_{\text{PF08 0106}}$  following pre-incubation with PBS, 5  $\mu\text{g/ml}$  anti-CD36 monoclonal antibody, or 5  $\mu\text{g/ml}$  anti-ICAM-1 monoclonal antibody. **B.** CD36 bound to HisAdEx (control), CIDR1 $\alpha_{\text{PF07 0049}}$ , CIDR1 $\alpha_{\text{MAL7P1.56}}$ , and CIDR1 $\alpha_{\text{PF08 0106}}$  following pre-incubation with PBS. **C.** CD36 bound to control, CIDR1 $\alpha_{\text{PF07 0049}}$ , CIDR1 $\alpha_{\text{MAL7P1.56}}$ , and CIDR1 $\alpha_{\text{PF08 0106}}$  following pre-incubation with PBS or anti-CD36. All experiments completed in duplicate and repeated at least twice. Error bars are SEM. Asterisks indicate P-value from Student *t* test. \*\* =  $P \leq 0.01$ ; \*\*\*\* =  $P \leq 0.0001$ .

The samples showed a clear difference in the amount of bound CD36 to the PfEMP1 protein (Figure 17A). Using Pearson's  $r$  Correlation analysis, we compared the MFI from each sample with their corresponding E-value from protein sequence similarity analysis. The relationship showed a strong negative correlation with an  $r$  value of -0.939 (Figure 17B). As the E-value increases, the MFI decreases. Therefore, in the context of CD36 binding, as a PfEMP1 protein's structure becomes more dissimilar to the protein structure of CIDR1 $\alpha$ <sub>PF08 0106</sub>, a proven and strong CD36 binding PfEMP1 protein, the ability to bind to CD36 will decrease.

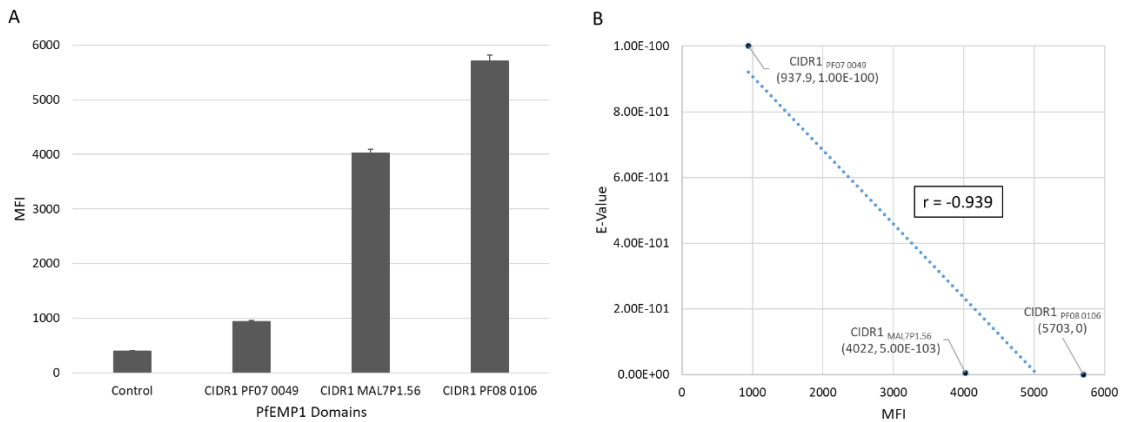


**Figure 17. Correlation between bound CD36 (MFI) and protein sequence similarity:** **A.** CD36 bound to HisAdEx (Control), CIDR1<sub>PF07 0049</sub>, CIDR1<sub>MAL7P1.56</sub>, and CIDR1<sub>PF08 0106</sub> following pre-incubation with PBS. **B.** Scatter plot of MFI values (x-axis) from **A** compared to E-values (y-axis). E-values are protein sequence similarity scores from NCBI Blast protein sequence comparisons.  $r$  is the Pearson Correlation Coefficient. Error bars are SEM. ( $r < 0.5$  = weak correlation,  $0.5 < r < 0.7$  = moderate correlation,  $0.7 < r$  = strong correlation).

#### Equilibrium constant ( $K_D$ ): CD36 avidity is correlated with E-value

Bio-Plex analysis demonstrated that there was a statistically significant amount of CD36 bound to CIDR1 $\alpha$ <sub>PF07 0049</sub> ( $P \leq 0.0001$ ), CIDR1 $\alpha$ <sub>MAL7P1.56</sub> ( $P \leq 0.0001$ ), and CIDR1 $\alpha$ <sub>PF08 0106</sub> ( $P \leq 0.0001$ , Figure 16B). Interacting 3.0 $\mu$ g/ml of CD36 with

CIDR1 $\alpha$ <sub>PF07 0049</sub>, CIDR1 $\alpha$ <sub>MAL7P1.56</sub>, and CIDR1 $\alpha$ <sub>PF08 0106</sub> coated beads resulted in average inverse velocities of  $0.006 \pm 0.002$ ,  $0.026 \pm 0.009$ ,  $0.002 \pm 0.0003$ , respectively.

Interacting 1.0 $\mu$ g/ml of CD36 with CIDR1 $\alpha$ <sub>PF07 0049</sub>, CIDR1 $\alpha$ <sub>MAL7P1.56</sub>, and CIDR1 $\alpha$ <sub>PF08 0106</sub> coated beads resulted in average inverse velocities of  $0.011 \pm 0.0009$ ,  $0.029 \pm 0.009$ ,  $0.006 \pm 0.0009$ , respectively. Interacting 0.3 $\mu$ g/ml of CD36 with CIDR1 $\alpha$ <sub>PF07 0049</sub>,

CIDR1 $\alpha$ <sub>MAL7P1.56</sub>, and CIDR1 $\alpha$ <sub>PF08 0106</sub> coated beads resulted in average inverse velocities of  $0.039 \pm 0.003$ ,  $0.119 \pm 0.028$ ,  $0.015 \pm 0.002$ , respectively. The inverse velocities ( $1/V = \Delta\text{Time}/\Delta\text{MFI}$ ) were plotted against their corresponding inverse concentrations ( $1/C$ ) on a Lineweaver-Burk double reciprocal plot. The line of best fit for CIDR1 $\alpha$ <sub>PF07 0049</sub> was  $y = 0.0111x + 0.0014$ , which produced a  $K_D$  value of 80.03nM (Figure 18A). The line of best fit for CIDR1 $\alpha$ <sub>MAL7P1.56</sub> was  $y = 0.0331x + 0.0067$ , which produced a  $K_D$  value of 67.68nM (Figure 18B). The line of best fit for CIDR1 $\alpha$ <sub>PF08 0106</sub> was  $y = 0.0042x + 0.0014$ , which produced a  $K_D$  value of 41.10nM (Figure 18C).

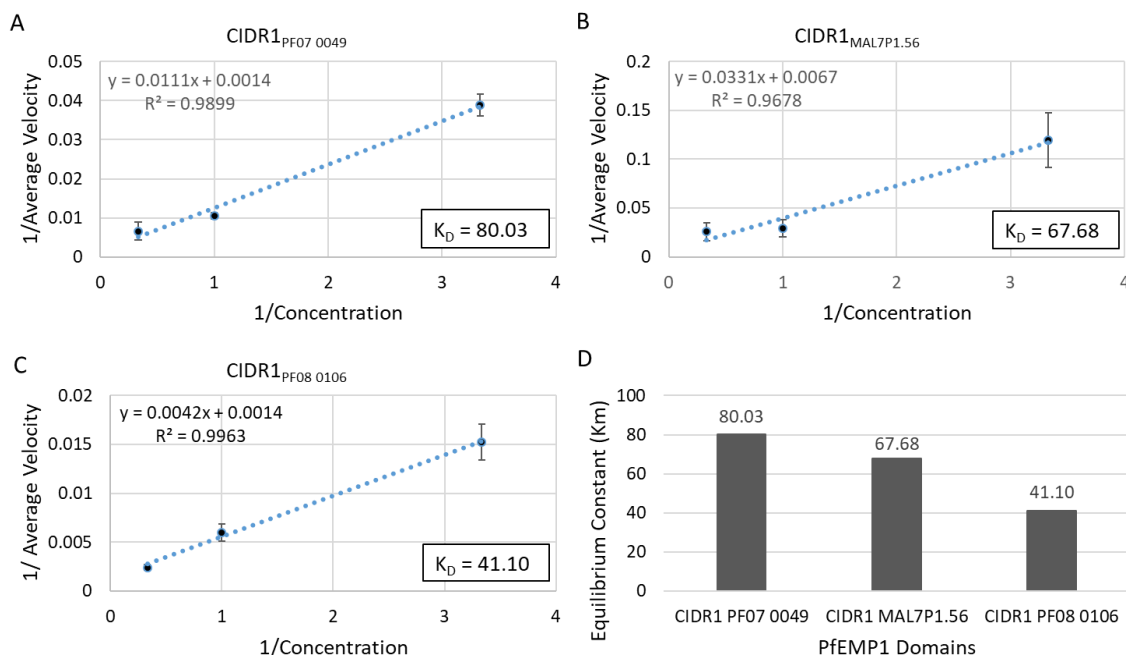


**Figure 18. Avidity of CD36 for PfEMP1 Domains:** The inverse of the CD36 concentrations (3.0 $\mu$ g/ml, 1.0 $\mu$ g/ml, 0.3 $\mu$ g/ml) are on the x-axis and the inverse of the average velocities are on the y-axis for **A.** CIDR1 $\alpha$ <sub>PF07 0049</sub>, **B.** CIDR1 $\alpha$ <sub>MAL7P1.56</sub>, **C.** CIDR1 $\alpha$ <sub>PF08 0106</sub>. **D.**  $K_D$  values are derived where the x-intercept =  $1/K_D$  for each graph. Error bars are SEM.

Using Pearson's  $r$  correlation analysis, we compared the  $K_D$  values from each sample with their corresponding E-value from protein sequence similarity analysis. The relationship between  $K_D$  and E-value showed a strong positive correlation with an  $r$  value of 0.747 (Figure 19). As the  $K_D$  decreases, the E-value also decreases. Therefore, as the avidity of CD36 for the PfEMP1 protein increases (decrease in  $K_D$ ), the protein structure similarities increase (decrease in E-value).

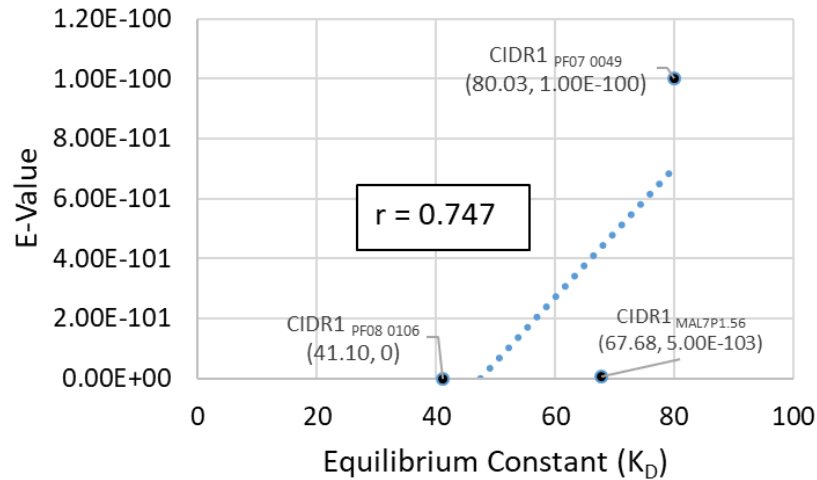


**Figure 19. Correlation between E-value and Equilibrium Constant of CD36: A.** Scatter plot of Equilibrium Constants (x-axis) compared to E-values (y-axis). E-values are protein sequence similarity scores from NCBI Blast protein sequence comparisons.  $r = 0.747$  demonstrating a strong positive correlation.  $r$  is the Pearson Correlation Coefficient. ( $r < 0.5$  = weak correlation,  $0.5 < r < 0.7$  = moderate correlation,  $0.7 < r$  = strong correlation)

*THP-1 surface bound CD36 ligates PfEMP1 coated beads; correlated with E-value and  $K_D$*

To determine if the direct-binding ability of PfEMP1 protein domains to CD36 translates to the ability to ligate to CD36 on monocyte-like THP-1 cells, control, CIDR1 $\alpha$ <sub>PF07\_0049</sub>, CIDR1 $\alpha$ <sub>MAL7P1.56</sub>, and CIDR1 $\alpha$ <sub>PF08\_0106</sub> coated beads were incubated with monocyte-like THP-1 cells. The percentage of control beads ligated by THP-1 cells when pre-incubated with PBS was  $17.51\% \pm 1.39$ , with anti-CD36 was  $14.81\% \pm 0.54$ , and with anti-ICAM-1 was  $14.81 \pm 0.93$ . The percentage of CIDR1 $\alpha$ <sub>PF07\_0049</sub> coated beads ligated by THP-1 cells when pre-incubated with PBS was  $18.72\% \pm 1.84$ , with anti-CD36 was  $11.97\% \pm 0.58$ , and with anti-ICAM-1 was  $18.60\% \pm 0.54$  (Figure 20A). CIDR1 $\alpha$ <sub>PF07\_0049</sub> coated beads showed a statistically significant ability to induce ligation by THP-1

cells compared to the control when the THP-1 cells were pre-incubated with the non-CD36 targeting anti-ICAM-1 antibody ( $p \leq 0.05$ ). Pre-incubation with anti-CD36 antibody reduced the ability of CIDR1 $\alpha_{\text{PF07 0049}}$  to ligate with THP-1 cells by 100% compared to the control. The reduction in ability to ligate by anti-CD36 was statistically significant compared to pre-incubation with non-CD36 targeting anti-ICAM-1 antibody ( $p \leq 0.05$ , Figure 20B).

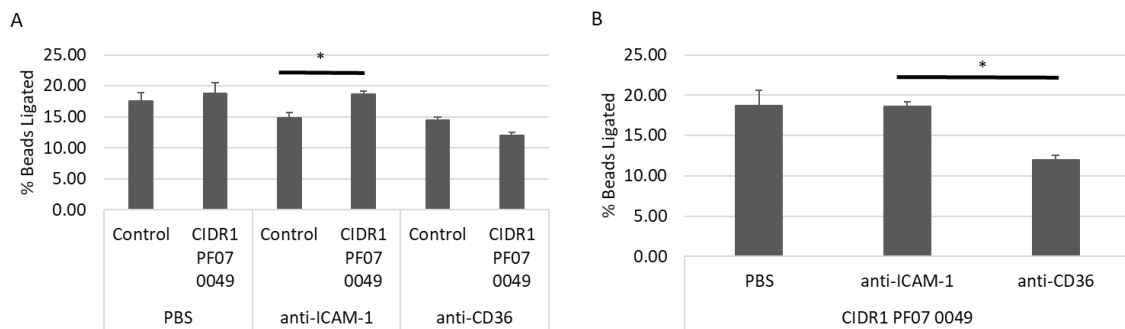


**Figure 20. Percentage of CIDR1 $\alpha_{\text{PF07 0049}}$  coated beads ligated by THP-1:** **A.** The percentage of control and CIDR1 $\alpha_{\text{PF07 0049}}$  coated beads ligated by THP-1 cells pre-incubated with PBS, anti-CD36 monoclonal antibody, and anti-ICAM-1 monoclonal antibody. **B.** The percentage of CIDR1 $\alpha_{\text{PF07 0049}}$  coated beads ligated by THP-1 cells pre-incubated with PBS, anti-CD36, and anti-ICAM-1. Error bars are SEM. Asterisks indicate P-value from Student *t* test. \* =  $P \leq 0.05$ .

The percentage of CIDR1 $\alpha_{\text{MAL7P1.56}}$  coated beads ligated by THP-1 cells when pre-incubated with PBS was  $21.40\% \pm 0.27$ , with anti-CD36 was  $16.78\% \pm 2.45$ , and with anti-ICAM-1 was  $21.04\% \pm 0.71$  (Figure 21A). CIDR1 $\alpha_{\text{MAL7P1.56}}$  coated beads showed a statistically significant ability to induce ligation by THP-1 cells compared to the control when the THP-1 cells were pre-incubated with the non-CD36 targeting anti-ICAM-1 antibody ( $p \leq 0.01$ ). Pre-incubation with anti-CD36 antibody reduced the ability



of CIDR1 $\alpha$ <sub>MAL7P1.56</sub> to induce ligation to THP-1 cells compared to pre-incubation with PBS and non-CD36 targeting anti-ICAM-1 antibody (Figure 21B).

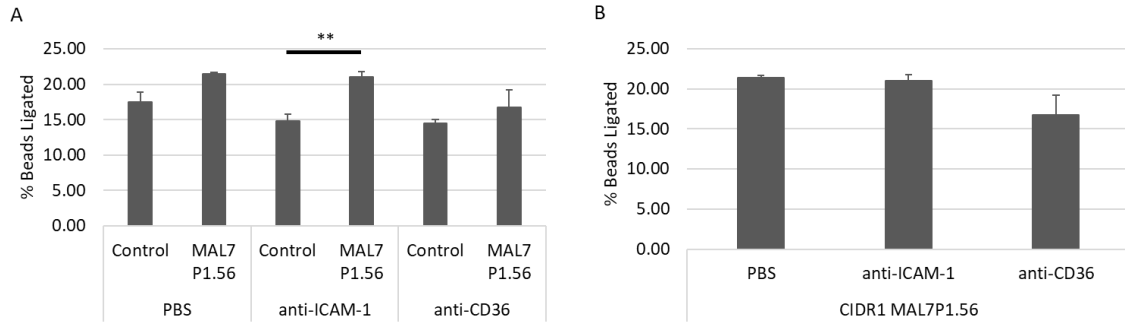


**Figure 21. Percentage of CIDR1 $\alpha$ <sub>MAL7P1.56</sub> coated beads ligated by THP-1:** **A.** The percentage of control and CIDR1 $\alpha$ <sub>MAL7P1.56</sub> coated beads ligated by THP-1 cells pre-incubated PBS, anti-CD36 monoclonal antibody, and anti-ICAM-1 monoclonal antibody. **B.** The percentage of CIDR1 $\alpha$ <sub>MAL7P1.56</sub> coated beads ligated by THP-1 cells pre-incubated with PBS, anti-CD36, and anti-ICAM-1. Error bars are SEM. Asterisks indicate P-value from Student *t* test. \*\* =  $P \leq 0.01$ .

The percentage of CIDR1 $\alpha$ <sub>PF08 0106</sub> coated beads ligated by THP-1 cells when pre-incubated with PBS was  $27.14\% \pm 1.02$ , with anti-CD36 was  $20.35\% \pm 0.88$ , and with anti-ICAM-1 was  $29.18\% \pm 5.42$  (Figure 22A). CIDR1 $\alpha$ <sub>PF08 0106</sub> coated beads showed a statistically significant ability to induce ligation by THP-1 cells compared to the control when the THP-1 cells were pre-incubated with PBS ( $p \leq 0.05$ ), anti-CD36 ( $p \leq 0.05$ ), and anti-ICAM-1 ( $p \leq 0.01$ ). The reduction in ability to ligate by anti-CD36 was statistically significant compared to pre-incubation with PBS ( $p \leq 0.05$ , Figure 22B).

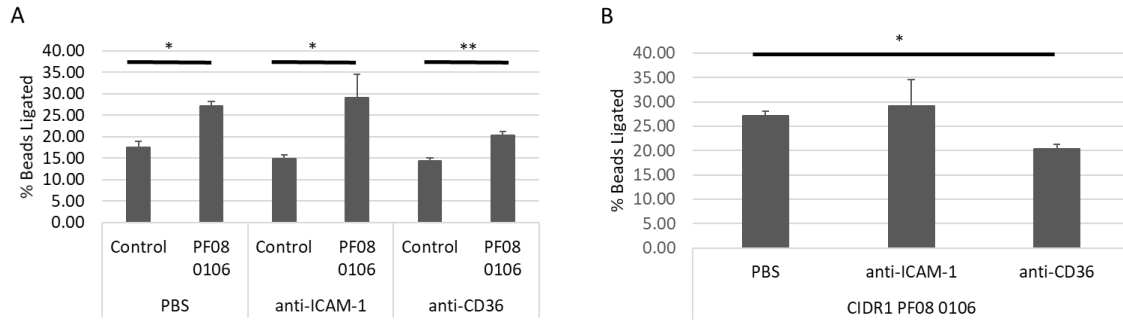


**Figure 22. Percentage of CIDR1 $\alpha$ PF08 0106 coated beads ligated by THP-1:** **A.** The percentage of control and CIDR1 $\alpha$ PF08 0106 coated beads ligated by THP-1 cells pre-incubated PBS, anti-CD36 monoclonal antibody, and anti-ICAM-1 monoclonal antibody. **B.** The percentage of CIDR1 $\alpha$ PF08 0106 coated beads phagocytosed by THP-1 cells pre-incubated with PBS, anti-CD36, and anti-ICAM-1. Error bars are SEM. Asterisks indicate P-value from Student *t* test. \* =  $P \leq 0.05$ , \*\* =  $P \leq 0.01$ .

The PfEMP1 coupled beads showed a varied ability to ligate to THP-1 cells via CD36, which was dependent on which PfEMP1 was attached to the beads. When adjusted for the control, 1.21% of CIDR1 $\alpha$ PF07 0049 coated beads were ligated by THP-1 cells, 3.89% of CIDR1 $\alpha$ MAL7P1.56 coated beads were ligated, and 9.63% of CIDR1 $\alpha$ PF08 0106 coated beads were ligated (Figure 23A). Using Pearson's *r* correlation analysis, we compared the percentage of PfEMP1 coated beads ligated by THP-1 cells to the corresponding E-value from protein sequence similarity analysis and PfEMP1 specific CD36 equilibrium constant ( $K_D$ ). The relationship between percentage of beads ligated and E-value showed a strong negative correlation with an *r* value of -0.748 (Figure 23B). As the percentage of beads ligated increased, the E-value decreased. Therefore, in the context of CD36 ligation, as the ability of the PfEMP1 protein to ligate to THP-1 cells increases, the PfEMP1 protein structure similarities increase (decrease in E-value). The relationship between percentage of beads ligated and  $K_D$  showed a very strong negative correlation with an *r* value of -1.0 (Figure 23C). As the percentage of beads ligated to

THP-1 cells increased, the  $K_D$  of bound CD36 decreased. Therefore, in the context of CD36 ligation, an increase in ligation to THP-1 cells is related to an increase in CD36 avidity (decrease in  $K_D$ ).

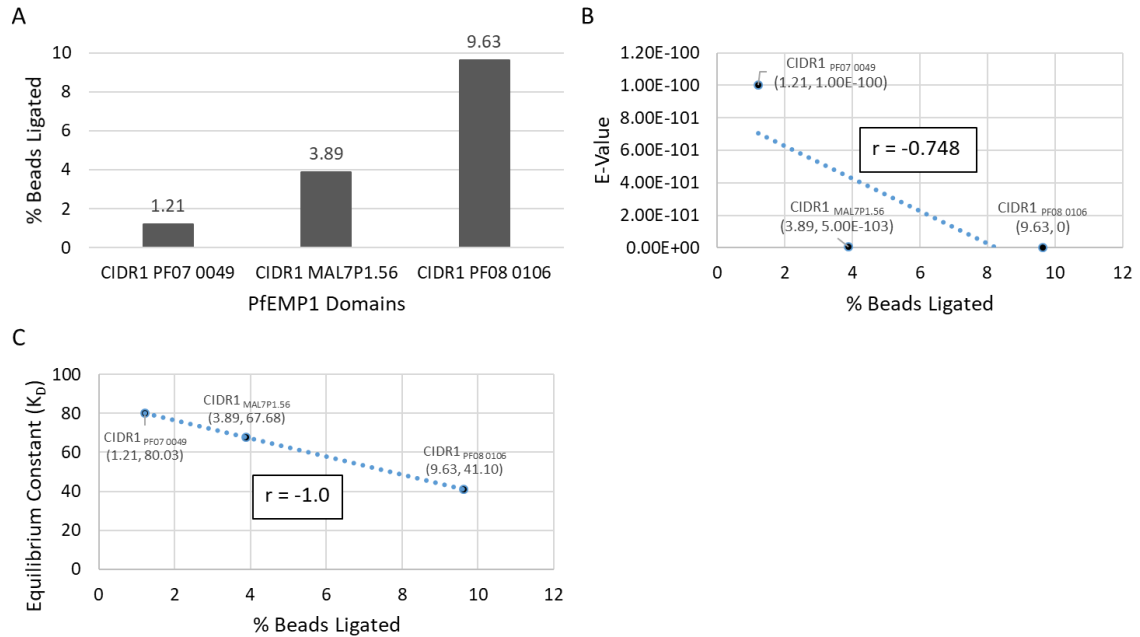


**Figure 23. Correlation between % beads ligated to THP-1, E-value and  $K_D$  of CD36:** **A.** The percentage of CIDR1 $\alpha$ <sub>PF07 0049</sub>, CIDR1 $\alpha$ <sub>MAL7P1.56</sub>, and CIDR1 $\alpha$ <sub>PF08 0106</sub> coated beads ligated by THP-1 cells. **B.** Scatter plot of % beads ligated (x-axis) compared to E-values (y-axis).  $r = -0.748$  demonstrating a strong negative correlation. **C.** Scatter plot of % beads ligated (x-axis) compared to  $K_D$  (y-axis) of PfEMP1-bound CD36.  $r = -1.0$  demonstrating a strong positive correlation.  $r$  is the Pearson Correlation Coefficient. ( $r < 0.5$  = weak correlation,  $0.5 < r < 0.7$  = moderate correlation,  $0.7 < r$  = strong correlation)

### THP-1 ligation to CIDR1 $\alpha$ -containing PfEMP1 subset produces anti-inflammatory effects

THP-1 cells were incubated for 0, 12, and 24 hours in a 48 well plate with empty wells, HAE (control) surface-immobilized wells, and DBL2 $\beta$ <sub>3PF11 0521</sub> surface-immobilized wells. The supernatants were collected and tested for the production of IL-

1ra, IL-1 $\beta$ , IL-2, IL-6, IL-8, IL-10, IL-12 (p40), IL-12 (p70), IL-13, IL-19, IL-20, IL-22, IL-26, IL-27, IL28a, IL29, IFN- $\gamma$ , MCP-1, MIP-1 $\alpha$ , and TNF- $\alpha$ . Only detected cytokines and statistically significant reductions or increases in the production of cytokines were reported.

THP-1 cells incubated in CIDR1 $\alpha$ <sub>PF07 0049</sub> coated wells for 24 hours produced less IL-1 $\beta$  ( $6.09 \pm 0.02$  pg/ml) than THP-1 cells alone ( $9.74 \pm 0.36$  pg/ml) and significantly less than the control incubated THP-1 cells ( $13.89 \pm 0.38$  pg/ml,  $P \leq 0.05$ , Figure 24A). THP-1 cells incubated for 24 hours in CIDR1 $\alpha$ <sub>PF07 0049</sub> coated wells produced  $197.94 \pm 9.25$  pg/ml of IL-8, which was less than THP-1 cells alone ( $636.73 \pm 36.09$  pg/ml) and significantly less than the control incubated THP-1 cells ( $290.85 \pm 4.45$  pg/ml,  $P \leq 0.05$ , Figure 24B).

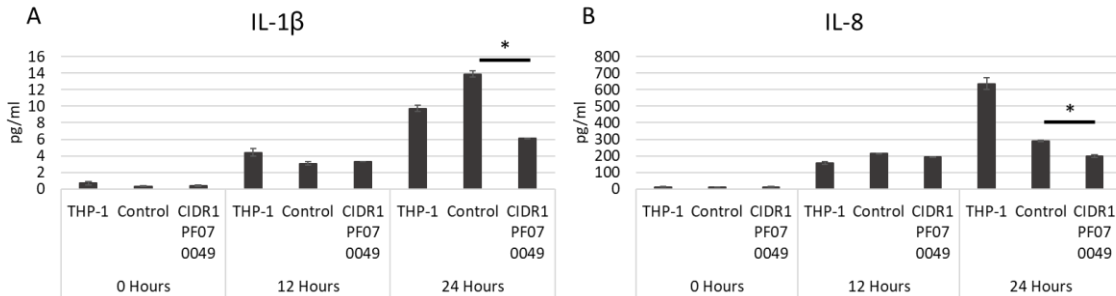


**Figure 24. Cytokine/Chemokine production from CD36::CIDR1 $\alpha$ <sub>PF07 0049</sub> ligation:** The amount of **A.** IL-1 $\beta$ , **B.** IL-8 produced after 0, 12, 24 hours of incubation in empty, HAE coated, or CIDR1 $\alpha$ <sub>PF07 0049</sub> coated wells. All samples were analyzed with a one-way ANOVA followed by a two-tailed T. Test with two sample equal variance and a 95% confidence (\* =  $P \leq 0.05$ ). Error bars are SEM.

THP-1 cells incubated in CIDR1 $\alpha$ <sub>MAL7P1.56</sub> coated wells for 12 hours produced more IL-1ra ( $7308.94 \pm 178.06$  pg/ml) than THP-1 cells alone ( $2903.33 \pm 133.28$  pg/ml)

and significantly more than the control incubated THP-1 cells ( $4850.39 \pm 256.30$  pg/ml,  $P \leq 0.05$ , Figure 25).

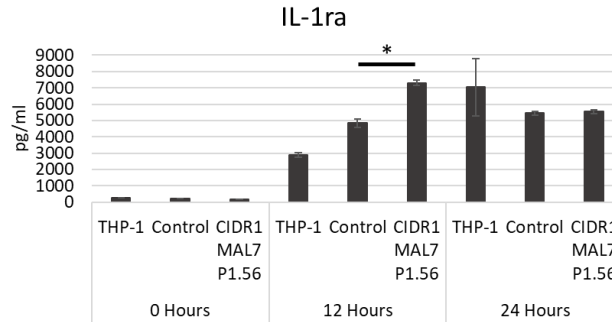


**Figure 25. Cytokine/Chemokine production from CD36::CIDR1αMAL7P1.56 ligation:** The amount of IL-1ra produced after 0, 12, 24 hours of incubation in empty, HAE coated, or CIDR1αMAL7P1.56 coated wells. All samples were analyzed with a one-way ANOVA followed by a two-tailed T. Test with two sample equal variance and a 95% confidence (\* =  $P \leq 0.05$ ). Error bars are SEM.

THP-1 cells incubated in CIDR1αPF08 0106 coated wells for 24 hours produced less IL-1β ( $7.09 \pm 0.28$  pg/ml) than THP-1 cells alone ( $9.74 \pm 0.36$  pg/ml) and significantly less than the control incubated THP-1 cells ( $13.89 \pm 0.38$  pg/ml,  $P \leq 0.01$ , Figure 26A). THP-1 cells incubated for 24 hours in CIDR1αPF08 0106 coated wells produced  $167.62 \pm 3.37$  pg/ml of IL-8, which was less than THP-1 cells alone ( $636.73 \pm 36.09$  pg/ml) and significantly less than the control incubated THP-1 cells ( $290.85 \pm 4.45$  pg/ml,  $P \leq 0.01$ , Figure 26B). After 12 hours of ligation, there was a decrease in IL-6 and an increase in both IL-1ra and MIP-1α, although not statistically significant compared to the control. After 24 hours of ligation, there was a decrease in MCP-1 and TNF-α while there was an increase in MIP-1α, although not statistically significant compared to the control.

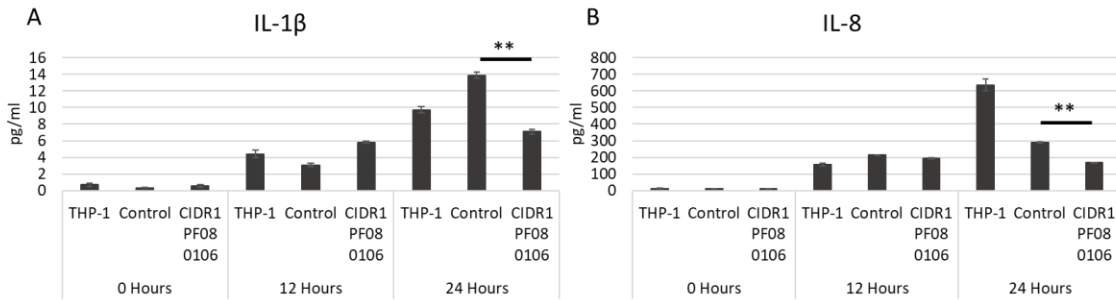


**Figure 26. Cytokine/Chemokine production from CD36::CIDR1αPF08 0106 ligation:** The amount of **A.** IL-1β, and **B.** IL-8 produced after 0, 12, 24 hours of incubation in empty, HAE coated, or CIDR1αPF08 0106 coated wells. All samples were analyzed with a one-way ANOVA followed by a two-tailed T. Test with two sample equal variance and a 95% confidence (\*\* =  $P \leq 0.01$ ). Error bars are SEM.

#### THP-1 cell ligation to CIDR1αPF08 0106 has a mixed effect on gene expression

The study demonstrated an extremely high level of reproducibility and precision based on Pearson r Correlation between all samples ( $R^2 \geq 0.991$ , Figure 27A). Cluster analysis of differentially expressed genes (DEG) demonstrated that there are some genes upregulated and others downregulated in THP-1 cells when incubated with CIDR1αPF08 0106 compared to HAE (Figure 27B). Analysis of the DEGs determined that the downregulation of specific genes, including keratin producing KRT14 and KRT18, fat-binding APOE, and pro-inflammatory TNF were statistically significant. Additionally, the upregulation of specific genes producing membrane associated EMP1, lipid-binding PLIN2, and pro-inflammatory CSF1 were statistically significant. Therefore, gene ontology (GO) analysis determined that there was a mixed reaction because some of the affected genes are involved in the inflammatory response were downregulated (TNF) and the others were upregulated (CSF1). Further analysis will be needed to determine why KRT14, KRT18, APOE, EMP1, and PLIN2 were also impacted by THP-1::CIDR1αPF08

0106 interaction. This is a significantly new data set and further analysis of the pathways and genes involved should be continued.

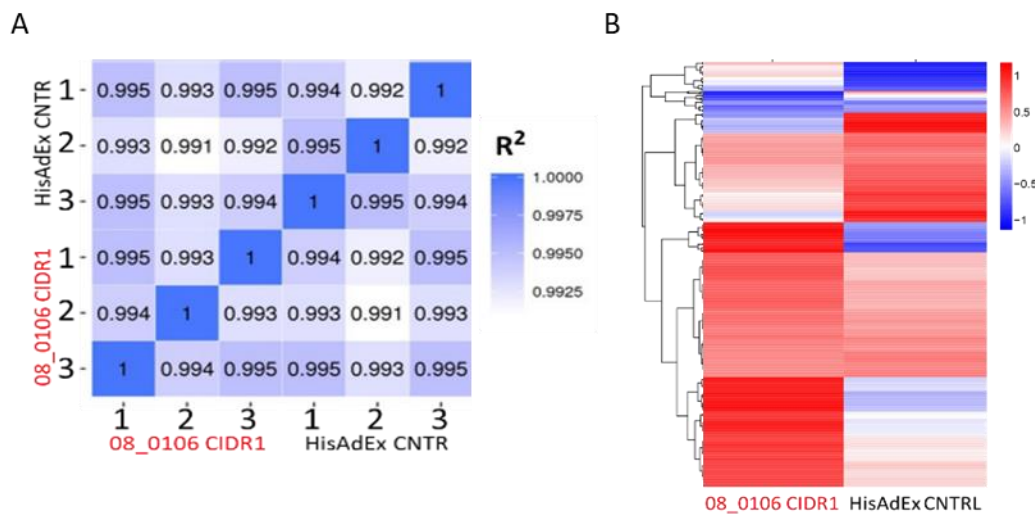


**Figure 27. RNASeq Analysis from THP-1 ligation to HAE and CIDR1 $\alpha$ PF08 0106:** **A.** Pearson correlation analysis of all samples **B.** Cluster analysis of differentially expressed genes (DEG).

## Discussion

CD36 ligation to PfEMP1 proteins has varying effects depending on the cells and tissues involved. In platelets, CD36::PfEMP1 ligation contributes to platelet clumping that is thought to be protective against malaria infection by activating platelets to release a platelet effector molecule (115). In endothelial cells, CD36::PfEMP1 ligation allows iRBCs to sequester in the vascular endothelium of tissues and organs (110, 116). In antigen-presenting immune cells (APCs), CD36::PfEMP1 ligation can mediate phagocytosis of iRBCs and production of pro-inflammatory TNF- $\alpha$  and IL-12 cytokines, which can promote a Th1 response and the further production of IFN $\gamma$  by T-cells (17, 114).

Several conserved structural features found within the CIDR domain region may determine the strength of CD36 binding (117). The CIDR $\alpha$  domain contains three-helical bundles with insertions between the helices that form a hydrophobic cavity for CD36 binding; this conserved region is present in approximately 85% of PfEMP1 proteins containing CIDR $\alpha$  domains (111, 112). Therefore, the PfEMP1 protein's sequence is important in understanding and possibly predicting CD36-mediated sequestration of malaria.

In this study, we predicted that protein sequence similarity toward the strong CD36-binding CIDR1 $\alpha$ <sub>PF08 0106</sub> PfEMP1 protein construct would predict similar CD36 binding strength and avidity. Using the NCBI-BLASTp sequence comparison database, we determined that the CIDR1 $\alpha$ <sub>MAL7P1.56</sub> and CIDR1 $\alpha$ <sub>PF07 0049</sub> constructs were the most closely related to CIDR1 $\alpha$ <sub>PF08 0106</sub>. In this limited set, CIDR1 $\alpha$ <sub>MAL7P1.56</sub> was more similar than CIDR1 $\alpha$ <sub>PF07 0049</sub>. Therefore, CD36 was predicted to have a lower  $K_D$  toward CIDR1 $\alpha$ <sub>MAL7P1.56</sub> compared to CIDR1 $\alpha$ <sub>PF07 0049</sub>. CIDR1 $\alpha$ <sub>PF08 0106</sub> expectedly had the lowest  $K_D$  (41.10nM), then CIDR1 $\alpha$ <sub>MAL7P1.56</sub> (67.68nM), and CIDR1 $\alpha$ <sub>PF07 0049</sub> (80.03nM, Figure 18D). Therefore, in-line with the hypothesis, CD36's avidity for PfEMP1 domain constructs decreased as the differences in PfEMP1 protein sequences toward CIDR1 $\alpha$ <sub>PF08 0106</sub> increased.

CD36 is one of the few cell surface receptors, implicated in malaria pathology, which has been studied for its role in immune recognition of PfEMP1 proteins (17, 110, 114, 116). Based on our CD36 binding and avidity results, we predicted that a strong CD36::PfEMP1 interaction will show a stronger ability to elicit a pro-inflammatory immune response, including the release of pro-inflammatory cytokine/chemokines by



immune cells, compared to weaker CD36::PfEMP1 interactions. Since we wanted to determine the immune response in naïve hosts, those who suffer the highest mortalities, we chose non-stimulated monocyte-like THP-1 cells to simulate a circulating monocyte, which would have a high probability of encountering a PfEMP1-expressing iRBC in the vasculature. Upon incubation of THP-1 cells with CIDR1 $\alpha$ <sub>PF08 0106</sub>, CIDR1 $\alpha$ <sub>MAL7P1.56</sub>, and CIDR1 $\alpha$ <sub>PF07 0049</sub> coated beads, the highest percentage of beads ligated by THP-1 cells were the CIDR1 $\alpha$ <sub>PF08 0106</sub> coated beads, the second highest was CIDR1 $\alpha$ <sub>MAL7P1.56</sub> beads, and the least able to ligate to THP-1 cells was the CIDR1 $\alpha$ <sub>PF07 0049</sub> coated beads (Figure 23A). This suggests PfEMP1 proteins with less protein sequence differences toward CIDR1 $\alpha$ <sub>PF08 0106</sub> have a stronger ability to bind CD36 with high avidity and possess a greater ability to ligate to monocyte-like THP-1 cells (Figure 25B & C). Interestingly, following 24 hours after initial ligation of CD36::CIDR1 $\alpha$ <sub>PF07 0049</sub>, the production of pro-inflammatory IL-1 $\beta$  and IL-8 was reduced, indicating suppression of an immune response (Figure 24). After 12 hours, ligation of CIDR1 $\alpha$ <sub>MAL7P1.56</sub> with CD36 on THP-1 cells produced significantly more IL-1ra than the control. An increase of IL-1ra would create competition for the interleukin-1 receptor (IL-1r), which could diminish the pro-inflammatory response from IL-1::IL-1r ligation, since there could be less IL-1r available. The ligation of CD36::CIDR1 $\alpha$ <sub>MAL7P1.56</sub> is not directly reducing the production of pro-inflammatory molecules like CIDR1 $\alpha$ <sub>PF07 0049</sub>, but instead, increasing the production of an anti-inflammatory molecule (Figure 25). Interestingly, ligation of CIDR1 $\alpha$ <sub>PF08 0106</sub> with CD36 on THP-1 cells produced a similar immune suppressive response as the ligation of CD36::CIDR1 $\alpha$ <sub>PF07 0049</sub>. After 24 hours the ligation of CD36::CIDR1 $\alpha$ <sub>PF08 0106</sub> reduced the production of pro-inflammatory IL-1 $\beta$  and IL-8,

which again, appears to be an immune suppressive response (Figure 26). Although not statistically significant, there was also a reduction in the production of TNF- $\alpha$ . Similarly, direct signaling through CD36 crosslinking on murine macrophage also resulted in a reduction in TNF- $\alpha$  production (118). Since CIDR1 $\alpha_{\text{PF08 0106}}$ , CIDR1 $\alpha_{\text{MAL7P1.56}}$ , and CIDR1 $\alpha_{\text{PF07 0049}}$  ligation to CD36 produced generally an anti-immune response, the malaria parasite might be trying to reduce the immune system's ability to mount an immune response through direct PfEMP1::CD36 ligation. It is worth noting that there was a detected increase in production of cytokines over time from our control THP-1 cells. Possible causes and solutions were discussed in Chapter II: ICAM-1 Studies – Discussion.

Analyzing supernatants for cytokine expression was a perfect exploratory assay to survey possible immune responses with a high-throughput design. Another effective method would be to look at the differentially expressed genes (DEG) from THP-1 cells interacting with PfEMP1 proteins. We compared the DEG from our THP-1 cells incubated with surface-immobilized CIDR1 $\alpha_{\text{PF08 0106}}$  to THP-1 cells incubated with surface-immobilized control, after 3 hours of incubation. Similar to cytokine analysis, there was a downregulation in the gene coding for TNF, which could lead to a reduction in inflammation. However, the CSF1 gene that codes for macrophage colony-stimulating factor 1 (CSF1) was upregulated, which could play a role in cell survival and differentiation of mononuclear phagocytes.

In conclusion, our study sought to determine if overall protein sequence similarity toward the CD36-binding CIDR1 $\alpha_{\text{PF08 0106}}$  protein construct plays a role in CD36 binding strength and avidity. Using our bead-based iRBC model expressing one target PfEMP1

protein at a time, the strength in binding ability and avidity of CD36 toward PfEMP1 proteins containing similar protein sequences, is in line with published literature that claims a highly conserved hydrophobic pocket found within ~85% of CIDR1 $\alpha$ -containing PfEMP1 proteins is responsible for providing a docking point for CD36 (112). Since CD36-dependent tissue sequestration is important for malaria growth and prolonged infection (119), the conserved hydrophobic pocket might serve as a possible vaccine or anti-adhesion drug target. Next, we wanted to understand if immune cell interaction with CD36-binding PfEMP1 proteins would contribute to a pro-inflammatory immune response and whether the intensity of the immune response would follow the same trend in CD36 binding based on sequence similarity. Interestingly, the strength in binding to CD36, determined by  $K_D$  value, was strongly correlated with the ability to induce ligation and, potentially, phagocytosis to THP-1 cells through CD36. Through immune cell ligation, cytokine production, and DEG analysis we found that PfEMP1 ligation to CD36 produces a mixed immune response, where some inflammatory genes were upregulated, while the production of some inflammatory cytokines were reduced and anti-inflammatory cytokines were increased. Thus, it appears that ligation of CD36 on the surface of THP-1 cells might produce mixed signaling and the net result may depend on the strength of CD36::PfEMP1 domain interaction or protein sequence identity of interacting CD36-binding PfEMP1 domain, which is worth further investigation.

## CHAPTER V: iRBC STUDIES AND CONCLUSION

### Abstract

Utilizing a PfEMP1-coated 5 $\mu$ m bead to simulate an iRBC displaying a specific PfEMP1 protein on the surface, we have shown that DBL2 $\beta$ <sub>PF11 0521</sub>, DBL2 $\delta$ <sub>PFL 2665c</sub>, and CIDR1 $\alpha$ <sub>PF08 0106</sub> strongly bind to ICAM-1, integrin  $\alpha$ V $\beta$ 3, and CD36, respectively. Depending on the naïve host's immune response, the parasite could be eliminated, severe complications could develop as a result of an overactive immune response, or the parasite could suppress an immune response. THP-1 cell ligation to surface-immobilized DBL2 $\beta$ <sub>PF11 0521</sub>, DBL2 $\delta$ <sub>PFL 2665c</sub>, and CIDR1 $\alpha$ <sub>PF08 0106</sub> resulted in anti-inflammatory effects (DBL2 $\beta$ <sub>PF11 0521</sub> and DBL2 $\delta$ <sub>PFL 2665c</sub>) or mixed immune effects (CIDR1 $\alpha$ <sub>PF08 0106</sub>). Characterizing specific PfEMP1::cell surface receptor interactions offers important information toward fully understanding and possibly predicting a host's immune response to the malaria parasite. Since the interaction of an iRBC with an immune cell is a complex interaction leading to various immune responses and evasion techniques, it is important to compare our naïve host immune interaction bead-based simulation model with actual iRBC::THP-1 interactions. Using the ICAM-1-binding 3G8 (IT4) clone and the integrin  $\alpha$ V $\beta$ 3/CD36-binding E9 (NF54) clone of *P. falciparum*, the elicited immune responses by THP-1 cells from the PfEMP1 surface-immobilized ligation experiments were compared to effects induced by incubation of THP-1 cells with live

iRBCs. The PfEMP1 surface-immobilized ligation experiments produced mainly anti-inflammatory effects, while the interaction with 3G8 and E9 iRBCs produced mainly pro-inflammatory effects.

## Introduction

In the previous chapters, utilizing a PfEMP1-coated 5 $\mu$ m bead to simulate an iRBC displaying a specific PfEMP1 protein on the surface, we have shown that DBL2 $\beta$ <sub>PF11 0521</sub>, DBL2 $\delta$ <sub>PFL 2665c</sub>, and CIDR1 $\alpha$ <sub>PF08 0106</sub> strongly bind to ICAM-1 ( $K_D$  = 7.62nM), integrin  $\alpha$ V $\beta$ 3 ( $K_D$  = 62.20nM), and CD36 ( $K_D$  = 41.10nM), respectively. Characterizing specific PfEMP1::cell surface receptor interactions offers important information toward fully understanding and possibly predicting a host's immune response to the malaria parasite.

Depending on the naïve host's immune response, the parasite could be eliminated (114), severe complications could develop as a result of an overactive immune response (129), or the parasite could suppress an immune response. To simulate a naïve circulating innate immune cell interacting with an iRBC, we incubated DBL2 $\beta$ <sub>PF11 0521</sub>, DBL2 $\delta$ <sub>PFL 2665c</sub>, and CIDR1 $\alpha$ <sub>PF08 0106</sub> coated beads or as surface-immobilized proteins with monocyte-like THP-1 cells to determine if ligation through PfEMP1 proteins would lead to inflammatory cytokine release. The DBL2 $\beta$ <sub>PF11 0521</sub> coated beads did not ligate to THP-1 cells better than control beads, but DBL2 $\delta$ <sub>PFL 2665c</sub> coated beads showed the ability to ligate, while CIDR1 $\alpha$ <sub>PF08 0106</sub> showed a statistically significant ability to ligate to monocyte-like THP-1 cells better than control beads. Ligation to surface-immobilized domains, precluding phagocytosis, through DBL2 $\beta$ <sub>PF11 0521</sub>, DBL2 $\delta$ <sub>PFL 2665c</sub>, and CIDR1 $\alpha$ <sub>PF08 0106</sub> resulted in decreases in the production of IL-1 $\beta$  and IL-8, while

increasing the production of IL-1ra. Therefore, PfEMP1 ligation to THP-1 surface receptors ICAM-1, integrin  $\alpha V\beta 3$ , and CD36 resulted in an anti-inflammatory response. Since the interaction of an iRBC with an immune cell is a complex interaction leading to various immune responses or evasion mechanisms (130), it is important to compare our naïve host immune interaction bead-based simulation model with actual iRBC::THP-1 interactions.

Using the ICAM-1-binding 3G8 (IT4) clone and the integrin  $\alpha V\beta 3$ /CD36-binding E9 clone of *P. falciparum*, the elicited immune responses from the bead-based experiments were compared to iRBC interactions with monocyte-like THP-1 cells.

## **Materials and Methods**

### **THP-1 Culture**

THP-1 cells, kindly provided by Dr. Yoshimi Shibata from Florida Atlantic University, were cultured in RPMI 1640 growth medium, supplemented with 25 $\mu$ g/ml gentamicin sulfate, 0.125 $\mu$ g/ml Amphotericin B, and 10% heat-inactivated FBS. The cells were cultured below 5X10<sup>5</sup> cells/ml in order to maintain an unstimulated, nonadherent monocyte population to simulate naïve host immune cells for cytokine analysis. Antibiotic and anti-fungal additives were withheld from the media for all experiments requiring binding.

### **Parasite Culture**

The 3G8 (IT4) and E9 (NF54) lines were cultured in O+ red blood cells at 2% hematocrit in complete RPMI 1640 growth medium, supplemented with 40 $\mu$ g/ml

gentamicin sulfate and 10% heat-inactivated human serum. The parasites were cultured at 37°C in a gas mixture of 5% CO<sub>2</sub>, 5% O<sub>2</sub>, and 90% N<sub>2</sub>. They were cultured for at least 5 cycles before trophozoite stage enrichment. Testing for the presence of mycoplasma in parasite cultures using PCF primers (5'-ACA CCA TGG GAG CTG GTA AT and 5'-CTT CWT CGA CTT YCA GAC CCA AGG CAT) was negative.

Before iRBC experimentation, trophozoite enrichment was completed to deplete cells not displaying PfEMP1 proteins on their surface (ring stage, RBC, etc.). The trophozoites, displaying PfEMP1 proteins on their surface, were retained by magnetic LD column separation (Milteni Biotec, Cat# 130-042-901), as described by the manufacturer. For experimentation, the elution of trophozoites was washed in RPMI 1640 and resuspended in RPMI 1640, supplemented with 10% heat-inactivated FBS. Experimental parasitemia levels were between 50-90% for experimentation.

#### *iRBC::THP-1 cytokine and chemokine analysis and statistical comparison*

4.0x10<sup>5</sup> THP-1 cells were incubated with 1.0x10<sup>6</sup> enriched 3G8 or E9 iRBCs in a 96 well plate at 37°C for 0, 12, and 24 hours. The supernatants were collected and analyzed using Bio-Plex Pro Human Cytokine kits testing for the presence of IL-1ra, IL-1β, IL-2, IL-6, IL-8, IL-10, IL-12 (p40), IL-12 (p70), IL-13, IL-19, IL-20, IL-22, IL-26, IL-27, IL28a, IL29, IFN-γ, MCP-1, MIP-1α, and TNF-α. 4 parameter logistic (4PL) or 5 parameter logistic (5PL) standard curves for each cytokine/chemokine were created using the provided standards with the concentration on the x-axis and the MFI on the y-axis. Unknown sample concentrations were determined by fitting the MFI values to the measured standard curves using the Bio-Plex Manager 5.0 software and confirmed by

MyCurveFit online-based application. All samples were analyzed with a one-way ANOVA followed by a two-tailed T. Test with two sample equal variance and a 95% confidence interval using both Microsoft Excel and Bio-Plex Manager 5.0 (\* =  $P \leq 0.05$ , \*\* =  $P \leq 0.01$ , \*\*\* =  $P \leq 0.001$ , \*\*\*\* =  $P \leq 0.0001$ ). Only statistically significant experimental values compared to the RBC control are reported. All graphical error bars are Standard Error of Means (SEM).

## Results

### THP-1::3G8 iRBC interaction produces mainly pro-inflammatory effects

THP-1 cells were incubated with ICAM-1-binding 3G8 iRBCs, control uninfected RBCs, and empty wells for 0, 12, and 24 hours. The supernatants were collected and tested for the production of IL-1 $\alpha$ , IL-1 $\beta$ , IL-2, IL-6, IL-8, IL-10, IL-12 (p40), IL-12 (p70), IL-13, IL-19, IL-20, IL-22, IL-26, IL-27, IL28a, IL29, IFN- $\gamma$ , MCP-1, MIP-1 $\alpha$ , and TNF- $\alpha$ . Only detected cytokines and statistically significant reductions or increases in the production of cytokines were reported.

THP-1 cells incubated for 12 hours with 3G8 iRBCs produced  $218.12 \pm 2.10$  pg/ml of IL-8, which was more than the THP-1 cells alone ( $156.64 \pm 8.03$  pg/ml) and significantly more than THP-1 cells incubated with RBC ( $160.03 \pm 2.96$  pg/ml,  $P \leq 0.01$ ). THP-1 cells incubated for 24 hours with 3G8 iRBCs produced  $1027.62 \pm 45.01$  pg/ml of IL-8, which was more than the THP-1 cells alone ( $636.73 \pm 36.09$  pg/ml) and significantly more than the THP-1 cells incubated with RBC ( $521.88 \pm 12.90$  pg/ml,  $P \leq 0.05$ , Figure 28A). THP-1 cells incubated for 24 hours with 3G8 iRBCs produced  $737.44 \pm 13.80$  pg/ml of MCP-1, which was more than the THP-1 cells alone ( $564.80 \pm 25.99$



pg/ml) and significantly more than the THP-1 cells incubated with RBC ( $493.52 \pm 13.67$  pg/ml,  $P \leq 0.01$ , Figure 28B). THP-1 cells incubated for 12 hours with 3G8 iRBCs produced  $124.84 \pm 1.96$  pg/ml of MIP-1 $\alpha$ , which was more than the THP-1 cells alone ( $48.32 \pm 0.65$  pg/ml) and significantly more than the THP-1 cells incubated with RBC ( $52.58 \pm 0.01$  pg/ml,  $P \leq 0.05$ ). THP-1 cells incubated for 24 hours with 3G8 iRBCs produced  $180.92 \pm 0.03$  pg/ml of MIP-1 $\alpha$ , which was more than the THP-1 cells alone ( $90.38 \pm 2.10$  pg/ml) and significantly more than the THP-1 cells incubated with RBC ( $77.05 \pm 0.98$  pg/ml,  $P \leq 0.01$ , Figure 28C). THP-1 cells incubated for 12 hours with 3G8 iRBCs produced  $1586.12 \pm 45.63$  pg/ml of TNF- $\alpha$ , which was more than the THP-1 cells alone ( $1087.91 \pm 5.76$  pg/ml) and significantly more than the THP-1 cells incubated with RBC ( $1144.82 \pm 19.02$  pg/ml,  $P \leq 0.05$ ). THP-1 cells incubated for 24 hours with 3G8 iRBCs produced  $2172.41 \pm 2.45$  pg/ml of TNF- $\alpha$ , which was more than the THP-1 cells alone ( $1542.91 \pm 104.69$  pg/ml) and significantly more than the THP-1 cells incubated with RBC ( $1652.63 \pm 15.13$  pg/ml,  $P \leq 0.05$ , Figure 28D).

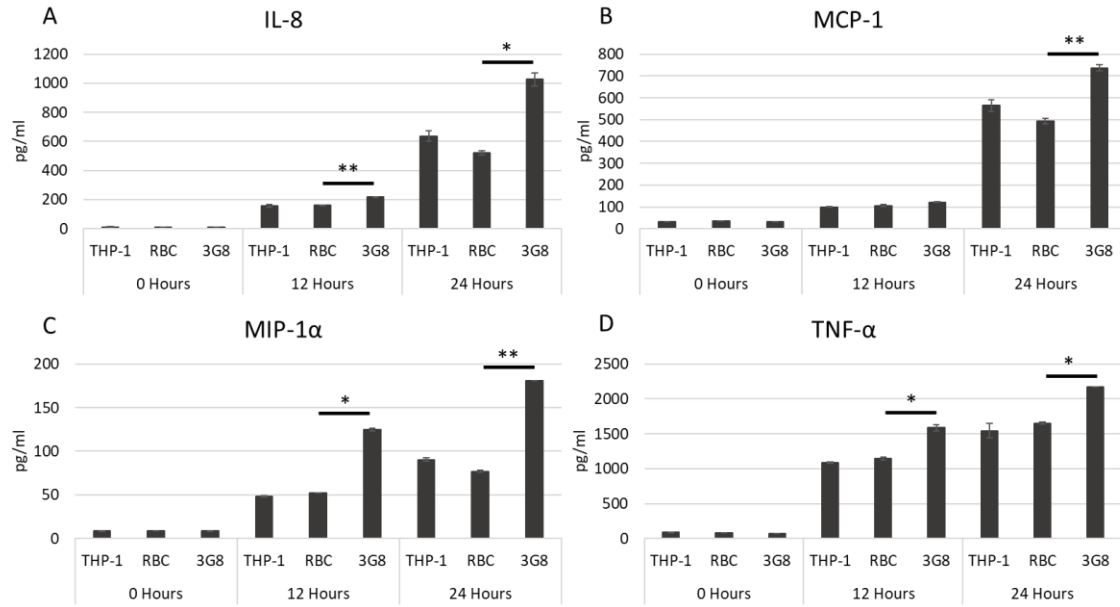


**Figure 28. Cytokine/Chemokine production from 3G8 iRBC::THP-1 interaction:** The amount of **A.** IL-8, **B.** MCP-1, **C.** MIP-1 $\alpha$ , and **D.** TNF- $\alpha$  produced after 0, 12, 24 hours of incubation in empty, with RBC, or with 3G8 iRBC. All samples were analyzed with a one-way ANOVA followed by a two-tailed T. Test with two sample equal variance and a 95% confidence (\* =  $P \leq 0.05$ , \*\* =  $P \leq 0.01$ ). Error bars are SEM.

*THP-1::E9 iRBC interaction produces mainly pro-inflammatory effects*

THP-1 cells were incubated with integrin and CD36 binding E9 iRBCs, control uninfected RBCs, and empty wells for 0, 12, and 24 hours. The supernatants were collected and tested for the production of IL-1 $\alpha$ , IL-1 $\beta$ , IL-2, IL-6, IL-8, IL-10, IL-12 (p40), IL-12 (p70), IL-13, IL-19, IL-20, IL-22, IL-26, IL-27, IL28a, IL29, IFN- $\gamma$ , MCP-1, MIP-1 $\alpha$ , and TNF- $\alpha$ . Only detected cytokines and statistically significant reductions or increases in the production of cytokines were reported.

THP-1 cells incubated for 24 hours with E9 iRBCs produced  $33.49 \pm 0.98$  pg/ml of IL-1 $\beta$ , which was more than the THP-1 cells alone ( $9.74 \pm 0.36$  pg/ml) and significantly more than the THP-1 cells incubated with RBC ( $8.12 \pm 0.34$  pg/ml,  $P \leq$

0.05, Figure 29A). THP-1 cells incubated for 24 hours with E9 iRBCs produced  $23.19 \pm 0.58$  pg/ml of IL-6, which was more than the THP-1 cells alone ( $2.69 \pm 0.16$  pg/ml) and significantly more than the THP-1 cells incubated with RBC ( $6.13 \pm 0.41$  pg/ml,  $P \leq 0.01$ , Figure 29B). THP-1 cells incubated for 12 hours with E9 iRBCs produced  $1242.10 \pm 4.02$  pg/ml of IL-8, which was more than the THP-1 cells alone ( $156.64 \pm 8.03$  pg/ml) and significantly more than the THP-1 cells incubated with RBC ( $160.03 \pm 2.96$  pg/ml,  $P \leq 0.0001$ ). THP-1 cells incubated for 24 hours with E9 iRBCs produced  $2025.91 \pm 70.422$  pg/ml of IL-8, which was more than the THP-1 cells alone ( $636.73 \pm 36.09$  pg/ml) and significantly more than the THP-1 cells incubated with RBC ( $521.88 \pm 12.90$  pg/ml,  $P \leq 0.05$ , Figure 29C). THP-1 cells incubated for 12 hours with E9 iRBCs produced  $280.22 \pm 4.19$  pg/ml of MCP-1, which was more than the THP-1 cells alone ( $99.63 \pm 2.35$  pg/ml) and significantly more than the THP-1 cells incubated with RBC ( $106.02 \pm 4.17$  pg/ml,  $P \leq 0.01$ ). THP-1 cells incubated for 24 hours with E9 iRBCs produced  $1030.36 \pm 9.19$  pg/ml of MCP-1, which was more than the THP-1 cells alone ( $564.80 \pm 25.99$  pg/ml) and significantly more than the THP-1 cells incubated with RBC ( $493.52 \pm 13.67$  pg/ml,  $P \leq 0.01$ , Figure 29D). THP-1 cells incubated for 12 hours with E9 iRBCs produced 1343 pg/ml of MIP-1 $\alpha$ , which was more than the THP-1 cells alone ( $48.32 \pm 0.65$  pg/ml) and significantly more than the THP-1 cells incubated with RBC ( $52.58 \pm 0.01$  pg/ml,  $P \leq 0.0001$ ). THP-1 cells incubated for 24 hours with E9 iRBCs produced 1343 pg/ml of MIP-1 $\alpha$ , which was more than the THP-1 cells alone ( $90.38 \pm 2.10$  pg/ml,  $P \leq 0.0001$ ) and significantly more than the THP-1 cells incubated with RBC ( $77.05 \pm 0.98$  pg/ml,  $P \leq 0.0001$ , Figure 29E). The MFI of MIP-1 $\alpha$  produced by THP-1 cells over 12 and 24 hours was at the top of the standard curve for MIP-1 $\alpha$ ; therefore, the concentrations were

estimated based on the standard value calculations for the highest concentration of MIP-1 $\alpha$ . THP-1 cells incubated for 12 hours with E9 iRBCs produced  $721.46 \pm 7.88$  pg/ml of TNF $\alpha$ , which was less than the THP-1 cells alone ( $1087.91 \pm 5.76$  pg/ml) and significantly less than the THP-1 cells incubated with RBC ( $1144.82 \pm 19.02$  pg/ml,  $P \leq 0.05$ ). THP-1 cells incubated for 24 hours with E9 iRBCs produced  $1309.59 \pm 23.08$  pg/ml of TNF- $\alpha$ , which was less than the THP-1 cells alone ( $1542.91 \pm 104.69$  pg/ml) and significantly less than the THP-1 cells incubated with RBC ( $1652.63 \pm 15.13$  pg/ml,  $P \leq 0.05$ , Figure 29F).

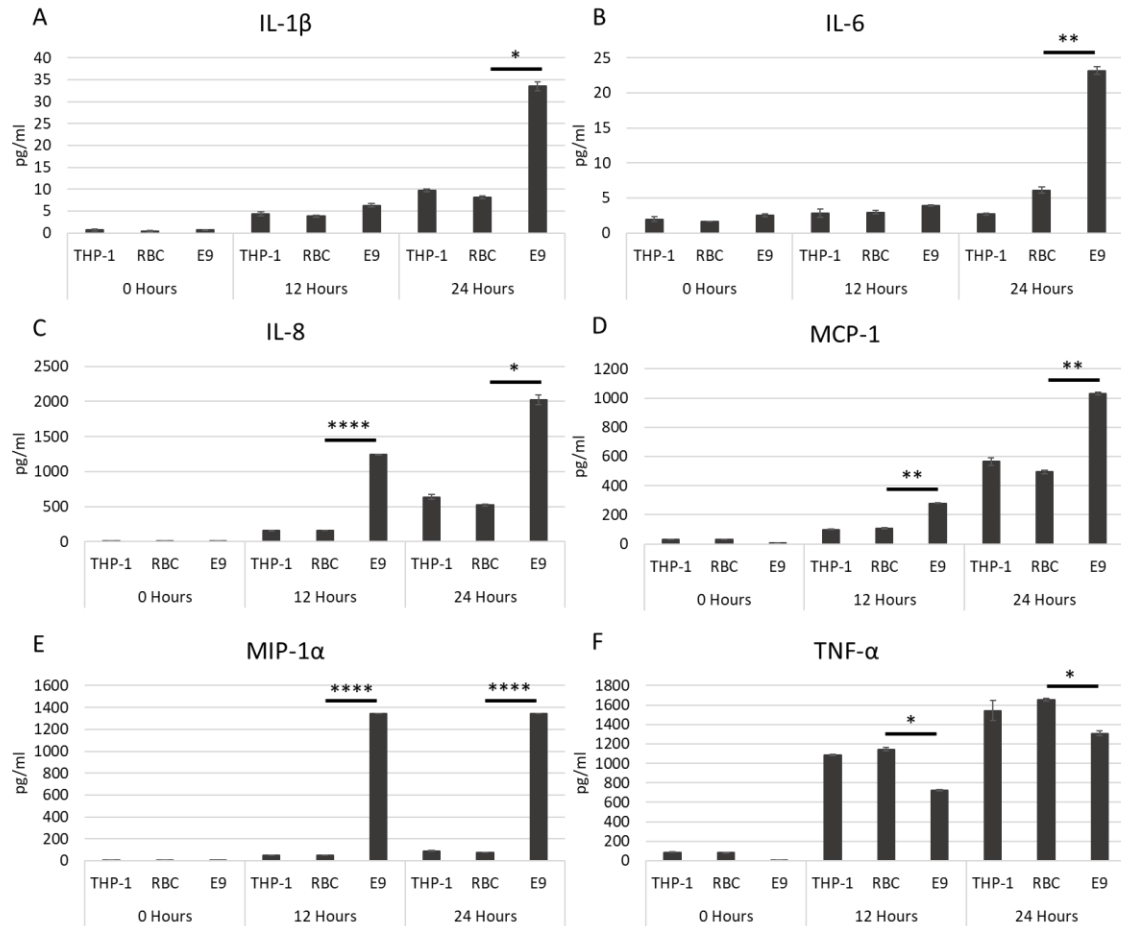


**Figure 29. Cytokine/Chemokine production from E9 iRBC::THP-1 interaction:** The amount of **A.** IL-1 $\beta$ , **B.** IL-6, **C.** IL-8, **D.** MCP-1, **E.** MIP-1 $\alpha$ , and **F.** TNF- $\alpha$  produced after 0, 12, 24 hours of incubation in empty wells, with RBC, or with E9 iRBC. All samples were analyzed with a one-way ANOVA followed by a two-tailed T. Test with two sample equal variance and a 95% confidence (\* =  $P \leq 0.05$ , \*\* =  $P \leq 0.01$ , \*\*\*\* =  $P \leq 0.0001$ ). Error bars are SEM.

## Discussion and Overall Conclusion

We selected the ICAM-1-binding 3G8 strain of malaria to determine if our simulated iRBC model, using PfEMP1 coated beads and surface-immobilized PfEMP1 protein constructs, compares to an actual iRBC in ICAM-1 binding ability and immune response profile. To confirm that 3G8 parasite line selected for these experiments binds

to the appropriate receptors, we immobilized BSA, ICAM-1, CSA, integrin  $\alpha V\beta 3$ , integrin  $\alpha V\beta 6$ , and CD36 on the surface of a petri dish, then added 3G8 iRBCs. The iRBCs were allowed to settle and interact with the surface-immobilized receptors, then after multiple washes, only ICAM-1 had a statistically significant amount of sequestered iRBC compared to the other surface-immobilized receptors (Figure 30,  $P \leq 0.001$ ) (16).

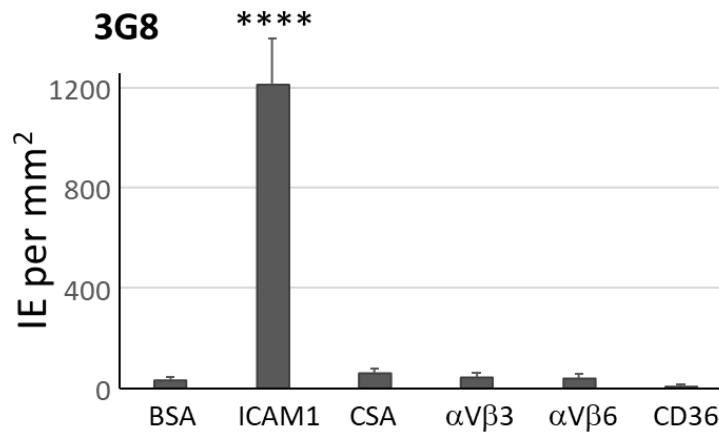


**Figure 30. 3G8 iRBC sequestered to ICAM-1:** 3G8 iRBC were incubated on surface immobilized BSA, ICAM-1, CSA,  $\alpha V\beta 3$ ,  $\alpha V\beta 6$ . 3G8 only sequestered to ICAM-1. Binding is measured by counting attached infected erythrocytes in 10 - 33 microscope fields. Bars indicate Means and Error bars indicate Standard Error of Means (SEM). Differences in binding were calculated by one-way ANOVA using Holm-Sidak's multiple comparison tests. These experiments were repeated at least once with similar qualitative results. \*\*\*\* =  $P \leq 0.0001$ . Adapted from (16).

After confirming that the 3G8 parasite binds to ICAM-1, the iRBC were incubated with THP-1 cells to determine their immune response profile. 3G8 iRBC stimulated THP-1 cells showed a statistically significant increase in the production of IL-8, MCP-1, MIP-1 $\alpha$ , and TNF- $\alpha$  following both 12 and 24 hours of incubation. Monocyte chemoattractant protein 1 (MCP-1), also known as CCL2, attracts other innate immune cells, including monocytes and dendritic cells, to areas of inflammation. Recruited dendritic cells, when co-cultured with iRBC, may activate NK cells and T cells to

increase production of IFN $\gamma$ , which would contribute to the overall inflammatory response (114). Macrophage inflammatory protein 1 $\alpha$  (MIP-1 $\alpha$ ), also known as CCL3, can activate other granulocytes to further release pro-inflammatory cytokines. Tumor necrosis factor  $\alpha$  (TNF- $\alpha$ ) is a pyrogen capable of inducing fever, inflammation, and apoptotic cell death. The production of IL-8, MCP-1, MIP-1 $\alpha$ , and TNF- $\alpha$  is a strong initial immune response from naïve THP-1 cells, with each of the produced cytokines/chemokines being able to recruit and stimulate more immune cells to increase the inflammatory immune response. Similarly, direct crosslinking of ICAM-1 on endothelial cells leads to increased production of IL-8 (126). Further, crosslinking of ICAM-1 on rheumatoid synovial cells leads to an upregulation of the IL-1 $\beta$  gene (127). In contrast, our surface-immobilized PfEMP1 ligation results showed mainly anti-inflammatory effects, including a decrease in the production of IL-1 $\beta$ .

Next, we selected the CD36 and integrin  $\alpha$ V $\beta$ 3-binding E9 strain of malaria to validate our simulated iRBC model, in a real iRBC model, for ability to bind and elicit an immune response through CD36 and integrin  $\alpha$ V $\beta$ 3. TO confirm binding specificity of this line to CD36 and integrin, we immobilized BSA, CD36, ICAM-1, CSA, and integrin  $\alpha$ V $\beta$ 3 on the surface of a petri dish, then added E9 iRBCs. The E9 iRBCs were allowed to settle and interact with the surface-immobilized receptors, then after multiple washes, CD36 ( $P \leq 0.0001$ ) and integrin  $\alpha$ V $\beta$ 3 ( $P \leq 0.0001$ ) had a statistically significant amount of sequestered iRBC compared to the other surface-immobilized receptors. When the E9 iRBCs were incubated with RGD-IP, during interaction with the surface-immobilized receptors, the double RGD-containing integrin  $\alpha$ V $\beta$ 3's interaction with E9 iRBCs was almost completely inhibited, but the interaction with CD36 was not (Figure 31A). When

E9 iRBCs were pre-incubated with soluble recombinant CD36 ( $P \leq 0.0001$ ) or the THP-1 cells were pre-incubated with anti-CD36 antibody ( $P \leq 0.0001$ ) the amount of bound E9 iRBC was significantly reduced (Figure 31B) (16).

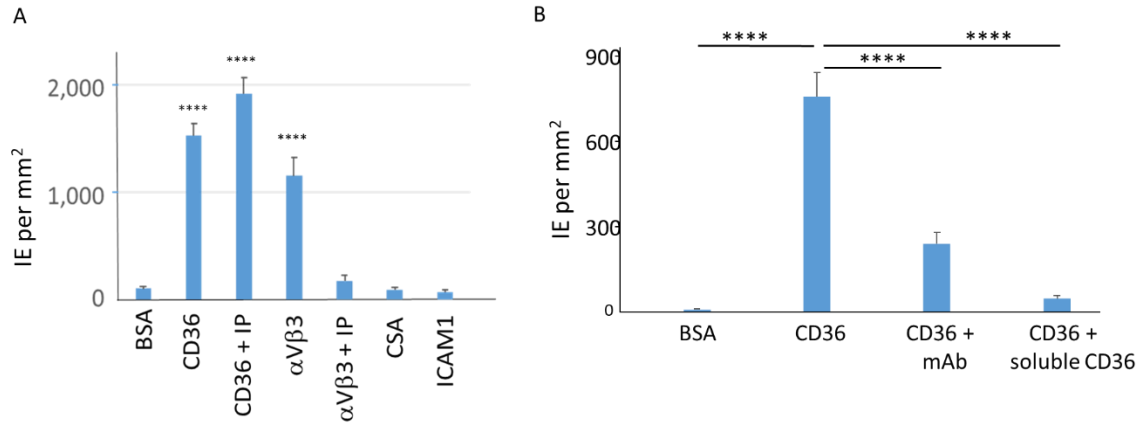


**Figure 31. E9 iRBC binding to surface-immobilized recombinant human receptors.** Binding of E9 iRBC to surface-immobilized receptors in absence and presence (10 µg/ml) of RGD-IP. Binding is measured by counting attached infected erythrocytes in 10 - 33 microscope fields. Bars indicate Means and Error bars indicate Standard Error of Means (SEM). Differences in binding were calculated by one-way ANOVA using Holm-Sidak's multiple comparison tests. These experiments were repeated at least once with similar qualitative results. \*\*\*\* =  $P \leq 0.0001$ . Adapted from (16).

After confirmation of binding through our target cell surface receptors, we incubated E9 iRBCs with THP-1 cells to determine their immune response profile. The immune response consisted mainly of increases in the production of pro-inflammatory cytokines and chemokines. THP-1 cells incubated with E9 iRBCs showed an increase in IL-1β and IL-6 after 12 hours of incubation and an increase in IL-8, MCP-1, and MIP-1α following both 12 and 24 hours of incubation. Similar to TNF-α, IL-6 is an acute phase response molecule that helps induce fever. Interestingly, through the interaction of THP-1::E9 iRBCs, there was a significant decrease in the production of TNF-α after 12 hours



of incubation. Using a similar model, CD36-mediated nonopsonic phagocytosis of ITG38 iRBCs by monocytes led to CD36 clustering around the phagocytosed iRBC and also a reduction in TNF- $\alpha$  (17). Further, interaction with CSA-binding parasites has also been shown to reduce the production of TNF- $\alpha$ , compared to iRBC not displaying the CSA-binding PfEMP1 protein (131). The consistency in reducing TNF- $\alpha$  over multiple parasite lines might imply that the parasite is attempting to suppress the immune response through PfEMP1-mediated ligation to immune cells. However, the production of IL-6, IL-8, MCP-1, and MIP-1 $\alpha$  is a strong initial immune response from naïve THP-1 cells, with each of the produced cytokines/chemokines being able to recruit and stimulate more immune cells to increase the inflammatory immune response. Similar to our E9 iRBC cytokine profile, wildtype mice infected with *Plasmodium berghei* produce elevated levels of IL-6, IL-8, MCP-1, TNF, IL-12, and RANTES, which were not produced in integrin  $\alpha$ D $\beta$ 2-deficient mice (95). It is worth noting that there was a detected increase in production of cytokines over time from our control THP-1 cells. Possible causes and solutions were discussed in Chapter II: ICAM-1 Studies – Discussion.

There was a stark difference in immune response between the surface-immobilized PfEMP1 ligation and iRBC::THP-1 cell line interactions. THP-1 ligation through DBL2 $\beta$ 3<sub>PF11 0521</sub>, DBL2 $\delta$ <sub>PF11 2665c</sub>, and CIDR1 $\alpha$ <sub>PF08 0106</sub> produced increases in anti-inflammatory IL-1 $\alpha$  and a decrease in the production of IL-1 $\beta$  and IL-8. Therefore, ligation produced mainly anti-inflammatory effects, which might signify that the PfEMP1 proteins are attempting to suppress the immune response. Alternatively, since our iRBC studies were more in-line with the literature, the whole iRBC might be needed to elicit a physiological immune response, but an immune suppressive ability of direct PfEMP1

ligation cannot be ruled out. Since we used an uninfected RBC as the control for our studies, the effect of other RBC surface molecules, like carbohydrates, on the immune response can be compared to the effect from PfEMP1 ligation. This rules out naturally occurring surface molecules as immune response stimulators. However, immune cells are able to recognize a reduction of naturally occurring RBC surface bound carbohydrates, including D-Glucose and sialic acid, on aged RBC (Chow 1979). Therefore, if iRBCs also display a reduction in surface bound carbohydrates, then receptors recognizing this reduction in expression may trigger different signaling pathways, which could influence the immune response in a way that our surface-immobilized PfEMP1 ligation study could not simulate. In addition, iRBC contain other molecules that can stimulate a pro-inflammatory response, like hemozoin (136).

The results of this study demonstrate that the high-throughput PfEMP1 bead-based assay is beneficial for determining new PfEMP1::receptor interactions involved in iRBC sequestration or the innate immune cell response. This model is also able to determine the strength of specific PfEMP1:cell surface receptor interactions. Further, THP-1 ligation through surface-immobilized PfEMP1 domains contributed a wealth of information about DEGs. DEG analysis can help determine key cell signaling pathway information on how PfEMP1 ligation may be disrupting or manipulating cell signaling for survival and to mediate the inflammatory response. If the parasite cannot be targeted directly for immune clearance, a better understanding of the pathways involved in iRBC::immune cell signaling could offer potential downstream targets for immune defensive therapies.

In our step-wise approach, testing THP-1 cell response using the simpler set-up of cell ligation to surface-immobilized PfEMP1 domains, with no phagocytosis, compared to the more complex set-up of cell interaction with iRBCs, with the possibility of phagocytosis, helps to delineate partial cellular activities to comprehend a more complex response most likely experienced in nature. Our findings may indicate that one of the functions of PfEMP1 proteins is to reduce immune response of innate immune cells, like monocytes, through signaling provided by interactions between PfEMP1 domains and monocyte surface receptors.

Without this evolutionary-adjusted signaling, the immune response to iRBC, which is in general pro-inflammatory, might be significantly stronger leading to negative consequences for the parasite or the host. This might be the case in unfortunate situations during field infections when expressed PfEMP1 variants possessing domains that are less inhibitory, may lead to overstimulation of the immune cells, and consequently, promote severe disease complications. Similarly, some domain variants might be pro-inflammatory upon interaction with immune-cell receptors and thus directly contributing to overall excessive immune responses. Understanding of the wealth of responses of immune cells upon their interactions with iRBCs expressing specific PfEMP1 proteins will provide better approaches to treat severe malaria cases and help in the design of better targets for vaccine development. In this respect, our work is a step toward further understanding these complex host-parasite relationships.

## REFERENCES

1. World Health Organization. (2018). *2018 World malaria report*. Geneva, Switzerland: World Health Organization.
2. D. C. Ghislaine Mayer *et al.*, Glycophorin B Is the Erythrocyte Receptor of *Plasmodium falciparum* Erythrocyte-Binding Ligand, EBL-1. *Proc. Natl. Acad. Sci. U. S. A.* **106**, 5348-5352 (2009).
3. A. F. Cowman, B. S. Crabb, Invasion of Red Blood Cells by Malaria Parasites. *Cell.* **124**, 755-766 (2006).
4. R. Fairhurst, C. Bess, M. Krause, Abnormal PfEMP1/knob display on *Plasmodium falciparum*-infected erythrocytes containing hemoglobin variants: fresh insights into malaria pathogenesis and protection. *Microb. Infect.* **14**, 851-862 (2012).
5. D. S. Khoury *et al.*, Effect of Mature Blood-Stage *Plasmodium* Parasite Sequestration on Pathogen Biomass in Mathematical and In Vivo Models of Malaria. *Infect. Immun.* **82**, 212-220 (2014).
6. D. Baruch, Adhesive receptors on malaria-parasitized red cells. *Best Practice & Research Clinical Haematology.* **12**, 747-761 (1999).
7. J. C. J. Calis *et al.*, Severe Anemia in Malawian Children. *N. Engl. J. Med.* **358**, 888-899 (2008).
8. G. Turner, Cerebral Malaria. *Brain Pathology.* **7**, 569-582 (1997).

9. E. Pongponratn *et al.*, An ultrastructural study of the brain in fatal *Plasmodium falciparum* malaria. *Am. J. Trop. Med. Hyg.* **69**, 345-359 (2003).
10. N. D. Pasternak, R. Dzikowski, PfEMP1: An antigen that plays a key role in the pathogenicity and immune evasion of the malaria parasite *Plasmodium falciparum*. *International Journal of Biochemistry and Cell Biology.* **41**, 1463-1466 (2009).
11. X. Su *et al.*, The large diverse gene family var encodes proteins involved in cytoadherence and antigenic variation of *plasmodium falciparum*-infected erythrocytes. *Cell.* **82**, 89-100 (1995).
12. M. J. Gardner *et al.*, Genome sequence of the human malaria parasite *Plasmodium falciparum*. *Nature.* **419**, 498-511 (2002).
13. S. M. Kraemer, J. D. Smith, Evidence for the importance of genetic structuring to the structural and functional specialization of the *Plasmodium falciparum* var gene family. *Mol. Microbiol.* **50**, 1527-1538 (2003).
14. J. D. Smith, G. Subramanian, B. Gamain, D. I. Baruch, L. H. Miller, Classification of adhesive domains in the *Plasmodium falciparum* Erythrocyte Membrane Protein 1 family. *Molecular & Biochemical Parasitology.* **110**, 293-310 (2000).
15. J. D. Smith *et al.*, Identification of a *Plasmodium falciparum* Intercellular Adhesion Molecule-1 Binding Domain: A Parasite Adhesion Trait Implicated in Cerebral Malaria. *Proc. Natl. Acad. Sci. U. S. A.* **97**, 1766-1771 (2000).
16. O. Chesnokov, J. Merritt, S. O. Tcherniuk, N. Milman, A. V. Oleinikov, *Plasmodium falciparum* infected erythrocytes can bind to host receptors integrins  $\alpha V\beta 3$  and  $\alpha V\beta 6$  through DBLd1\_D4 domain of PFL2665c PfEMP1 protein. *Scientific Reports.*, 1 (2018).

17. I. McGilvray, L. Serghides, A. Kapus, O. Rotstein, K. Kain, Nonopsonic monocyte/macrophage phagocytosis of *Plasmodium falciparum*-parasitized erythrocytes: a role for CD36 in malarial clearance. *Blood*. **96**, 3231-3240 (2000).
18. J. D. Smith, B. Gamain, D. I. Baruch, S. Kyes, Decoding the language of var genes and *Plasmodium falciparum* sequestration. *Trends in Parasitology*. **17**, 538-545 (2001).
19. B. A. Robinson, T. L. Welch, J. D. Smith, Widespread functional specialization of *Plasmodium falciparum* erythrocyte membrane protein 1 family members to bind CD36 analysed across a parasite genome. *Mol. Microbiol.* **47**, 1265-1278 (2003).
20. A. Oleinikov *et al.*, High Throughput Functional Assays of the Variant Antigen PfEMP1 Reveal a Single Domain in the 3D7 *Plasmodium falciparum* Genome that Binds ICAM1 with High Affinity and Is Targeted by Naturally Acquired Neutralizing Antibodies. *Plos Pathogens*. **5**, e1000386-e1000386 (2009).
21. J. Gullingsrud, T. Saveria, E. Amos, P. Duffy, A. Oleinikov, Structure-Function-Immunogenicity Studies of PfEMP1 Domain DBL2 beta (PF11\_0521), a Malaria Parasite Ligand for ICAM-1. *Plos One*. **8** (2013).
22. M. Fried, P. E. Duffy, A. Brockman, B. J. Brabin, F. Nosten, Maternal antibodies block malaria. *Nature*. **395**, 851-852 (1998).
23. A. Scherf *et al.*, Antigenic variation in malaria: in situ switching, relaxed and mutually exclusive transcription of var genes during intra-erythrocytic development in *Plasmodium falciparum*. *Embo j.* **17**, 5418-5426 (1998).

24. A. V. Oleinikov *et al.*, Effects of Sex, Parity, and Sequence Variation on Seroreactivity to Candidate Pregnancy Malaria Vaccine Antigens. *J. Infect. Dis.* **196**, 155-164 (2007).
25. E. Hempelmann, Hemozoin Biocrystallization in *Plasmodium falciparum* and the antimalarial activity of crystallization inhibitors. *Parasitol. Res.* **100**, 671-676 (2007).
26. Drugs and Medications: Chloroquine Phosphate." *WebMD*. WebMD, n.d. Web. <<http://www.webmd.com/drugs/2/drug-8633/chloroquine-oral/details#side-effects>>
27. P. Singhasivanon, Mekong malaria. Malaria, multi-drug resistance and economic development in the greater Mekong subregion of Southeast Asia. *Southeast Asian J. Trop. Med. Public Health.* **30 Suppl 4**, i (1999).
28. N. J. White, Antimalarial drug resistance. *J. Clin. Invest.* **113**, 1084-1092 (2004).
29. E. Schwartz, Prophylaxis of malaria. *Mediterranean Journal of Hematology and Infectious Diseases.* **4**, e2012045-e2012045 (2012).
30. M. J. Hamel *et al.*, The Combination of Indoor Residual Spraying and Insecticide-Treated Nets Provides Added Protection against Malaria Compared with Insecticide-Treated Nets Alone. *Am. J. Trop. Med. Hyg.* **85**, 1080-1086 (2011).
31. WHO. Global plan for insecticide resistance management in malaria vectors. Geneva: World Health Organization; 2012.
32. Y. Fang *et al.*, Resistance to pyrethroid and organophosphate insecticides, and the geographical distribution and polymorphisms of target-site mutations in voltage-gated sodium channel and acetylcholinesterase 1 genes in *Anopheles sinensis* populations in Shanghai, China. *Parasites & Vectors.*, 1 (2019).

33. RTS,S Clinical Trials Partnership, A Phase 3 Trial of RTS,S/AS01 Malaria Vaccine in African Infants. *N. Engl. J. Med.* **367**, 2284-2295 (2012).
34. RTS,S Clinical Trials Partnership, Efficacy and safety of RTS,S/AS01 malaria vaccine with or without a booster dose in infants and children in Africa: final results of a phase 3, individually randomised, controlled trial. *The Lancet.* **386**, 31-45 (2015).
35. M. Baratin *et al.*, Natural Killer Cell and Macrophage Cooperation in MyD88-Dependent Innate Responses to Plasmodium Falciparum. *Proc. Natl. Acad. Sci. U. S. A.* **102**, 14747-14752 (2005).
36. D. Hansen, Inflammatory Responses Associated with the Induction of Cerebral Malaria: Lessons from Experimental Murine Models. *Plos Pathogens.* **8**, e1003045 (2012).
37. M. W. Mosesson, Fibrinogen and fibrin structure and functions. *Journal of Thrombosis and Haemostasis.* 1894 (2005).
38. S. T. Lord, E. Strickland, E. Jayjock, Strategy for recombinant multichain protein synthesis: fibrinogen B-beta-chain variants as thrombin substrates. *Biochemistry.*, 2342 (1996).
39. J. W. M. Heemskerk, E. M. Bevers, T. Lindhout, Platelet Activation and Blood Coagulation. *Journal of Thrombosis and Haemostasis.* **88**, 186-193 (2002).
40. S. Palta, R. Saroa, A. Palta, Overview of the coagulation system. *Indian J. Anaesth.*, 515 (2014).



41. D. H. Farrell, P. Thiagarajan, D. W. Chung, E. W. Davie, Role of Fibrinogen  $\alpha$  and  $\gamma$  Chain Sites in Platelet Aggregation. *Proc. Natl. Acad. Sci. U. S. A.* **89**, 10729 (1992).
42. T. Bombeli, B. R. Schwartz, and J. M. Harlan, Adhesion of Activated Platelets to Endothelial Cells: Evidence for a GPIIbIIIa-dependent Bridging Mechanism and Novel Roles for Endothelial Intercellular Adhesion Molecule 1 (ICAM-1),  $\alpha v \beta 3$  Integrin, and GPIb $\alpha$ . *J. Exp. Med.*, 329 (1998).
43. L. R. Languino *et al.*, Fibrinogen mediates leukocyte adhesion to vascular endothelium through an ICAM-1-dependent pathway. *Cell.*, 1423 (1993).
44. D. C. Altieri, J. Plescia, E. F. Plow, The structural motif glycine 190-valine 202 of the fibrinogen gamma chain interacts with CD11b/CD18 integrin (alpha M beta 2, Mac-1) and promotes leukocyte adhesion. *J. Biol. Chem.* **268**, 1847-1853 (1993).
45. W. S. Somers, J. Tang, G. D. Shaw, R. T. Camphausen, Insights into the molecular basis of leukocyte tethering and rolling revealed by structures of P- and E-selectin bound to SLe(super.x) and PSGL-1. *Cell.*, 467 (2000).
46. A. E. Daniel, J. D. van Buul, Endothelial Junction Regulation: A Prerequisite for Leukocytes Crossing the Vessel Wall. *Journal of Innate Immunity.* **5**, 324-335 (2013).
47. M. S. Diamond, D. E. Staunton, S. D. Marlin, T. A. Springer, Binding of the integrin Mac-1 (CD11b/CD18) to the third immunoglobulin-like domain of ICAM-1 (CD54) and its regulation by glycosylation. *Cell.* **65**, 961-971 (1991).
48. M. L. Dustin, T. A. Springer, Lymphocyte Function-Associated Antigen-1 (LFA-1) Interaction with Intercellular Adhesion Molecule-1 (ICAM-1) Is One of at Least

- Three Mechanisms for Lymphocyte Adhesion to Cultured Endothelial Cells. *J. Cell Biol.* **107**, 321 (1988).
49. J. Millan *et al.*, Lymphocyte transcellular migration occurs through recruitment of endothelial ICAM-1 to caveola- and F-actin-rich domains. *Nat. Cell Biol.*, 113 (2006).
  50. W. A. Muller, Leukocyte–endothelial-cell interactions in leukocyte transmigration and the inflammatory response. *Trends Immunol.* **24**, 326-333 (2003).
  51. S. K. Shaw *et al.*, Coordinated redistribution of leukocyte LFA-1 and endothelial cell ICAM-1 accompany neutrophil transmigration. *J. Exp. Med.* **200**, 1571-1580 (2004).
  52. A. R. Berendt, *et al.*, Intercellular adhesion molecule-1 is an endothelial cell adhesion receptor for *Plasmodium falciparum*. *Letters to Nature.* **341**. (1989).
  53. L. B. Ochola *et al.*, *Plasmodium falciparum* cytoadherence to ICAM-1 is associated with cerebral malaria. *Malaria Journal.* P27 (2010).
  54. S. Etienne-Manneville, N. Chaverot, A. D. Strosberg, P. O. Couraud, ICAM-1-coupled signaling pathways in astrocytes converge to cyclic AMP response element-binding protein phosphorylation and TNF- $\alpha$  secretion. *Journal of Immunology.* **163**, 668-674 (1999).
  55. S. Dragoni *et al.*, Endothelial MAPKs Direct ICAM-1 Signaling to Divergent Inflammatory Functions. *Journal of Immunology.* **198**, 4074-4085 (2017).
  56. C. Lawson, S. Wolf, ICAM-1 signaling in endothelial cells. *Pharmacological Reports.* **61**, 22-32 (2009).

57. D. Mittar *et al.*, Flow Cytometry and High-Content Imaging to Identify Markers of Monocyte-Macrophage Differentiation. *BD Biosciences*. Application Note (2011).
58. T. Lavstsen, A. Salanti, A. Jensen, D. E. Arnot, T. G. Theander, Sub-grouping of *Plasmodium falciparum* 3D7 var genes based on sequence analysis of coding and non-coding regions. *Malaria Journal*. **2**(2003).
59. A. Jensen *et al.*, *Plasmodium falciparum* associated with severe childhood malaria preferentially expresses PfEMP1 encoded by group A var genes. *J. Exp. Med.* **199**, 1179-1190 (2004).
60. S. J. Chakravorty, A. Craig, The role of ICAM-1 in *Plasmodium falciparum* cytoadherence. *Eur. J. Cell Biol.* **84**, 15-27 (2005).
61. D. A. Cunningham *et al.*, ICAM-1 is a key receptor mediating cytoadherence and pathology in the *Plasmodium chabaudi* malaria model. *Malaria Journal*. **1** (2017).
62. J. M. Casasnovas, T. Stehle, Jin-Huan Liu, Jia-Huai Wang, T. A. Springer, A Dimeric Crystal Structure for the N-Terminal Two Domains of Inter Cellular Adhesion Molecule-1. *Proc. Natl. Acad. Sci. U. S. A.* **95**, 4134 (1998).
63. K. M. F. Mustaffa, J. Storm, M. Whittaker, T. Szeszak, A. G. Craig, In vitro inhibition and reversal of *Plasmodium falciparum* cytoadherence to endothelium by monoclonal antibodies to ICAM-1 and CD36. *Malaria Journal.*, **1** (2017).
64. M. E. Labadia, D. D. Jeanfavre, G. O. Caviness, M. M. Morelock, Molecular regulation of the interaction between leukocyte function-associated antigen-1 and soluble ICAM-1 by divalent metal cations. *J. Immunol.* **161**, 836-842 (1998).
65. A. Weber, P. Wasiliew, M. Kracht, Interleukin-1 (IL-1) Pathway. *Science signaling*. **3**. (2010).

66. B. Shen, M. K. Delaney, X. Du, Inside-out, outside-in, and inside–outside-in: G protein signaling in integrin-mediated cell adhesion, spreading, and retraction. *Curr. Opin. Cell Biol.* **24**, 600-606 (2012).
67. S. Tadokoro *et al.*, Talin Binding to Integrin  $\beta$  Tails: A Final Common Step in Integrin Activation. *Science*. **302**, 103 (2003).
68. M. Moser, B. Nieswandt, S. Ussar, M. Pozgajova, R. Fässler, Kindlin-3 is essential for integrin activation and platelet aggregation. *Nat. Med.* **14**, 325-330 (2008).
69. Y. Takada, X. Ye, S. Simon, The integrins. *Genome Biol.* **8**(2007).
70. C. Zeltz, J. Orgel, D. Gullberg, Molecular composition and function of integrin-based collagen glues—Introducing COLINBRIs. *BBA - General Subjects*. **1840**, 2533-2548 (2014).
71. R. O. Hynes, The Extracellular Matrix: Not Just Pretty Fibrils. *Science*. **326**, 1216 (2009).
72. J. S. Munger, D. Sheppard, Cross Talk among TGF-beta Signaling Pathways, Integrins, and the Extracellular Matrix. *Cold Spring Harbor Perspectives in Biology*. **3**(2011).
73. J. Emsley, C. G. Knight, Structural basis of collagen recognition by integrin  $\alpha 2 \beta 1$ . *Cell*. **101**, 47 (2000).
74. C. Zeltz, D. Gullberg, The integrin-collagen connection - a glue for tissue repair? *J. Cell. Sci.* **129**, 653-664 (2016).
75. M. Aumailley, The laminin family. *Cell Adhesion & Migration.*, 48 (2013).

76. R. Nishiuchi *et al.*, Ligand-binding specificities of laminin-binding integrins: A comprehensive survey of laminin–integrin interactions using recombinant  $\alpha 3\beta 1$ ,  $\alpha 6\beta 1$ ,  $\alpha 7\beta 1$  and  $\alpha 6\beta 4$  integrins. *Matrix Biology*. **25**, 189-197 (2006).
77. M. D. Pierschbacher, E. Ruoslahti, Variants of the Cell Recognition Site of Fibronectin That Retain Attachment-Promoting Activity. *Proc. Natl. Acad. Sci. U. S. A.* **81**, 5985 (1984).
78. E. Ruoslahti, RGD and other recognition sequences for integrins. *Annu. Rev. Cell Dev. Biol.* **12**, 697-715 (1996).
79. T. Xiao, J. Takagi, B. Coller, J. Wang, T. Springer, Structural basis for allostery in integrins and binding to fibrinogen-mimetic therapeutics. *Nature.*, 59 (2004).
80. Jian-Ping Xiong *et al.*, Crystal Structure of the Extracellular Segment of Integrin  $\alpha V\beta 3$  in Complex with an Arg-Gly-Asp Ligand. *Science*. **296**, 151 (2002).
81. I. D. Campbell, M. J. Humphries, Integrin Structure, Activation, and Interactions. *Cold Spring Harbor Perspectives in Biology*. **3**(2011).
82. E. Ruoslahti, Fibronectin and its receptors. *Annu. Rev. Biochem.* **57**, 375-413 (1988).
83. L. V. Valenick, H. C. Hsia, J. E. Schwarzbauer, Fibronectin fragmentation promotes  $\alpha 4\beta 1$  integrin-mediated contraction of a fibrin–fibronectin provisional matrix. *Exp. Cell Res.* **309**, 48-55 (2005).
84. H. A. M. Hussein *et al.*, Beyond RGD: virus interactions with integrins. *Arch. Virol.*, 2669 (2015).

85. P. Aksoy, C. Y. Abban, E. Kiyashka, W. Qiang, P. I. Meneses, HPV16 infection of HaCaTs is dependent on  $\beta$ 4 integrin, and  $\alpha$ 6 integrin processing. *Virology*. **449**, 45-52 (2014).
86. N. Cheshenko *et al.*, Herpes Simplex Virus Type 2 Glycoprotein H Interacts with Integrin alpha v beta 3 To Facilitate Viral Entry and Calcium Signaling in Human Genital Tract Epithelial Cells. *J. Virol.* **88**, 10026-10038 (2014).
87. D. Veessler *et al.*, Single-particle EM reveals plasticity of interactions between the adenovirus penton base and integrin  $\alpha$ v $\beta$ 3. *Proc. Natl. Acad. Sci. U. S. A.* **111**, 8815 (2014).
88. L. Renia *et al.*, Cerebral malaria Mysteries at the blood-brain barrier. *Virulence*. **3**, 193-201 (2012).
89. J. P. Siano, K. K. Grady, P. Millet, T. M. Wick, Short report: Plasmodium falciparum: cytoadherence to  $\alpha$ (v) $\beta$ 3 on human microvascular endothelial cells. *Am. J. Trop. Med. Hyg.* **59**, 77-79 (1998).
90. D. Weerasinghe *et al.*, A role for the  $\alpha$  v  $\beta$  3 integrin in the transmigration of monocytes. *J. Cell Biol.* **142**, 595-607 (1998).
91. R. Hanayama *et al.*, Identification of a factor that links apoptotic cells to phagocytes. *Nature.*, 182 (2002).
92. A. G. Dupuy, E. Caron, Integrin-dependent phagocytosis - spreading from microadhesion to new concepts. *J. Cell. Sci.* **121**, 1773-1783 (2008).
93. T. S. Rask, D. A. Hansen, T. G. Theander, A. G. Pedersen, T. Lavstsen, Plasmodium falciparum Erythrocyte Membrane Protein 1 Diversity in Seven Genomes - Divide and Conquer. *Plos Computational Biology*. **6**(2010).

94. B. Alberts *et al.* Molecular Biology of the Cell. 4<sup>th</sup> Edition. New York:Garland Science; 2002. Integrins. Available from <http://www.ncbi.nlm.nih.gov/books/NBK26867/>
95. I. G. de Azevedo-Quintanilha *et al.*, Integrin alpha(D)beta(2) (CD11d/CD18) mediates experimental malaria-associated acute respiratory distress syndrome (MA-ARDS). *Malaria Journal*. **15**(2016).
96. L. Zhao, Z. Varghese, J. F. Moorhead, Y. Chen, X. Z. Ruan, CD36 and lipid metabolism in the evolution of atherosclerosis. *Br. Med. Bull.* **126**, 101-112 (2018).
97. R. L. Silverstein, W. Li, Y. M. Park, S. O. Rahaman, Mechanisms of cell signaling by the scavenger receptor CD36: implications in atherosclerosis and thrombosis. *Trans. Am. Clin. Climatol. Assoc.* **121**, 206-220 (2010).
98. Min-Mei Huang, J. B. Bolen, J. W. Barnwell, S. J. Shattil, J. S. Brugge, Membrane Glycoprotein IV (CD36) is Physically Associated with the Fyn, Lyn, and Yes Protein-Tyrosine Kinases in Human Platelets. *Proc. Natl. Acad. Sci. U. S. A.* **88**, 7844 (1991).
99. H. A. Bull, P. M. Brickell, P. M. Dowd, Src-related protein tyrosine kinases are physically associated with the surface antigen CD36 in human dermal microvascular endothelial cells. *FEBS Lett.* **351**, 41-44 (1994).
100. S. M. Thomas, J. S. Brugge, Cellular functions regulated by Src family kinases. *Annu. Rev. Cell Dev. Biol.* **13**, 513-609 (1997).
101. Y. C. Zeng, N. B. Tao, K. N. Chung, J. E. Heuser, D. M. Lublin, Endocytosis of oxidized low density lipoprotein through scavenger receptor CD36 utilizes a lipid

- raft pathway that does not require caveolin-1. *J. Biol. Chem.* **278**, 45931-45936 (2003).
102. P. Tontonoz, L. Nagy, J. G. A. Alvarez, V. A. Thomazy, R. M. Evans, PPARgamma promotes monocyte/macrophage differentiation and uptake of oxidized LDL. *Cell.*, 241 (1998).
  103. Y. Jiang *et al.*, Oxidized low-density lipoprotein induces secretion of interleukin-1[beta] by macrophages via reactive oxygen species-dependent NLRP3 inflammasome activation. *Biochem. Biophys. Res. Commun.*, 121 (2012).
  104. H. Kirii *et al.*, Lack of interleukin-1 beta decreases the severity of atherosclerosis in ApoE-deficient mice. *Arteriosclerosis Thrombosis and Vascular Biology*. **23**, 656-660 (2003).
  105. Y. Q. Huo, A. Hafezi-Moghadam, K. Ley, Role of vascular cell adhesion molecule-1 and fibronectin connecting segment-1 in monocyte rolling and adhesion on early atherosclerotic lesions. *Circ. Res.* **87**, 153-159 (2000).
  106. M. Namiki *et al.*, Local overexpression of monocyte chemoattractant protein-1 at vessel wall induces infiltration of macrophages and formation of atherosclerotic lesion - Synergism with hypercholesterolemia. *Arteriosclerosis Thrombosis and Vascular Biology*. **22**, 115-120 (2002).
  107. L. M. Stuart *et al.*, Response to Staphylococcus aureus Requires CD36-Mediated Phagocytosis Triggered by the COOH-Terminal Cytoplasmic Domain. *J. Cell Biol.* **170**, 477 (2005).



108. D. Cao *et al.*, CD36 regulates lipopolysaccharide-induced signaling pathways and mediates the internalization of *Escherichia coli* in cooperation with TLR4 in goat mammary gland epithelial cells. *Scientific Reports.*, 23132 (2016).
109. I. N. Baranova *et al.*, Role of human CD36 in bacterial recognition, phagocytosis, and pathogen-induced JNK-mediated signaling. *J. Immunol.* **181**, 7147-7156 (2008).
110. C. F. Ockenhouse, N. N. Tandon, C. Magowan, G. A. Jamieson, J. D. Chulay, Identification of a Platelet Membrane Glycoprotein as a *Falciparum Malaria* Sequestration Receptor. *Science.* **243**, 1469 (1989).
111. J. D. Smith, J. A. Rowe, M. K. Higgins, T. Lavstsen, Malaria's deadly grip: cytoadhesion of *Plasmodium falciparum*-infected erythrocytes. *Cell. Microbiol.*, 1976 (2013).
112. F. Hsieh *et al.*, The structural basis for CD36 binding by the malaria parasite. *Nature Communications.* **7**(2016).
113. B. G. Yipp *et al.*, Src-family kinase signaling modulates the adhesion of *Plasmodium falciparum* on human microvascular endothelium under flow. *Blood.* **101**, 2850-2857 (2003).
114. N. M. Gowda, X. Wu, S. Kumar, M. Febbraio, D. C. Gowda, CD36 Contributes to Malaria Parasite-Induced Pro-Inflammatory Cytokine Production and NK and T Cell Activation by Dendritic Cells. *Plos One.* **8**(2013).
115. A. Pain *et al.*, Platelet-Mediated Clumping of *Plasmodium Falciparum*-Infected Erythrocytes is a Common Adhesive Phenotype and is Associated with Severe Malaria. *Proc. Natl. Acad. Sci. U. S. A.* **98**, 1805 (2001).

116. J. A. Rowe, A. Claessens, R. A. Corrigan, M. Arman, Adhesion of Plasmodium falciparum-infected erythrocytes to human cells: molecular mechanisms and therapeutic implications. *Expert Reviews in Molecular Medicine*. **11**(2009).
117. B. A. Robinson, T. L. Welch, J. D. Smith, Widespread functional specialization of Plasmodium falciparum erythrocyte membrane protein 1 family members to bind CD36 analysed across a parasite genome. *Mol. Microbiol.*, 1265 (2003).
118. L. K. Erdman *et al.*, CD36 and TLR interactions in inflammation and phagocytosis: implications for malaria. *J. Immunol.* **183**, 6452-6459 (2009).
119. J. Fonager *et al.*, Reduced CD36-dependent tissue sequestration of Plasmodium-infected erythrocytes is detrimental to malaria parasite growth in vivo. *J. Exp. Med.* **209**, 93-107 (2012).
120. A. V. Oleinikov *et al.*, A plasma survey using 38 PfEMP1 domains reveals frequent recognition of the Plasmodium falciparum antigen VAR2CSA among young Tanzanian children. *Plos One.*, e31011 (2012).
121. A. Mahamar *et al.*, Host factors that modify Plasmodium falciparum adhesion to endothelial receptors. *Sci Rep.* **7**, 13872-13872 (2017).
122. A. Bengtsson *et al.*, A Novel Domain Cassette Identifies Plasmodium falciparum PfEMP1 Proteins Binding ICAM-1 and Is a Target of Cross-Reactive, Adhesion-Inhibitory Antibodies. *Journal of Immunology.* **190**, 240-249 (2013).
123. F. Lennartz *et al.*, Structure-Guided Identification of a Family of Dual Receptor-Binding PfEMP1 that Is Associated with Cerebral Malaria. *Cell Host & Microbe.* **21**, 403-414 (2017).

124. A. Brown *et al.*, Molecular Architecture of a Complex between an Adhesion Protein from the Malaria Parasite and Intracellular Adhesion Molecule 1. *J. Biol. Chem.* **288**, 5992-6003 (2013).
125. J. Gullingsrud *et al.*, High-Throughput Screening Platform Identifies Small Molecules That Prevent Sequestration of Plasmodium falciparum-Infected Erythrocytes. *J. Infect. Dis.* **211**, 1134-1143 (2015).
126. H. Sano *et al.*, Cross-linking of intercellular adhesion molecule-1 induces interleukin-8 and RANTES production through the activation of MAP kinases in human vascular endothelial cells. *Biochem. Biophys. Res. Commun.* **250**, 694-698 (1998).
127. Y. Koyama *et al.*, Cross-linking of intercellular adhesion molecule 1 (CD54) induces AP-1 activation and IL-1beta transcription. *J. Immunol.* **157**, 5097-5103 (1996).
128. P. D. Arora, M. F. Manolson, G. P. Downey, J. Sodek, C. McCulloch, A novel model system for characterization of phagosomal maturation, acidification, and intracellular collagen degradation in fibroblasts. *J. Biol. Chem.* **275**, 35432-35441 (2000).
129. I. A. Clark, A. C. Budd, L. M. Alleva, W. B. Cowden, Human malarial disease: a consequence of inflammatory cytokine release. *Malaria Journal.* **5**, 85 (2006).
130. E. B. Belachew, Immune Response and Evasion Mechanisms of Plasmodium falciparum Parasites. *Journal of Immunology Research.* (2018).

131. N. G. Sampaio, E. M. Eriksson, L. Schofield, Plasmodium falciparum PfEMP1 Modulates Monocyte/Macrophage Transcription Factor Activation and Cytokine and Chemokine Responses. *Infect. Immun.* **86**(2017).
132. L. Chen, Z. Zhang, and F. Sendo, Neutrophils play a critical role in the pathogenesis of experimental cerebral malaria. *Clin. Exp. Immunol.*, 125 (2000).
133. W. Chanput, J. Mes, R. A. M. Vreeburg, H. F. J. Sayelkoul, H. J. Wichers, Transcription profiles of LPS-stimulated THP-1 monocytes and macrophages: a tool to study inflammation modulating effects of food-derived compounds. *Food & Function.* **1**, 254-261 (2010).
134. M. A. Jones, S. Totemeyer, D. J. Maskell, C. E. Bryant, P. A. Barrow, Induction of proinflammatory responses in the human monocytic cell line THP-1 by *Campylobacter jejuni*. *Infect. Immun.* **71**, 2626-2633 (2003).
135. Kirikae, T. et al. Endotoxin contamination in fetal bovine serum and its influence on tumor necrosis factor production by macrophage-like cells J774.1 cultured in the presence of the serum. *Int. J. Immunopharmacol.* 19, 255-262 (1997).
136. Shio, M. T., Kassa, F. A., Bellemare, M. & Olivier, M. Innate inflammatory response to the malarial pigment hemozoin. *Microb. Infect.* **12**, 889-899 (2010).